Evaluation of Rotating Packed Beds for Distillation

Zur Erlangung des akademischen Grades eines

Dr.-Ing.

von der Fakultät Bio- und Chemieingenieurwesen
der Technischen Universität Dortmund
genehmigte Dissertation

vorgelegt von

M.Sc. Hina Qammar

aus

Lahore

Tag der mündlichen Prüfung: 13.10.2025

1. Gutachter/-in: Prof. Dr.-Ing. Gerhard Schembecker
2. Gutachter/-in: Prof. Dr. Christoph Held

Dortmund 2025

This thesis is dedicated to Univ.-Prof. Dr.-Ing. Andrzej Górak, whose early guidance and mentorship made this work possible.

Abstract

In the chemical industry, centrifugal contactors have been proven to enhance separation processes, including distillation and absorption. Due to intensified mass and heat transfer, these contactors offer lower equipment volume, faster processing, and greater flexibility and performance. Rotating packed beds (RPBs), a centrifugal contactor, have been investigated for decades; however, their industrial implementation remains limited despite several benefits reported in the literature. One key limitation is the lack of a fundamental understanding of mass transfer within the packing and the absence of appropriate scaling rules. This work evaluates the rotating packed bed (RPB) technology for distillation by developing a fundamental understanding of mass transfer in RPB packings through comprehensive investigations.

Firstly, a pilot plant was developed to facilitate large-scale distillation experiments and enable temperature measurements. It was automated using LabVIEW for instrumentation, control, and data acquisition. Secondly, total reflux distillation experiments were conducted at atmospheric pressure using conventional RPB packings, such as knit mesh and metal foam, with varying radial packing lengths, and without packing. Based on these results, a novel Zickzack packing was designed, resulting in slightly improved separation efficiency and easier scalability due to more homogeneous conditions inside the packing. Experiments with varying rotational speeds, vapor loads, and packing lengths demonstrate the flexibility of RPB operation while maintaining separation efficiency.

Lastly, rotor telemetry was implemented for the first time to estimate the radial temperature profile and to develop an understanding of mass transfer within the packing, revealing that, in addition to the packing, the casing also contributes to the total separation efficiency of an RPB. Moreover, the separation efficiency of conventional RPB packings does not increase linearly with radial packing length, unlike Zickzack packing. The mass transfer performance was estimated using available correlations, and their limitations were identified. The key design and operational findings are summarized.

Zusammenfassung

In der chemischen Industrie haben sich Zentrifugalkontaktoren als vorteilhaft für die Intensivierung von Trennprozessen wie Destillation und Absorption erwiesen. Durch den Einsatz von Zentrifugalkräften wird der Stoff- und Wärmeübergang intensiviert, wodurch kompaktere Apparate, schnellere Prozesse sowie eine höhere Flexibilität und Leistungsfähigkeit ermöglicht werden. Rotating Packed Beds (RPBs), eine Form von Zentrifugalkontaktoren, werden seit Jahrzehnten untersucht; ihre industrielle Umsetzung ist jedoch trotz zahlreicher in der Literatur beschriebener Vorteile bislang begrenzt. Ein wesentlicher Grund hierfür ist das fehlende grundlegende Verständnis des Stoffübergangs innerhalb der Packung sowie das Fehlen geeigneter Skalierungsregeln. Ziel dieser Arbeit war es, die RPB-Technologie für die Destillation durch umfassende Untersuchungen zu bewerten und ein grundlegendes Verständnis des Stoffübergangs in RPB-Packungen zu entwickeln.

Hierzu wurde zunächst eine Pilotanlage aufgebaut, um großskalige Destillationsversuche durchzuführen und Temperaturmessungen zu ermöglichen. Die Anlage wurde mithilfe von LabVIEW zur Messung, Steuerung und Datenerfassung automatisiert. Anschließend wurden Totalrücklauf-Destillationsversuche bei Atmosphärendruck mit konventionellen RPB-Packungen, wie Drahtgestrick und Metallschaum, bei variierenden radialen Packungslängen sowie ohne Packung durchgeführt. Auf Grundlage dieser Ergebnisse wurde eine neuartige Zickzack-Packung entwickelt, die aufgrund homogenerer Bedingungen innerhalb der Packung eine leicht verbesserte Trennleistung und eine einfachere Skalierbarkeit ermöglicht. Untersuchungen mit variierenden Drehzahlen, Gasbelastungen und Packungslängen zeigen die hohe Betriebsflexibilität von RPBs bei gleichzeitig konstanter Trennleistung.

Darüber hinaus wurde erstmals ein Rotortelemetriesystem eingesetzt, um das radiale Temperaturprofil zu bestimmen und ein besseres Verständnis des Stoffübergangs innerhalb der Packung zu gewinnen. Dabei konnte gezeigt werden, dass neben der Packung auch das Gehäuse zur Gesamttrennleistung eines RPB beiträgt. Zudem nimmt die Trennleistung konventioneller RPB-Packungen im Gegensatz zur Zickzack-Packung nicht linear mit zunehmender radialer Packungslänge zu. Die Stoffübergangsleistung wurde mithilfe verfügbarer Korrelationen abgeschätzt und deren Grenzen identifiziert. Abschließend werden die wichtigsten Erkenntnisse hinsichtlich Auslegung und Betrieb zusammengefasst.

Table of Contents

Abstract ..... **I**

Zusammenfassung ..... **II**

Table of Contents ..... **III**

List of Abbreviations and Symbols ..... **VI**

Chapter 1 Introduction **1**

1.1. Scope of this Work 3

Chapter 2 State of the Art **4**

2.1. Process Intensification 5

2.2. Fundamentals of RPBs 7

2.2.1. Analogy of RPB and Conventional Column 8

2.2.2. Rotor and Packing Types 10

2.3. Vapor-Liquid Contacting in RPBs 13

2.3.1. Industrial Applications 14

2.3.2. Pressure Drop 19

2.3.3. Mass Transfer Fundamentals and Correlations 20

2.3.4. Measurement Techniques to Understand Mass Transfer in RPBs 25

Chapter 3 Mass Transfer Investigation in RPBs **30**

3.1. Materials and Methods 31

3.1.1. Experimental Set-up 31

3.1.2. Experimental Procedure 35

3.1.3. Measurement of Separation Efficiency 36

3.1.4. Vapor Bypass 37

3.2. Influence of Design Parameters 38

3.2.1. Radial Packing Length (Scale-ability) 38
3.2.2. Effect of Rotor Diameter 42
3.2.3. Effect of Packing Type 45
3.3. Influence of Operating Parameters 46
3.3.1. Rotational Speed and Vapor Load (Operating ranges) 46
3.4. Development of Zickzack Packing Design 48
3.4.1. Performance Evaluation of the Advanced Zickzack Packing Design 52
3.4.2. Comparison with Reported Literature 53
3.5. Comparison with Conventional Column 55
3.6. Summary 56
Chapter 4 Temperature Profile Investigations in RPBs 58
4.1. Fundamentals 59
4.2. Materials and Methods 61
4.2.1. Experimental Setup 61
4.2.2. Experimental Procedure 64
4.3. Calculation of Theoretical Stages Using Temperature Measurements 65
4.3.1. Overall Composition Profile in an RPB 67
4.3.2. Contribution of Packing and Casing to the Overall Mass Transfer 68
4.3.3. Radial Temperature Profile in Packed and Empty Rotor 71
4.3.4. Change in the Separation Efficiency Along the Radial Packing Length 72
4.4. Contribution of Mass Transfer Zones 76
4.5. Summary 78
Chapter 5 Mass Transfer Modeling 79
5.1. Mass Transfer Rate 80
5.2. Experimental Mass Transfer Coefficient 80

5.3. Simulated Mass Transfer Coefficient 85

Chapter 6 Key Design and Operation Findings for Distillation in RPBs 90

6.1. Overview of Parameters Investigated in this Work 90

Chapter 7 Conclusion 100

Chapter 8 Outlook 102

Chapter 9 References 103

Chapter 10 Appendix 112

A-1: List of Dimensionless Numbers 112

A-2: P&ID of Distillation in RPBs 113

A-3: Calculation of Geometrical Surface Area of RPB Casing 116

A-4: Mass transfer of Conventional RPB Packing at an F-factor of 0.6 $Pa^{0.5}$ 117

A-5: Equilibrium Curve of Ethanol-Water Test System at 1.0133 bar Pressure 118

A-6: Vapor Density Data of Ethanol-Water Test System at 1.013 bar Pressure 130

A-7: Temperature Measurement Data of Rotor Telemetry 133

A-8: Vapor-liquid equilibrium data of the methanol-ethanol test system 136

Chapter 11 Declaration 137

Chapter 12 List of Publications 138

Chapter 13 List of Supervised Theses 140

List of Abbreviations and Symbols

Latin letters

a_c	centrifugal acceleration	m s^{-2}
A	surface area	m^2
A_c	cylindrical surface area	m^2
a_p	specific geometric packing surface area per unit	m^2 m^{-3}
d	diameter	m
D	radial length	m
D_G	diffusion coefficient gas phase	m^2 s^{-1}
d_p	effective diameter of the packing	m
F_{factor}	gas capacity factor	$Pa^{0.5}$
F_{eye}	gas capacity factor at the inner radius of the rotor	$Pa^{0.5}$
g	gravitational acceleration	m s^{-2}
h	axial length	m
K_Ga	overall volumetric gas- or vapor-side mass transfer coefficient	s^{-1}
kga	local mass transfer coefficient in the packing	s^{-1}
L_{pack}	radial packing length	m
$\dot{m}$	mass flow rate	kg s^{-1}
r	radius	m
T	temperature	°C
u	velocity	m s^{-1}
x	liquid molar fraction	—
y	vapor molar fraction	—
y^{eq}	equilibrium vapor composition	—

Greek letters

α	relative volatility	—
ε	porosity	—
ϵ	hold-up	—
ρ	density	kg m^{-3}
Ø	pore diameter of foam packing	mm
σ_{lv}	vapor-liquid surface tension	kg s^{-2}
ν	kinematic viscosity	m^2 s^{-1}
ω	angular velocity	rad s^{-1}

Subscripts

avg	average
c	casing
col	column
empty	without a packing installed
G or g	gas
i	inner
int	integrated
l	liquid
o	outer
pack	packing
v or vap	vapor

Dimensionless numbers

Bo	Bond number	
Gr	Grashof number	—
Re	Reynolds number	—
Sc	Schmidt number	—
We	Weber number	—

List of abbreviations

ATU	area of a transfer unit
CRZB	compound rotating zigzag bed
ER	empty rotor
HETP	height equivalent to a theoretical plate
HTU	height of a transfer unit
KM	knit mesh packing
MF	Metal foam packing
NTU	number of transfer unit
Nth	Number of theoretical stages
OD	outer diameter
RPB	rotating packed bed
RSRM	raschig super ring metal
RZB	rotating zig-zag bed
TI	Temperature indicator
VLE	Vapor-liquid equilibrium
ZZ	Zickzack packing

Chapter 1 Introduction

Fluctuations in customer demand bring new challenges to the chemical industry, requiring energy-efficient, cost-effective, and modular processes [3]. While distillation remains the most widely used fluid-separation technology, it is a space-demanding and energy-intensive process in the chemical industry [6]. Traditionally, multistage counter-current distillation is implemented in static columns with different types of trays or packed beds, where liquid flows downward under gravity while vapor flows upward. Process intensification has received increasing attention for decades to address the remarkable challenges of the chemical, specialty, and pharmaceutical industries, such as more efficient production and economical separation processes. Although many approaches to process intensification exist, they generally intensify the fundamental phenomena with apparatuses or their interplay [7]. Many technologies and methodologies for process intensification to achieve operational or structural improvements have been established over the last three decades [9,10]. Despite this, other advanced technologies have not yet been fully integrated into industrial applications due to insufficient understanding of the techniques; as a result, they remain under investigation at the academic level. This is also true for applying centrifugal fields in separation technologies, such as absorption, distillation, and stripping, to enhance efficiency. Promising concepts for intensified distillation equipment include the so-called high gravity (HIGEE) technology and rotating packed beds (RPBs), which have gained considerable attention in recent years, especially in Asia [13,14]. Compared to static equipment, they bear the potential for significant mass transfer improvements and extended operating windows, providing compact equipment with added flexibility. In RPBs, the centrifugal force induced by the rotation of a packed-bed rotor enhances the interaction between a gas and a liquid stream that passes counter-currently through the packing. It is claimed that applying high shear forces creates thin films and fine droplets, thereby intensifying contact between the phases [15–17]. Intense mixing, reduced equipment size, the use of high-specific-surface-area packings, and an enlarged operating window are the primary benefits of this technology compared to conventional gravity-based separation [18].

Centrifugal process intensification was introduced more than 80 years ago by Podbielniak (1935) [19]. However, the design of today's RPBs is related to the patents by Pilo and Dahlbeck (1960) [20] and Ramshaw and Mallinson (1981) [21]. The work of Ramshaw at ICI on RPBs was vital in promoting the concept of process intensification to the chemical engineering community [17]. Owing to the increasing interest in RPBs, some rotor types and packing designs have been developed specifically in the last two decades. The review article by Cortes-Garcia et al. (2017) [14] provides a concise overview and analysis of available distillation designs. Experimental investigations have been expanded from conventional single-block packings for RPBs, like wire mesh [22,23], knit mesh [23], and metal foams [1], to more complex packing and rotor configurations, as in split packing [8] for enhanced vapor angular slip velocity and several other alternatives [24–26]. Continuous distillation applications, especially the so-called Rotating Zigzag Beds (RZBs), developed mainly by Wang et al. (2008) [27,28] have shown superior performance compared to known single-block packings in RPB and have been adopted in several industrial applications, primarily in Asia [13,14]. Unlike classical RPBs with so-called single-block packings, which are fixed between two simultaneously rotating disks, the RZB rotor consists of a rotating and stationary disk on which two series of circular baffles are mounted alternately [29]. The RZB concept is more closely linked to tray columns, whereas conventional RPBs are closely related to packed columns.

Although many attempts have been made to exploit the full potential of HIGEE technology, initially promoted to enable a 10-100× reduction in equipment size, the industrial application of RPBs, especially in Europe and the U.S., remains severely limited [18]. Potential reasons include general caution regarding rotating equipment, energy consumption, the lack of dedicated analysis of mass transfer within the RPB, and the absence of proper scale-up rules. Furthermore, there is still a severe need for reliable mass transfer analysis and modeling, as most published data for RPBs reflect results from relatively small-scale laboratory equipment, assuming that all mass transfer in the RPB can be attributed to the packing. Nevertheless, differentiation between mass transfer in the packing and the casing is of significant importance when characterizing the performance of a specific type of packing under different operating parameters, such as rotational speed and F-factor. Therefore, different rotor configurations, with and without packing, must be evaluated to quantify mass transfer within the packing accurately and to develop scaling guidelines. Developing reliable scale-up rules is an essential

step in paving the way for the industrial applications of RPBs. Moreover, understanding and quantifying the mass transfer inside the packing is critical for packing scalability.

1.1. Scope of this Work

This work conducts various experimental investigations to evaluate different types of conventional RPB packing (Chapter 3.2.3) and to address their limitations. Investigations are extended to develop a new single block additively manufactured packing (Chapter 3.4) offering potential for easy scale-up and compared with conventional knit mesh and metal foam packings as well as traditional column packings (Chapter 3.5) based on dedicated batch distillation experiments under total reflux for the dehydration of ethanol (Chapters 3.1). Additionally, experiments with varying vapor loads and rotational speeds (Chapter 3.3) enabled the creation of a database highlighting the operating range and flexibility of RPBs. To understand and quantify the mass transfer inside the packing, investigations on the local mass transfer inside the rotor are conducted using two approaches: (1) varying radial packing lengths (Chapter 3.2.1), and (2) using wireless temperature sensors to record radial temperature profiles in different rotor configurations (Chapter 4). The overall vapor-side volumetric mass transfer coefficient in the RPB and the local mass transfer coefficient within the packing are calculated from the current work's experimental data and compared with the simulated mass transfer coefficients obtained from available literature correlations (Chapter 5). Finally, based on the wide range of experimental data collected in this work, the summarized results are expected to serve as a basis for developing consistent and reliable guidelines for distillation in RPBs (Chapter 6).

Chapter 2 State of the Art

The chapter presents the necessary foundation and background on process intensification, specifically centrifugally enhanced separation processes, followed by an overview of the fundamentals and background of rotating packed beds (RPBs). The first part of the chapter explains basic terminology, separation principles, and analogies to conventional columns, with a focus on distillation processes. The final section of the chapter focuses on current industrial applications, mass transfer in RPBs, and an overview of existing measurement techniques for estimating liquid hold-up, flow patterns, and mass transfer phenomena in RPBs.

Parts of Chapter 2 are published in:

Neumann, K.; Gladyszewski, K.; Groß, K.; Qammar, H.; Wenzel, D.; Górak, A.; Skiborowski, M.: A guide on the industrial application of rotating packed beds, CHERD, 2018, 134, 443 – 462, http://doi.org/10.1016/j.cherd.2018.04.024

Qammar, H; Gładyszewski, K; Górak, A; Skiborowski, M: Towards the Development of Advanced Packing Design for Distillation in Rotating Packed Beds, Chem. Ing. Tech., 2019, 91, 11, 1663 – 1673, https://doi.org/10.1002/cite.201900053

Qammar, H.: Rotating Packed Beds in Distillation: Binary Distillation, in: M. Skiborowski, A. Górak (Eds.), Process Intensification, De Gruyter, 2022, pp. 159–188.

https://doi.org/10.1515/9783110724998-006

Qammar, H; Hecht, F.; Skiborowski, M; Górak, A.: Experimental Investigation and Design of Rotating Packed Beds for Distillation, Chemical Engineering Transactions, 69, 655-660

https://doi.org/10.3303/CET1869110

.

2.1. Process Intensification

Products manufactured by industries such as the chemical, specialty, and pharmaceutical sectors are necessary for today's society. However, these industries face challenges in responding to rapidly changing markets, as they must produce more sustainably, efficiently, and environmentally friendly products at lower costs due to increasing global competition. Moreover, the demand for innovative products has led to shorter lifetimes for these products and processes. Environmental laws and regulations are evolving, and stricter boundaries are being established for the chemical industry. With the increasing pressure to meet environmental regulations, there is a need to evaluate whether existing technology is flexible enough to meet these demands in the future. Therefore, introducing and implementing new technological innovations is necessary in the future to reduce costs and improve environmental safety. For example, the equipment must be upgraded or modified to meet global challenges. New reaction pathways that employ different catalysts, solvents, or operating conditions need to be developed to improve efficiency in resource consumption, solvent use, and energy expenditure. Improving the design of existing processes and creating new ones to address future challenges that exceed those addressed by the conventional process unit toolbox is the only effective way to address them. The new norm is ``using much less to produce much more´´ [30]. Process intensification is a crucial tool for addressing the latest challenges in the process industry. Process intensification involves developing and optimizing chemical or industrial processes to substantially improve efficiency, productivity, and sustainability. It integrates and synergizes several unit operations and process steps into a single system or equipment to maximize outputs and minimize energy consumption, waste production, and overall environmental impact. Heat and mass transfer enhancement methods have existed for a long time, even before they were called "Process Intensification". For example, electric fields and centrifugal forces were among the famous options. Rotation to enhance heat and mass transfers has been one of the most effective tools in several unit operations, from reactors to separators. However, the initial application of rotation in industrial plants primarily focused on heat transfer operations, which consisted of two phases. Process intensification continues to evolve as an interdisciplinary field, with ongoing research and development efforts focused on process miniaturization, intensified mixing and reaction technologies, and the integration of renewable energy sources [30,31].

Although many approaches to process intensification exist, they generally intensify the fundamental phenomena with apparatuses or their interplay [7]. Many technologies and methodologies for process intensification to achieve operational or structural improvements have been established over the last three decades [9,10]. The ultimate goal is to achieve highly efficient, environmentally friendly industrial processes that address the challenges of resource scarcity, energy efficiency, and climate change in the modern world. Despite this, some of the advanced technologies have not yet been fully integrated into industrial applications due to insufficient understanding of the techniques; therefore, they remain under investigation at the academic level. It is also true for applying centrifugal fields in separation technologies like absorption, distillation, and stripping to enhance efficiency. The concept of exploiting centrifugal force to intensify separation processes dates back to the 19th century, for example, centrifugal milk separators for milk processing [32], and centrifugal filters for separating liquids and solids [33]. In the 1930s, patents were filed for the development of centrifugal contactors for liquid-liquid and gas-liquid operations [17,19]. Reported benefits were a more efficient process, reduced equipment size due to the improvement in mass and heat transfer, and enlargement of the operating window due to replacing the gravitational field with the centrifugal acceleration of 100-1000 times Earth's gravity [34]. This technology is usually referred to as *HiGee*-technology. Podbielniak (1935) [19] was one of the first to realize the limitations imposed by gravity, introducing a centrifugal countercurrent contact apparatus in the 1930s, consisting of a spirally wound tube mounted on a rotating support. This design was further improved, as evidenced by a 1940 patent. The construction of most modern high gravity (Higee) apparatus is similar to the design initially patented by Pilo and Dahlbeck (1960) [20]. However, Stankiewicz and Moulijn [35] point out that the current form of high gravity (Higee) technology was predominantly developed and initially demonstrated for distillation by Imperial Chemical Industries (London), which started working on rotating packed beds (RPBs) in the late 1970s as a spinoff from a NASA research project [21,36]. Since then, Higee technology has evolved into one of the most promising branches of process intensification (PI), aiming to improve heat and mass transfer through high centrifugal forces [15]. Rotating packed beds (RPBs) are an example of HiGee technology equipment. According to Figure 2.1 [37], process intensification can occur at different levels. RPB is an example of PI done simultaneously at the operation & equipment level and the phase & transport level.

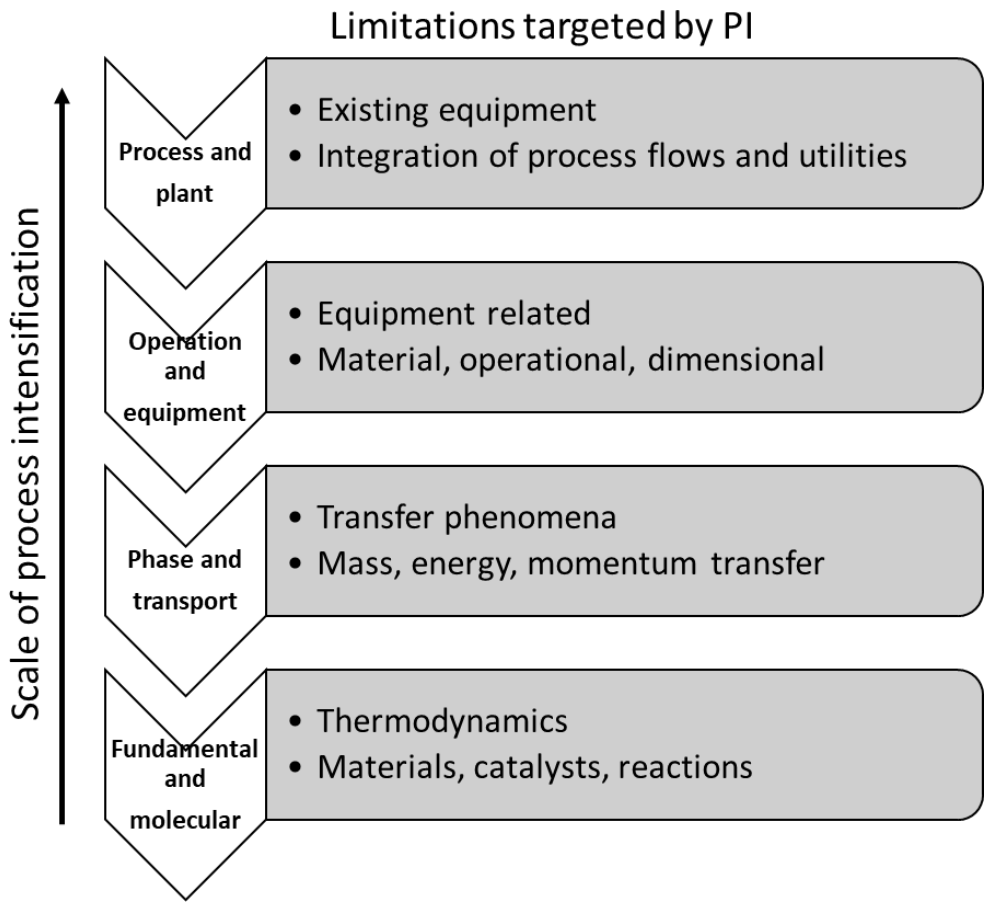

Figure 2.1: Different levels of process intensification [37].

2.2. Fundamentals of RPBs

Rotating packed bed (RPB) is an example of a process intensification device that utilizes additional energy and manipulation of structural parameters to meet the demands for efficient, flexible, and innovative production facilities [38]. The extra energy from high centrifugal forces facilitates intense mixing, enhanced mass transfer, shorter residence times, and higher capacities than in conventional distillation apparatus. Moreover, transforming the longitudinal geometry of conventional columns into a radial geometry yields compact, modular devices. The scope of this work is based on the unit operation of distillation. The following sections introduce the terminology used for RPBs and present the separation principles and rotor designs.

2.2.1. Analogy of RPB and Conventional Column

An RPB mainly consists of a rotor enclosed in a stationary casing. In an RPB (Figure 2.2), a packing is mounted on a shaft and serves as a rotor. In other versions of this machine, non-packing rotors are employed, as presented in 2.2.2. In general, for a counter-current operation, the liquid is introduced at the eye of the rotor through a liquid distributor. After entering the rotating packing, the liquid is accelerated towards the outer radius by the centrifugal forces and collected in the casing. The vapor is introduced through the casing and, under externally applied pressure, flows towards the center of the rotor. Seals between the rotating and non-rotating parts are necessary to prevent bypassing of liquid and vapor.

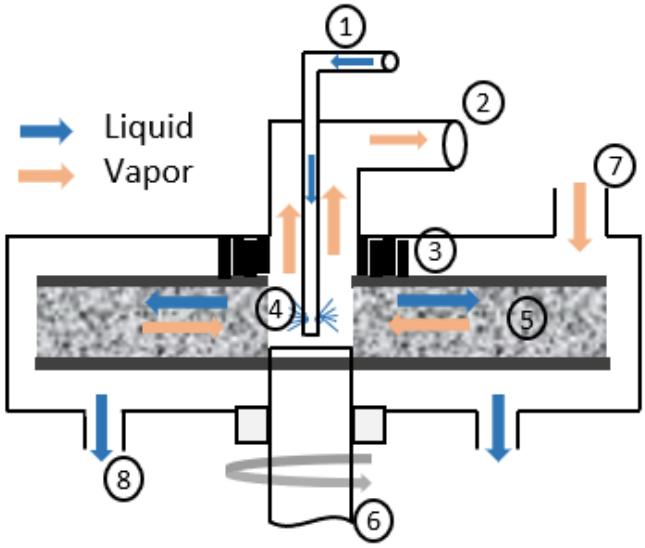

Figure 2.2: Sketch of a rotating packed bed for distillation. 1: liquid inlet, 2: vapor outlet, 3: seals, 4: nozzles, 5: packing, 6: shaft, 7: vapor inlet, 8: liquid outlet.

The basic principles and characteristics of RPB can be better understood through an analogy with conventional distillation columns, as shown in Figure 2.3. In a conventional distillation column, the liquid generally flows from top to bottom under the influence of gravitational force ‘g’ and countercurrently to vapors flowing upwards, whereas in an RPB, the liquid and vapor flow radially under the influence of applied centrifugal forces. In a conventional distillation column, the vertical height of the packing represents the separation efficiency, and the radial diameter represents the column capacity. However, in an RPB, the separation efficiency is

defined by the radial length of the packing, and the vertical height of the packing primarily determines the capacity.

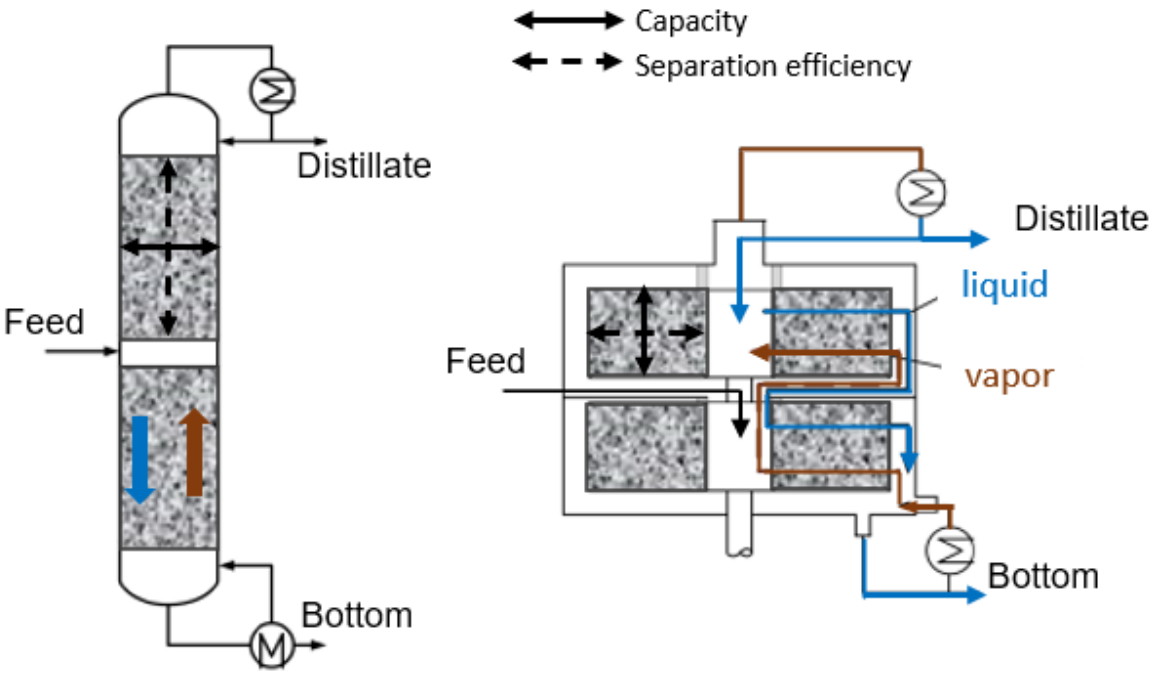

Figure 2.3: Analogy of a conventional distillation column and an RPB.

Unlike in columns, introducing liquid feed in RPBs is complex due to the combination of rotating and non-rotating parts. For the distillation operation, two rotors are attached to the same shaft. A liquid collector/casing and a liquid redistributor separate the two rotors. The liquid from the upper rotor is collected at the casing and redistributed to the eye of the lower rotor. In contrast, the vapor follows counter-currently from the eye of the lower rotor to the outer casing of the upper rotor. A rectifying section in the upper and a stripping section in the lower rotor are formed.

Another advantage of RPBs over conventional columns is their rotational speed, which provides an additional degree of operational freedom. This operational variable can be varied by several orders of magnitude relative to the gravitational force to alter the operating window and separation efficiency [15,39]. Centrifugal acceleration is a function of rotational speed as well as of radius. Intense mixing and increased mass transfer in an RPB can be achieved at high rotational speeds and large radii. However, the radial dependence of the centrifugal

acceleration results in inhomogeneous centrifugal fields within the packing, ranging from low at the center to high at the outer edge of the rotor. Conversely, the liquid and vapor loads are higher at the center and lower at the outer radii of the packing. The inverse relationship between load and centrifugal force leads to differences in separation efficiency across radial packing lengths. The fundamental mass-transfer process in RPBs remains poorly understood and will be discussed in Chapter 3.

2.2.2. Rotor and Packing Types

The rotor is the central component of HiGee devices, as it determines their performance characteristics. Over the last two decades, various packing types and rotors have been investigated, and developments have been proposed. The rotors can be divided into packed and non-packed (tray-type rotors). RPB is a classic example of a packed rotor, and a Rotating zigzag bed (RZB) is an example of a tray-type rotor. For packed rotors, not only have various conventional packing types been investigated, e.g., wire mesh and metal foams, but many new packing designs have also been developed to understand mass transfer fundamentals and improve rotor separation efficiency. Advanced packing includes split and spiral packing, etc. (Figure 2.4). Li et al. (2014) [40] presented an interesting overview of the various rotor types for RPB and RZB. It proposed a counterflow concentric ring rotating bed with a higher gas side mass transfer coefficient than an RPB and a 5.6 times higher gas-liquid throughput than an RZB. However, owing to the current industrial applications, the two main rotor variations of HiGee devices, i.e., RPB and RZB, will be discussed in the following section.

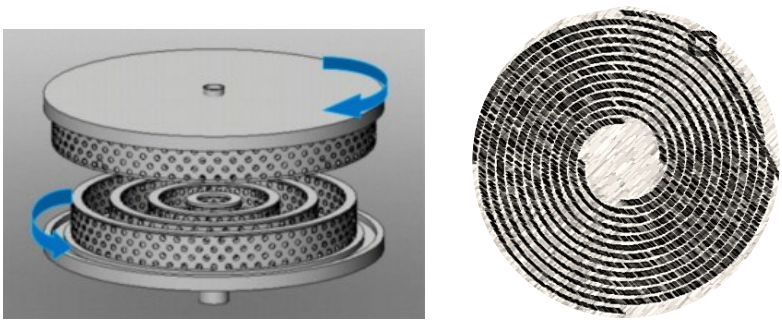

Figure 2.4: Schematic of split packing (left) and spiral packing (right). (Reprinted/adapted with permission from [41–43])

The main challenge in continuous distillation in a single RPB is supplying the feed along the apparatus's longitudinal axis as conventionally done in a distillation column [27,28]. Since the

rotor moves with the shaft, the only way to introduce the feed is either from the top as liquid (at the center of the rotor) or from the bottom as vapor (at the outer edge of the rotor). Consequently, two single-stage connected RPBs or an RPB with at least two stages (multirotor) would be required [27,28]. With recent developments in RPB, a novel rotating baffle distributor has been developed that rotates with the rotor [44]. Due to the rotating baffle distributor, continuous distillation can be performed in a single RPB with multiple rotors, thereby increasing separation performance [45].

There is an alternative rotor design to the single-block packing called RZB. This innovative geometrical modification of conventional RPBs was first patented and commercialized in 2005 [46,47]. Contrary to an RPB, an RZB is not constructed from a rotor equipped with a packing material but is built from two parts, one static, while the other rotates (Figure 2.5).

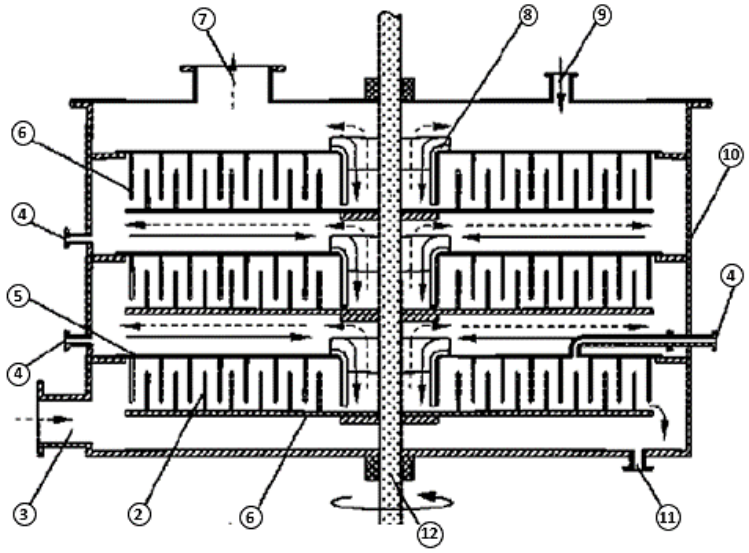

Figure 2.5: Sketch of a multirotor RZB. 1: rotational disc, 2: rotational baffle, 3: gas inlet, 4: liquid inlets, 5: Stationary disc, 6: Stationary baffle, 7: gas outlet, 8: guide pipe, 9: reflux pipe, 10: rotor casing, 11: liquid outlet, 12: rotating shaft. [27]

The reported advantages of RZBs over RPBs are the elimination of the dynamic seal between the vapor outlet and the rotor, as well as the elimination of the collection and drainage system in the case of a multirotor RPB, which is necessary to direct the liquid from one stage to the center of the next stage. It is further reported that the same mass transfer rates as in RPBs can

be achieved in RZBs [27,28]. The reason for this comparability is that in an RZB, the rotor consists of stationary and rotating baffles without packing, which reduces the contacting surface area while improving the tangential slip velocity of the vapor. On the contrary, in an RPB, the packing offers a higher surface area for contact, but the tangential slip velocity of the vapor is lower. Therefore, the average mass transfer rates in an RPB and RZB are reportedly comparable [27,28].

In contrast, it is essential to recognize that differences depend on the specific mass transfer resistances of a particular problem. An additional advantage of RZBs is that the feed can be introduced at any point along the rotor due to the stationary top rotor plate. However, the power consumption for operating an RZB is reported to be higher than that of an RPB, mainly due to a higher liquid hold-up in the rotor and a higher pressure drop resulting from the zigzag flow [29]. Li et al. (2012) [29] concluded that the power requirement of an RZB was roughly 2.5 times higher than that of an RPB, making further development of the RZB technology necessary [29]. Similarly, Qammar et al., 2019, [43] showed that the pressure drop in an RPB packed with Zickzack packing is almost ten times lower than in an RZB under comparable operating conditions. Loll et al. (2022) [48] further developed the Zickzack packing for deaeration, improving the sealing of the packing, to minimize vapor bypass and enhance the mass transfer within the packing.

Nevertheless, owing to their superior operability, RZBs have been applied for continuous distillation in industrial applications. Xu et al. (2012) [47] reported around 300 RZB installations in industrial applications for pharmaceutical material and intermediates, fine chemicals, bio-diesel, and environmental protection [47]. Most industrial applications of RZBs for distillation are in China. They are also called rotating distillation machines, supergravity separators, or Higee distillation systems. Almost thirty thousand chemical companies in China can potentially apply RZB in product separation and solvent recovery [39,49].

2.3. Vapor-Liquid Contacting in RPBs

Distillation was the first unit operation of RPBs. In 1983, Ramshaw [50] reported the concept of HiGee distillation, based on research by Imperial Chemical Industries (ICI). They conducted intensive pilot and large-scale research using separate RPBs for the stripping and rectifying sections. The outer diameter of the rotor was 80 cm, and the height of the rotor was 30 cm, including the wire mesh packaging. During their tests, HETP (height equivalent to theoretical plates) values of 1–2 cm were achieved with an average centrifugal acceleration of 1000 times the acceleration due to gravity [51]. Although extensive research was conducted, details of the results could not be obtained from the open literature.

After Ramshaw, about a decade later, Kelleher and Fair (1996) [1] reported subsequent distillation research on RPBs. Their slightly smaller RPB consisted of a single rotor with a metal sponge packing, measuring 15 cm in axial height, allowing for a large capacity. The first experimental results on the number of transfer units (NTU) were presented in the literature at total reflux. Various experimental and theoretical studies, including modeling methods, have been conducted over the last few years using a range of rotors, packings, and chemical systems. However, the number of investigations is limited. One of the essential developments was Chandra et al.'s split packing in 2005 [52] (Figure 2.4), which showed that light turbulence in the vapor phase limits vapor-side mass transfer. Wang et al. [27] also introduced RZBs, and their subsequent development is essential, as they offer new possibilities due to their rather tray-like design. Finally, Luo et al. (2012) [53] developed a design that combines stationary discs with pores and rotating packing rings. This design combines the packed and zigzag rotor designs to reduce pressure drop and increase separation efficiency compared to RPB and RZB. Although some milestones and advantages have been demonstrated, further in-depth investigations are still needed to thoroughly understand and identify the phenomena and potential of RPB for distillation. Some RZB distillation applications and a very recent RPB carbon capture application are discussed in the following section.

2.3.1. Industrial Applications

Over the past few years, several applications of RPBs have been reported [14,24]. Some applications benefit from the short residence time and intense mixing of the contacting phases in the RPB, while others benefit from the reduced equipment size. Sudhoff (2015) [54] presented an interesting overview of the potential benefits of RPBs over conventional equipment and their potential fields of application within a process. Later on, Neumann et al. (2018) [18] summarized some industrial applications of RPBs containing gas-liquid [55–58], vapor-liquid [39,47,49], and liquid-liquid mixtures [9,59] in a recent review [18]. In a single RPB, supplying the feed along the rotor's radial axis is challenging because the rotor rotates with the shaft. However, recent geometrical modifications to the rotor have enabled other options, such as an RZB, for continuous distillation [27]. The details of the design and structure of an RZB are discussed in section 2.2.2.

Solvent Recovery

In recent years, the most prominent application of RZBs in vapor-liquid contacting processes has been solvent recovery from products or waste streams. Methanol, for instance, is one of the most significant commodity chemicals in the world, mainly used as a base material in the production of other chemicals, such as formaldehyde and acetic acid, and as a chemical agent in pharmaceuticals, synthetic fabrics, paints, adhesives, and plastics. Owing to the health and environmental hazards associated with methanol, it is often necessary to recover it from the waste liquid or exhaust gas streams [60]. Solvent recovery is also essential for the economic feasibility of an industrial process. The recovery reduces the fresh solvent requirement and possibly the cost of expensive waste treatment.

An example in which the use of an RZB not only reduced the occupied space for the equipment but also improved product purity is the binary separation of the methanol-water mixture [18,39]. An RZB of diameter 0.83 m and a total height of 0.8 m, excluding the motor, is reported to separate a binary methanol-water mixture with a total capacity of 500 kg/h [49]. Furthermore, with these dimensions, 99.8 wt.% pure methanol is produced at the top and 0.2 wt.% at the bottom. Neumann et al. performed a theoretical study to enable a potential comparison between the packed column and the RZB. The separation of the methanol-water mixture serves as a reference for simulating the process in Aspen Plus® using the built-in

RADFRAC model and Sulzer BX500 structured packing. All the input data, such as feed, top and bottom compositions, reflux ratio, etc., are compared on the same basis and presented in Table 2.1. The reported packed column for the above case has a height of 11 m, a diameter of 0.6 m, and 3 wt.% methanol in the bottom product [39,49].

Table 2.1: Simulation data for methanol-water distillation [61].

Item	**Feed**	**Top**	**Bottoms**
Flowrate [kg/h]	500	350.4	149.6
Methanol [wt./wt.]	0.7	0.998	0.002
Water [wt./wt.]	0.3	0.002	0.998
Column Operating Conditions			
Pressure [bar]	1.01	Reflux ratio	1.5
Feed condition	Saturated liquid	Distillate to feed ratio (mass)	0.7
Packing	Sulzer BX500		

The simulation results for column sizing showed that a packed column 13 m tall would be required to achieve a top product purity of 99.8 wt%, similar to that reported for the RZB. Consequently, applying RZB reduces equipment size by an order of magnitude compared to the conventional distillation column. Furthermore, a sensitivity study conducted as part of the theoretical study mentioned above [18] showed that variations in feed and product compositions affect column height. The authors showed that when the feed composition varies from 70 wt.% methanol to 50 wt.% methanol, keeping the column height (13 m), distillate-to-feed ratio (0.7), and reflux ratio (1.5) constant, the top product purity dropped from 99.8 wt.% methanol to 71.4 wt.% [18]. In contrast, in an RZB, changes during operation can be accommodated by varying the rotational speed without altering the design or other critical operating parameters (such as temperature), thereby avoiding the time-consuming effort required to maintain process stability. It implies that the rotational speed of an RZB can be adjusted to respond to changes in feed or product composition, providing a degree of flexibility absent in the static column equipment used as a benchmark.

Processing Heat-Sensitive Materials

An interesting example of solvent recovery is the separation of methanol from an aqueous stream containing heat-sensitive, viscous materials that are prone to decomposition. Wang et al. [39] used this application and compared the performance of a distillation column with that of an RZB. However, it is not a comparison of equipment exchange only, as two different operations, i.e., batch distillation in the packed column and continuous steam stripping in RZB, are compared. As this makes comparison with other equipment difficult, it should be noted that applying the steam stripping operation in the conventional column would be ineffective due to the higher residence time, as the longer contact time with the high-temperature steam would result in product decomposition. Therefore, batch distillation must be performed at low temperatures under vacuum, which reduces mass transfer rates due to the increased viscosity of the liquid mixture.

A distinct advantage of using RZB is the significantly reduced residence time, which enables continuous steam stripping [39]. Therefore, it is reasonable to compare both pieces of equipment while considering the mode of operation and the specific operating conditions, as they apply only through RZB. The RZB application offers lower utility and equipment costs due to higher operating temperatures and smaller equipment. Moreover, the applied centrifugal forces in an RZB generate intense turbulence and higher liquid velocities, resulting in thinner liquid films and increased mass transfer rates. Although the power consumption of operating an RZB is generally higher than that of a reboiler and condenser, in this comparison, the total power consumption of a packed column is 35 kW, including refrigeration and vacuum. In contrast, the RZB has 18 kW since cooling water is used in the condenser. Using RZB, the reduction in the area occupied is four times less than that of the packed column [39].

Carbon Capture

Another vital application of RPBs is in carbon capture. Carbon dioxide (CO_2), a significant greenhouse gas from power plants and industries, significantly impacts climate change, and its mitigation and achieving net-zero carbon are the most critical global standards. To reduce CO_2 emissions in the atmosphere, chemical absorption from large CO_2 emitters is a common and effective mechanism for capturing carbon after combustion, in which the gas is absorbed into a solvent. Primarily, traditional columns are used for this process. Process intensification technology has been gaining attention in this field due to the high capital costs, high absorption column heights, and low energy efficiency of traditional columns. In this regard, RPB has been identified as an appropriate technology to improve carbon capture via absorption [62].

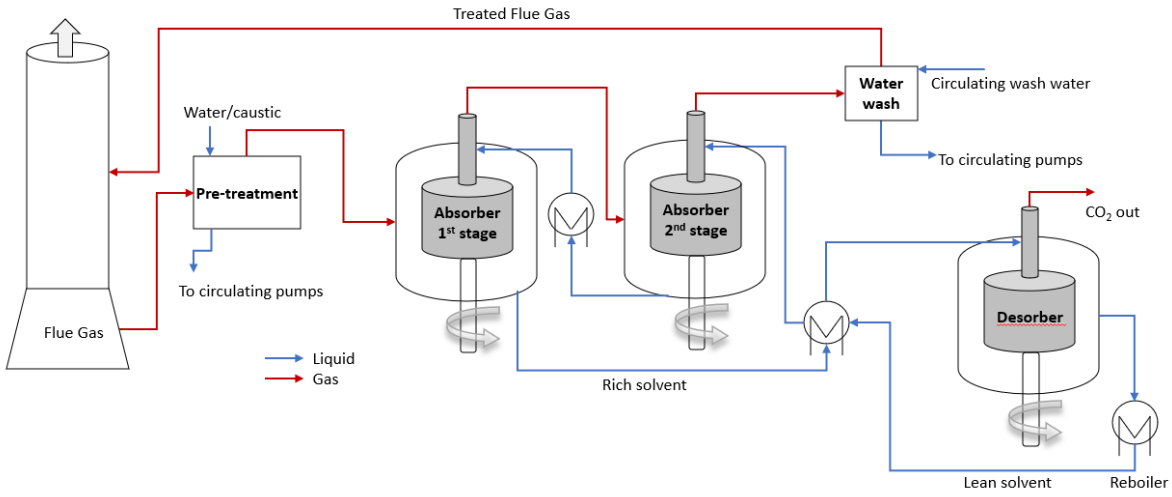

Figure 2.6: Process flow diagram of CO_2 absorption process using RPBs and solvent regeneration [63].

Carbon Clean recently implemented its first CO_2 capture process, cycloneCC, using RPB and innovative solvents. A simplified process scheme is shown in Figure 2.6. CO_2 is scrubbed from the flue gas using Carbon Clean's special solvent. The rich solvent is regenerated in the desorber, producing a CO_2 stream at the top. The CO_2-regenerated lean solvent is recycled back to the absorber. CycloneCC is particularly suitable for small to medium-sized emission sources. According to company research, cycloneCC has shown that carbon capture costs will be reduced by 50%. Although footprints are 50% lower than those of conventional technologies,

traditional capture methods still match their performance [63]. It enables CycloneCC to be implemented where traditional carbon capture technologies are not typically considered. The significantly reduced size of the equipment means the entire technology is manufactured in-house. This modular approach is scalable across any industrial application. The process intensification technology combines Carbon Clean's advanced, proprietary amino-based buffer salt solvent (APBS-CDRMax®) with two rotating packed beds (RPBs). CycloneCC is built on a prefabricated skid and can be installed in less than 8 weeks, thereby avoiding a long, complex design, construction, and engineering process. CycloneCC can be expanded to capacity by adding additional standard modular units [63].

2.3.2. Pressure Drop

Pressure drop is the most extensively researched topic in RPBs. However, it is not the focus of this work; therefore, this section is kept brief. Various factors influence the pressure drop in RPBs, as it increases with higher gas and liquid flow rates, higher rotational speeds, and reduced packing voidage. Rao et al., 2004, [15] summarised the different contributing effects into four parts:

(1) Pressure loss due to the momentum gain of the gas,

(2) frictional losses of vapor and liquid,

(3) pressure drop due to centrifugal acceleration, and

(4) pressure loss due to expansion and contraction of gas entering and exiting the rotor.

It is assumed that the 2nd and 3rd effects contribute primarily to the pressure drop, and that the other effects are negligible [15]. Several experimental studies have been conducted to develop correlations for gas flow rate, Reynolds number, rotation speed, packing characteristics, and specific resistance parameters [2,22,56]. Several mathematical models were also drawn from theoretical considerations with different levels of complexity [52,56]. Singh et al. (1992) [64] published a semi-empirical approach to describe the pressure drop. The correlation is the sum of the pressure drop due to rotation and that due to flow. Similarly, Neumann et al. [65] suggested two main effects contributing primarily to the dry pressure dr: the centrifugal head, which depends primarily on the rotor outer diameter, and the frictional pressure drop due to gas flow, which depends primarily on rotor geometry, packing properties, and operating conditions. Neumann et al. [65,66] also found that the wet pressure drop is larger than the dry pressure drop and increases with increasing liquid loads. However, the difference between wet and dry pressure drop fades away at higher rotational speeds, most likely due to decreasing liquid holdup and film thickness. Gross et al. [67,68] further validated that dry pressure drop in an RPB can be satisfactorily predicted by the method of Neumann et al., with ±30% error, which can be increased upto ±10 % by expanding the experimental operating conditions with rotational speeds ranging from 300 to 2000 min^{-1} and $F_{G,max}$ between 0 and 12 Pa$^{0.5}$. Furthermore, Gross et al. [68] validated experimentally that for packed rotors, the wet pressure drop is always higher than the dry pressure drop and supports the hypothesis that the liquid

increases the resistance for the gas to flow through the packing as described by other authors [69–71].

2.3.3. Mass Transfer Fundamentals and Correlations

Mass transfer in RPBs is more intense than in conventional gravity-operated columns. Many investigations have shown that the intensified mass transfer is due to the larger interfacial area between the phases and the high mass transfer rates [72,73]. There are a few ways to increase the interfacial area between the vapor and liquid phases, e.g., by increasing the packing surface area, wetting a larger portion of the packing surface, and producing different flow regimes with larger interfacial areas. In RPBs, packing types having surface areas up to 3300 m^2 m^{-3} have been investigated, and even higher surface areas have been proposed [36,50]. Along with the possibility of using high-surface-area packing, the intensification of mass transfer rates on both the liquid and vapor sides must be considered independently. Mass transfer phenomena in an RPB are complex and need a systematic understanding and estimation of various underlying mass transfer fundamentals. This section discusses mass transfer phenomena and different modeling approaches for distillation in RPBs.

Although distillation was the first unit operation investigated in the patent of Ramshaw and Mallinson [21], minimal experimental studies have been published on distillation in RPBs. Absorption and stripping operations are most studied in RPBs, and since these operations are primarily limited to the liquid-side mass transfer, the liquid-side mass transfer rates are the most examined in RPBs. In many distillation processes, mass transfer limitations primarily occur in the vapor phase, and vapor-side mass transfer rates in RPBs are less well researched than those on the liquid side. One of the interesting studies is by Sudhoff et al. (2014) [74], who investigated the separation efficiency of RPBs across different distillation processes in a theoretical study to demonstrate their flexibility in responding to changing flow rates and feed compositions. They proposed a model and an integrated design method to assist and accelerate the implementation of RPBs for distillation processes in the future [75]. In another study, Rao et al. [15] suggested developing packing types that generate turbulent flow regimes and using higher-surface-area packing. They also examined volumetric vapor-side mass transfer coefficients (k_Ga) and found values up to 120 s^{-1} at high gas velocities, due to the high centrifugal forces. For the vapor-side mass transfer coefficients (k_G), it was found that the values are similar to those for conventional columns [76,77]. Some authors assume that the

turbulence generated in the vapor phase inside the rotating packing is limited since the vapor entering the packing will be accelerated to the packing's velocity [77], and the slip velocity will become negligible [15]. Rao et al. (2004) [15] also proposed a packing design to increase vapor-phase turbulence and enhance vapor-side mass transfer rates. Many packings have been developed and proposed to increase the vapor-side mass transfer rates, as mentioned in section 2.2.2. Some of the essential correlations for distillation in RPBs are summarized in

Table 2.2.

Chen et al. (2011) [78] conducted a comprehensive study that combined results from the literature into a single correlation to predict the volumetric vapor-side mass transfer coefficient. As in an RPB, the packing area continuously increases from the inner to the outer side of the rotor, resulting in varying liquid loads and separation efficiency; therefore, the concept of HETP (height equivalent to a theoretical plate) can not be applied to RPBs. Singh et al. (1992) [64] proposed an ATU–NTU concept (area of a transfer unit–number of transfer units) for RPBs similar to the HTU-NTU concept (height of a transfer unit–number of transfer units) for columns. The idea is based on two-film theory, driving a material balance for a differential volume element within the packing and integrating along its radial length, i.e., from r_i to r_o. Additionally, the vapor flow rate is assumed constant when integrating the packing equation from the inner to the outer radius. The final equation is shown in Equation (2.1), where r_o represents the outer radius of the packing and r_i represents the inner radius.

$$\pi({r_o}^2 - {r_i}^2) = ATU \cdot NTU \tag{2.1}$$

Other investigators have also adopted this concept because it is more suitable, as the geometry of the RPB packing is also considered [1]. Kelleher and Fair (1996) [1] developed a two-phase model for high liquid-to-gas ratios, such as distillation. They derived a correlation for the vapor-side mass transfer coefficient from distillation experiments with cyclohexane and n-heptane, given in Equations (2.2) and (2.4).

$$K_G a \left(\frac{d_p}{a_p D_G}\right) = 2.3(10)^{-7} Re^2 Gr^{1/3} Sc^{-1/3} \tag{2.2}$$

$$d_p = \frac{6(1-\epsilon)}{a_p} \tag{2.3}$$

$$ATU_G = \frac{\dot{m}_g}{K_G a \rho_G h} \quad 2.4$$

d_p is the effective diameter of the packing, $\dot{m}_g$ is the vapor flow rate, h is the packing height ρ_G is the vapor density and $K_G a$ is the overall volumetric mass transfer coefficient. The authors used the ATU-NTU concept by Singh et al. (1992) [64] to evaluate the mass transfer efficiency of an RPB, and the correlation developed could estimate the ATU data with a ±30% error. ATU represents the ground area of a ring in a total packing arrangement. Kelleher and Fair (1996) [1] adapted the concept and defined ATU_g and NTU_g for the vapor side according to Equations (2.5) and (2.6), respectively. In these equations, y_o, and y_i denote the composition at the outlet and inlet of the RPB, respectively, and y^{eq} represents the equilibrium composition. Using the ATU-NTU concept, the effect of varying the operation condition can be seen directly on $K_G a$.

$$K_G a = \frac{\dot{m}_g}{\rho_g \cdot h \cdot ATU_g} \quad 2.5$$

$$NTU_g = \int_{y_i}^{y_o} \frac{dy}{(y^{eq} - y)} \quad 2.6$$

Li et al. (2008) [4] used two single-rotor RPBs to conduct continuous distillation experiments with an ethanol-water test mixture using three different packing types. They derived an empirical correlation for NTU values, thereby evaluating the effects of the high gravity factor (dimensionless average centrifugal acceleration), the distillate-to-feed ratio, the reflux ratio, and the feed and distillate compositions on NTU. In 2011, Mondal et al. [8] developed a correlation for the overall volumetric vapor-side mass transfer coefficient using a methanol-ethanol test mixture with split packing under total reflux conditions. They used a more straightforward approach, correlating the overall vapor-side volumetric mass transfer coefficient with the vapor capacity factor (F-factor) and the centrifugal acceleration, as shown in Equation (2.7).

$$K_G a = 1.06\ (F_{factor})^{\,2.14}\ (\omega^2\, r_{avg})^{0.51} \quad 2.7$$

In the Equation above $\omega^2 r_{avg}$ is the centrifugal acceleration at the average radius of the packing (r_{avg}) and F_{factor} is the vapor capacity factor calculated by the product of the vapor velocity and the square root of vapor density ($u \cdot \sqrt{\rho_v}$). The last term in the above equation shows the separation efficiency's dependency on the rotational speed.

Hilpert et al. (2022) [12] recently developed a rate-based model for multicomponent distillation in RPBs using MERSHQ methodology (Material balances, Energy balances, Rate equations, Summation equations, Hydraulic equations, and eQuilibrium equations). They modified the existing correlations to capture the maxima in separation efficiency often observed by many authors [11,12]. They used ethanol/n-propanol distillation experiments in an empty and a packed rotor to develop correlations for the volumetric gas-side mass transfer coefficient, $k^V a$, and deaeration of water experiments for the liquid-side mass transfer coefficient, $k^L a$. The developed model is also validated for a ternary system and shows that the model can predict the experimental overall volumetric mass transfer coefficient, $K^V a$, with ±30% error [11].

Table 2.2: List of essential investigations on mass transfer correlations for distillation in RPBs.

Authors	**Chemical system**	**Correlation**	**RPB-type**	**Reference**
Kelleher and Fair (1996)	Cyclohexane + n-heptane	ATU-NTU concept, local k_Ga, overall K_Ga	RPB, metal sponge	[1]
Liu et al. (1996)	Ethanol + water	Film-flow, K_Ga	RPB, random plastic grains	[2]
Li et al. (2008)	Ethanol + water	HETP and HTU-NTU concept	Double RPBs, corrugated discs, wire mesh, wave thread	[4]
Nascimento et al. (2009)	n-hexane + n-heptane	ATU-NTU concept, K_Ga	RPB, Raschig rings, wire mesh	[5]
Mondal et al. (2011)	Methanol + ethanol	HETP concept, K_Ga	Split packing RPB, metal foam	[8]
Hilpert et al. (2021)	Ethanol + n-propanol	K^La and K^va for binary and ternary systems	RPB, metal foam	[11,12]

2.3.4. Measurement Techniques to Understand Mass Transfer in RPBs

Maldistribution between the gas and liquid phases has been a challenge in both conventional columns and RPB. Both equipment types tend to show maldistribution, especially for the liquid phase [79,80]. Since in an RPB the cross-sectional area of the packing increases from the inner to the outer packing diameter, the liquid load decreases throughout the packing, which may result in dewetting of the packing surface in some areas. Therefore, liquid maldistribution along the rotor radius is expected to be responsible for reduced mass transfer performance in RPBs. Several measurement techniques [80,81] have been used to characterize flow and mass transfer in RPBs, which are discussed in the following section.

Liquid Hold-up and Flow Patterns

Burns et al. (1996) [81] conducted a visual study on the liquid flow patterns in an RPB. They concluded that rivulet flow is prominent at low rotational speeds, leading to severe liquid maldistribution. At high rotational speed, the rivulet flow changes to droplet flow, and the onset of film flow is established. The authors [82] later conducted a detailed study using a packing resistance method to measure the liquid hold-up (ϵ_l) at the inner and outer radial positions, and the tracer response technique is used to estimate the hold-up at the middle radial position for varying rotational speeds. They proposed Equation (2.8) for the liquid hold-up.

$$\epsilon_l = 0.039\left(\frac{g}{g_0}\right)^{-0.5}\left(\frac{U}{U_o}\right)^{0.6}\left(\frac{\nu}{\nu_0}\right)^{0.22} \qquad 2.8$$

Where g is the centrifugal acceleration, U is the liquid flow rate per unit area (superfacial velocity), and ν is the kinematic viscosity of the liquid. g_0 (100 ms^{-2}), U_0 (1 cms^{-1}), and ν_0 (1 $x10^{-6}$ m^2s^{-1}) are characteristic values. This equation describes the dependence of liquid hold-up on liquid flow rate, acceleration, and viscosity, with the influence of gas flow assumed negligible. Yang et al. (2015) [83] used a noninvasive X-ray technique to study the hydrodynamics of RPB. They captured time-average tomographic cross-sectional images of the packing under various operating conditions. The authors proposed a correlation to estimate liquid hold-up quantitatively, with most experimental data falling within ±22% of the estimated

values. They found that liquid hold-up increases with liquid flow rate and viscosity, and decreases with increasing rotational speed. Wire mesh and nickel foam packing were tested, and the result was that the foam packing had a higher liquid holdup than the wire mesh packing under the same operating conditions.

Groß et al. (2019) [80] reported Gamma-ray tomography results and concluded that rotational speed affects liquid holdup in the packing. At higher rotational speeds, the liquid holdup decreases rapidly along the radial length of the packing. Not only does the liquid load become smaller, but the strength of the centrifugal field increases linearly with the radial position in the rotor. Furthermore, at the inner diameter of the packing, a liquid ring exists that diminishes almost linearly towards the outer diameter of the packing. Guo et al. (2017) [70] conducted a theoretical study using a three-dimensional simulation in an RPB to understand the liquid flow behavior, droplet size, specific surface area, and residence time. The results show that the particular area of liquid droplets increases, whereas the residence time of liquid in an RPB decreases rapidly with increasing rotational speed. They proposed that increasing the rotational speed or the liquid inlet velocity could help to minimize the liquid maldistribution. Chen et al. (2005) [84] conducted an experimental investigation in an RPB with changing packing radii. They concluded that centrifugal force, liquid load, and end effects may affect the mass transfer coefficient differently at different radial positions in the packed bed. The results showed that the mass transfer coefficient decreases with increasing radial distance in the packed bed due to the decreasing liquid load in the outer packing regions. However, the decrease in mass transfer coefficient may also result from the inlet liquid not being adequately distributed in the outer packing regions. The authors concluded that the end effects might overestimate the mass transfer coefficient at the inner radius of the packed bed. Therefore, one has to be careful when characterizing mass transfer in an RPB using interpretations based on the mass transfer coefficient.

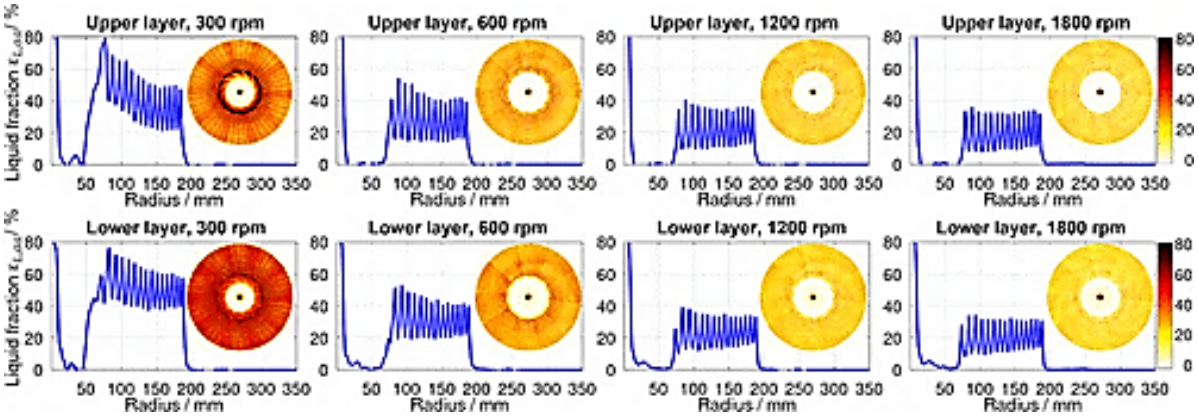

Figure 2.7: Effect of the rotational speed on the angular-averaged radial profiles of the liquid fraction and the liquid fraction distributions in the upper and lower baffle layers of the Zickzack packing in an RPB. The change in liquid hold-up in the packing is indicated by the color change (yellow to black). The lighter the color, the lower the liquid hold-up. (Reprinted/adapted with permission from [85]).

Following conventional packings, Loll et al. (2023) [85] used γ-ray computed tomography (CT) to investigate the liquid distribution in an advanced structured packing, the Zickzack, non-invasively. The Zickzack packing was developed in the scope of this thesis (section 3.4, Figure 3.10) and, in parallel, has been improved by other researchers [85]. They characterized the fluid dynamics of this packing using an air-water system at atmospheric pressure. They found a uniform liquid distribution throughout the packing at rotational speeds above 1200 rpm. In Figure 2.7, the donut represents the packing, and the shift in liquid hold-up with rotational speed (indicated by the color change from dark red or black to yellow) is shown. The liquid hold-up is higher at lower rotational speeds and at the inner side of the packing. However, there are more radial non-uniformities in liquid distribution inside the packing at lower rotational speed.

Mass Transfer Distribution in an RPB

Several measurement techniques are currently employed to characterize the flow conditions in packed columns and RPBs. An overview of recent research on the measurement principles of liquid flow and holdup, and the most essential techniques in an RPB, is provided in the article by Groß et al. (2019) [80]. Despite techniques for investigating flow patterns in an RPB, there

is only limited knowledge of the mass transfer fundamentals within the packing, especially for gas-side-controlled operations such as distillation. A few studies have been published to understand the distribution of mass transfer (aka mass transfer zones) in an RPB. For example, Guo et al. (1997) [55] introduced the concept of three mass transfer zones in an RPB: the end zone, the bulk zone, and the cavity zone, based on a physical absorption process using an oxygen-water system. The end zone comprises the initial few centimeters of the packing on the inner side of the rotor. According to their analysis, the end zone contributes the most to the total mass transfer in an RPB, followed by the bulk zone and cavity zone. Later, Groß et al. (2020) [67] used a slightly modified approach. They defined the surface areas of the rotor, packing, and casing, using the rotor volume as a common reference point. According to their analysis, the empty rotor and casing contribute to the total mass transfer in an RPB, in addition to the packing. They also conducted scale-up experiments to improve mass transfer performance and concluded that the mass transfer coefficient does not increase linearly with increasing radial packing length. Care should be taken while interpreting K_La values for smaller and larger radial packing lengths to avoid overestimating the mass transfer coefficient.

Temperature Measurements in an RPB

Understanding the fundamentals of mass transfer within the packing is essential for developing reliable scaling rules. However, there is hardly any experimental study related to the radial mass transfer distribution inside the packing of an RPB. Our earlier studies (2018) [86] presented a temperature measurement approach that measured casing, vapor inlet, and outlet temperatures to improve understanding of mass-transfer distribution in an RPB. The studies showed that although the overall separation efficiency of an RPB reaches a maximum with increasing rotational speed, the packing's separation efficiency decreases with increasing rotational speed. These studies demonstrated the potential of such a technique and laid the foundation for the wireless temperature measurements inside the rotating packing (telemetry technique) discussed in detail in Chapter 4. The radial temperature profile in the packing can be measured using the rotor telemetry technique. Determining the radial temperature profile for the distillation of a binary system at atmospheric pressure in a packed bed allows estimation of the composition profile, which can be used to calculate the mass transfer along the rotor under various operating conditions. These mass transfer data may help characterize mass transfer in an RPB and develop reliable design and scale-up rules. Similarly, Ressemann et al.

(2023) [87] employed a slightly modified, offline measurement technique and data loggers to measure the radial temperature profile in an RPB. They presented a methodology for analyzing raw data under different assumptions and included the compensations for maldistribution. The analysis divided the whole packing (metal foam) into four regions, including the casing. They characterized the mass transfer in these regions using the number of transfer units (NTU) and the volumetric mass transfer rate. The data showed a greater effect of changing rotational speed on NTU values at the outer radius than at the inner radius of the packing [87].

Chapter 3 Mass Transfer Investigation in RPBs

This chapter outlines the experimental setup and method, preceding the presentation of the mass transfer results for ethanol dehydration in RPBs. The calculation of mass transfer efficiency in terms of the number of theoretical stages is explained, followed by experimental results showing how variations in design and operating parameters affect the separation efficiency of an RPB. Eventually, based on the investigations of conventional RPB packings, an advanced packing design is presented and compared with a traditional distillation column.

Parts of Chapter 3 are published in:

Qammar, H; Hecht, F.; Skiborowski, M; Górak, A.: Experimental Investigation and Design of Rotating Packed Beds for Distillation, Chemical Engineering Transactions, 69, 655-660

https://doi.org/10.3303/CET1869110

Qammar, H; Gładyszewski, K; Górak, A; Skiborowski, M: Towards the Development of Advanced Packing Design for Distillation in Rotating Packed Beds, Chem. Ing. Tech., 2019, 91, 11, 1663 – 1673,

https://doi.org/10.1002/cite.201900053

Qammar, H.: Rotating Packed Beds in Distillation: Binary Distillation, in: M. Skiborowski, A. Górak (Eds.), Process Intensification, De Gruyter, 2022, pp. 159–188.

https://doi.org/10.1515/9783110724998-006

3.1. Materials and Methods

An overview of the experimental setup, details of the RPB used, and different packing types investigated are presented. Furthermore, the experimental procedure, including the method for calculating separation efficiency, the sealing test, and start-up, is described.

3.1.1. Experimental Set-up

Figure 3.1 [43] shows the pilot-scale RPB, with a diameter of 1 m and a height of 1.15 m, used for the experiments within the scope of the investigation. The P&ID for the setup is shown in Appendix A-2, Figure 10.1. This RPB has a maximum rotational speed of 1500 rpm provided by a motor with a maximum power of 2.2 kW [43]. The investigated RPB has one vapor inlet, a vapor outlet, three liquid inlets at the top, and four liquid outlets at the bottom. The simplified flow diagram of the experimental set-up for distillation at total reflux under atmospheric pressure is further shown in Figure 3.2. All experiments are performed at counter-current operation and under total reflux conditions. Nitrogen was introduced into the reboiler as an inert gas to ensure safe operation. The liquid is introduced via three flat fan nozzles (Lechler 686.406, with a 0.79 mm² hole cross-sectional area) with a 90° spray angle and are positioned 120° apart to cover the full inner circumference at the eye of the rotor. A labyrinth seal at the top prevents the vapors from bypassing the rotor, and a liquid seal at the bottom of the rotating shaft prohibits any leakages. PT100 sensors (accuracy class A) are used at the vapor inlet, the vapor outlet, and inside the RPB casing to measure temperature. Two types of conventional packing, namely metal foam and knit mesh, used for the experiments are also shown in Figure 3.1. Based on experience with conventional RPB packings, an advanced Zickzack packing was also developed and is discussed in section 3.4. The design specifications of the investigated RPB, rotor, and packing types, along with their dimensions, are listed in Table 3.1. The metal foam packing, NCX1116, consists of five packing rings that fit together smoothly. This packing is investigated with all five rings and with only two rings, using a rotor with an outer diameter of 400 mm. In Table 3.2, the dimensions of five metal foam rings are mentioned, which are used to determine the effect of radial packing length on the separation efficiency of the RPB. Water-ethanol is used as a test mixture for all the experiments. The dehydration of ethanol is, in fact, one of the most studied chemical systems in RPBs and also one of the standard test mixtures for distillation recommended by Onken and Arlt [88]. The feed mixture, consisting of 10 wt.% ethanol, is charged into the reboiler before each experiment. The reboiler is

electrically heated, with a total heating power of 20 kW and a capacity of 65 l. The reboiler heating duty can be varied between 1 kW and 20 kW. Deionized water (998 kg m^{-3} at 20 ºC) and absolute ethanol (789 kg m^{-3} at 20 ºC) are used to prepare the feed mixture. Density measurements are used to evaluate the composition of the test mixture used. For this purpose, a Densito 30PX by Mettler-Toledo GmbH is used, with a density accuracy of ± 1 kg m^{-3}. The reflux flow rate is measured with a Coriolis flowmeter from SIEMENS, featuring a SITRANS FC300 sensor with a MASS 6000 transmitter, with a flow accuracy of ±0.1% of the rate.

Table 3.1: Overview of RPB dimensions and the properties of internals used in this work.

RPB				
Total height	1100 mm		Outer diameter (OD)	1000 mm
Casing				
Inner diameter	860 mm		Inner height	129 mm
Rotors				
Inner diameter	146 mm		height	10 mm
Rotor-1 OD	400 mm		Rotor-2 OD	600 mm
Packings				
Rotor-1				
Knit mesh	OD_{pack} = 360 mm	ε = 86.6 %,	a_p = 2672 m^2m^{-3}	$Ø_{wire}$ = 0.2 mm
Metal foam, NCX1116	OD_{pack} = 380 mm	ε = 92%,	a_p = 1000 m^2m^{-3}	$Ø_{pore}$ = 1.4 mm
Rotor-2				
Knit mesh	OD_{pack} = 560 mm	ε = 86.3%	a_p = 2748 m^2m^{-3}	$Ø_{wire}$ = 0.2 mm
Zickzack packing	Details in section 3.4			
Distributor				
Flat flan nozzle, 3 nozzles with 1 hole each, 120° apart, 90° spray angle				$Ø_{hole}$ = 1 mm

Table 3.2: Metal foam NCX1116 rings inner and outer diameters

	Ring 1	**Ring 2**	**Ring 3**	**Ring 4**	**Ring 5**
Inner diameter [m]	0.146	0.165	0.200	0.250	0.300
Outer diameter [m]	0.165	0.199	0.250	0.300	0.380

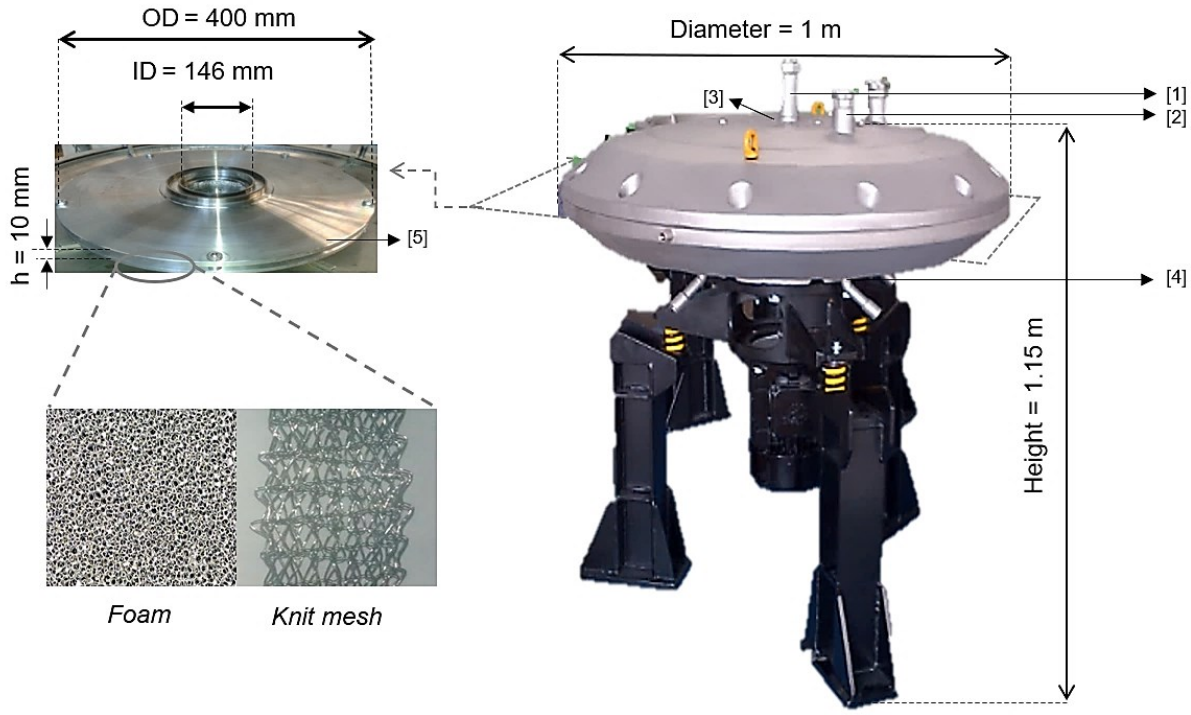

Figure 3.1: Pilot-scale RPB on the right with the rotor shown in an opened casing on the top left and conventional RPB packing types (metal foam and metal knit mesh) on the bottom left. 1: vapor outlet, 2: vapor inlet, 3: liquid inlet, 4: liquid outlet, 5: rotor plate [43].

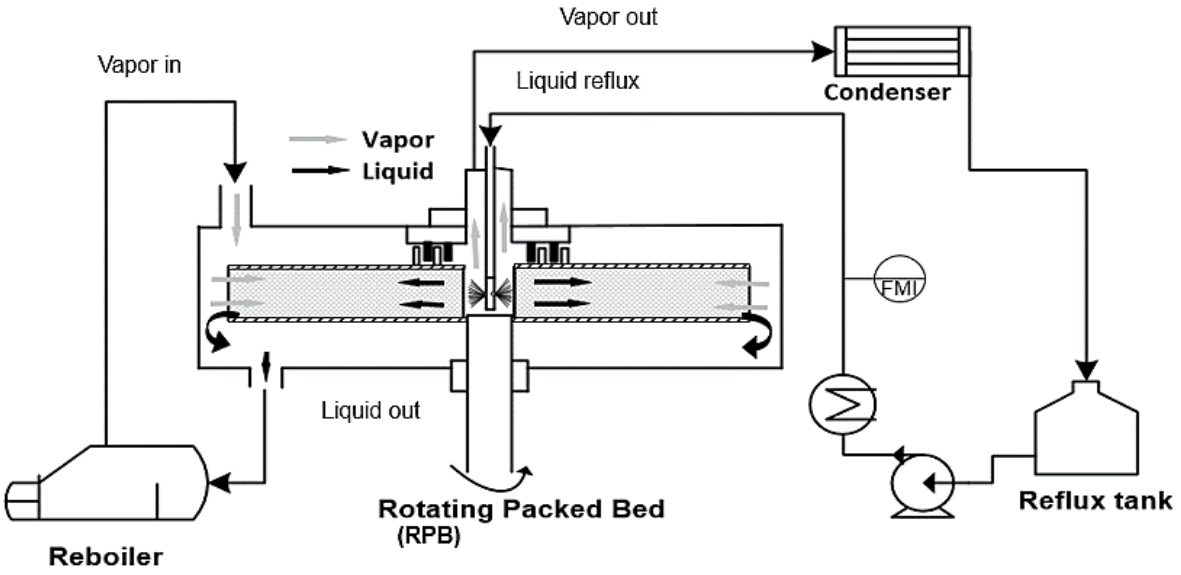

Figure 3.2: Flow scheme of RPB pilot plant under total reflux at atmospheric pressure [43].

3.1.2. Experimental Procedure

A leakage test was conducted before operating the plant with a water-ethanol mixture; it indicates whether all connections, fittings, and devices are adequately sealed. At first, the leakage test is performed with Nitrogen on the pressurized parts. A water-soap mixture is sprayed onto the connections and fittings, and bubbles that form indicate an improperly sealed connection. Afterward, a water/steam leakage test is performed. The testing procedure is similar to the plant's actual operational procedure, except that the medium used is nonhazardous. Therefore, it provides the first experience operating the plant, ensuring it operates safely during investigations involving potentially hazardous chemicals. The following experimental procedure investigates the influence of different design and operational parameters. Firstly, the rotational speed of the RPB was set to a value between 1 s^{-1} and 20 $s^{-1,}$ and a 10 wt.% ethanol-water mixture of approximately 55 kg was pumped into the reboiler. Before starting the reboiler, nitrogen, used as an inert gas, was supplied to ensure safe operation. The electrically heated reboiler was set to a power level that yielded the required F-factor at the eye of the rotor. As the feed mixture boils in the reboiler, a constant stream of vapor is introduced into the RPB through the vapor inlet located at the outer edge of the casing. It flows radially inward through the packing and leaves the RPB through the eye of the rotor.

The vapor stream exiting the RPB was condensed in the overhead condenser, and the condensate was collected in the reflux tank. A constant mass of the liquid in the reflux tank was used to control the pump and ensure operation under total reflux. The liquid reflux flow rate and density were measured online using a Coriolis mass flow meter. Once a steady state was reached, liquid samples were drawn from the liquid reflux, the bottom stream of the RPB, and the reboiler. Steady-state was assumed once the temperature change was less than 0.3 °C and the liquid reflux density change was less than 0.5 kg m^{-3} over 10 minutes. The liquid samples were further analyzed using a Mettler Toledo Densitometer 30 PX. The first steady state is achieved in approximately 2 hours, and it takes approximately 20-30 minutes to attain a new steady state after modifying the rotational speed. Although the extended initial period to reach the steady state is attributed to heat uptake by the solid steel casing of the RPB, the short time to reach the new steady state indicates the RPB's ability to adjust to changes during operation quickly. Each experiment was performed twice. Initially, the rotational speed was increased stepwise from 1 s^{-1} to 20 s^{-1}, and afterward it was reduced stepwise over the same intervals to complete the cycle and examine potential hysteresis effects.

The RPB pilot plant is designed to record (temperature) automatically and control (flow rate) essential measurements using the DAQ system. Communication is via Modbus TCP/IP. The measurement and control scheme for the pilot plant is developed using LabVIEW (Laboratory Virtual Instrument Engineering Workbench) dataflow programming software from National Instruments (NI) Corporation. All essential data is continuously recorded and saved. A picture of the interface showing measured and controlled variables during operation is shown in Appendix A-2, Figure 10.1a.

3.1.3. Measurement of Separation Efficiency

This chapter shows the mass transfer efficiency of distillation in RPB in terms of the number of theoretical stages (Nth) calculated using an analytic description of the vapor-liquid equilibrium (VLE) curve. The general VLE curve of a binary and ideal system can be defined by Equation (3.1), where (x) represents the liquid composition, (α) represents the relative volatility, and y^{eq} shows the equilibrium vapor composition. In the scope of this thesis, the liquid and vapor compositions are estimated in two ways: (1) using the samples collected from

the top and bottom of RPB (used in Chapter 3), and (2) using the temperature measurements at the vapor inlet and outlet of the RPB (used in Chapter 4).

$$y^{eq} = \frac{\alpha\, x}{x(\alpha - 1) + 1} \tag{3.1}$$

In a non-ideal system, relative volatilities change with the liquid composition. In this regard, Li et al. (2014) [40] proposed an empirical approach that correlated the relative volatility of the ethanol-water system with the liquid composition using a composite function in Equation (3.2).

$$\alpha = \begin{cases} 1.1213 \cdot (x + 0.2)^{-1.523} & x \leq 0.292 \\ 0.8938 \cdot (x)^{-1.062} & x > 0.292 \end{cases} \tag{3.2}$$

With the explicit description of the VLE curve, the number of theoretical stages can be calculated together by employing total reflux criteria ($x = y$) iteratively.

3.1.4. Vapor Bypass

There are very limited studies on vapor bypass in RPBs. One of these studies [89] investigated vapor bypass in distillation RPBs by comparing a labyrinth seal (LS) and a floating ring seal (FRS). Their study showed that the LS led to lower separation performance at higher rotational speeds, while the FRS gave nearly constant or improved performance. They interpreted this as evidence that vapor bypass through the LS increases with rotational speed and reduces the measured NTU. Their bypass-detection method was based on temperature measurements at three positions: vapor in the casing, vapor leaving the rotor eye, and vapor leaving the RPB. If the outlet temperature was higher than the rotor-eye temperature, this was interpreted as mixing with bypassed vapor from the casing. Using this method, they calculated relative bypass fractions of 9.2% at 600 rpm and 27.0% at 900 rpm for the LS [89].

However, this conclusion should be interpreted carefully. The study demonstrates that seal design can influence RPB performance, but it does not prove that every maximum in separation efficiency observed in the literature is caused by vapor bypass. The temperature-based method relies on the assumption that the measured temperature difference is caused only by mixing

with bypassed vapor. Other effects, such as local heat generation, heat transfer near the seal, or thermal non-uniformities, may also influence the measured temperature. Therefore, temperature measurements alone are a useful indicator of possible bypass, but they are not a fully independent proof of bypass flow.

Moreover, maxima in separation efficiency have also been reported for other types of rotating packed beds, where the upper rotor plate is stationary and an equivalent upper vapor seal is not required (similar to the concept of RZB) [24,90]. This indicates that such maxima can also originate from hydrodynamic effects inside the rotor, for example, liquid maldistribution, reduced liquid hold-up, or inefficient wetting at high rotational speeds.

Neumann's CO_2 absorption experiments further show that leakage through a labyrinth seal can be negligible under certain operating conditions [91]. Authors compared a labyrinth seal with a hermetic liquid seal and found similar CO_2 capture efficiencies within the experimental uncertainty. This supports the assumption that bypass through a labyrinth seal is not necessarily dominant in all RPB systems [91].

Therefore, for the present work, it is reasonable to assume that vapor bypass through the upper labyrinth seal has no significant influence on the comparative interpretation of the results. Since all experiments were conducted with the same seal configuration, the trends remain internally comparable. Nevertheless, a definitive quantification of vapor bypass would require an independent measurement method, such as tracer experiments, direct flow or pressure drop measurements, or local concentration measurements.

3.2. Influence of Design Parameters

3.2.1. Radial Packing Length (Scale-ability)

Chen et al. (2005) [84] studied the mass transfer efficiency of an RPB with various inner and outer radii. They investigated mass transfer coefficients as a function of liquid flow rate, rotational speed, inner and outer radii of the packed bed, and radial position within the bed during various water-deaeration experiments. Experimental results showed that the liquid side mass transfer coefficient, k_La, increased with increasing rotational speed and liquid flow rate. Furthermore, they correlated the increased k_La at reduced packing volume with the more prominent end effects at the same packing volume. They proposed a predictive equation for k_La that accounts for end effects.

Similarly, Groß et al. [67] evaluated the scale-up of packing in an RPB by deaerating water with nitrogen for two different radial packing lengths. They also showed that increasing the packing volume improves the overall mass transfer coefficient, enabling a specific degassing value to be achieved with a significantly lower rotational speed. However, the k_La value decreases significantly with increasing radial packing length, indicating nonuniform flow along the radial length of the packing. Such a study of distillation is rarely found. Therefore, several experiments were conducted with varying packing lengths to evaluate the effect of increasing packing length on distillation separation efficiency.

An essential question for developing the packing scale-up rules for RPB is the contribution of each radial segment of packing, i.e., whether the entire packing contributes equally to mass transfer. A few practical approaches include experiments with varying radial packing lengths, withdrawing samples at different radial positions of the rotor, using wireless temperature measurements along the radial packing length for a binary test mixture, etc. In the scope of this work, two approaches are used: experiments with varying radial packing lengths, discussed in this section, and rotor telemetry discussed in the next Chapter 4.
To evaluate the effect of increasing packing length on the separation efficiency of distillation, experiments were conducted with the following packing lengths (L_{pack}): 0 m (empty rotor), 0.1 m, 0.125 m, and 0.19 m. Chromium-nickel metal foam NCX1116 by Recemat is used as the packing. The inner radius of the packing is kept constant at 0.073 m while the outer radius is varied as mentioned above. The whole metal foam packing is cut into rings to facilitate the investigation with different packing lengths, as shown in Figure 3.3.

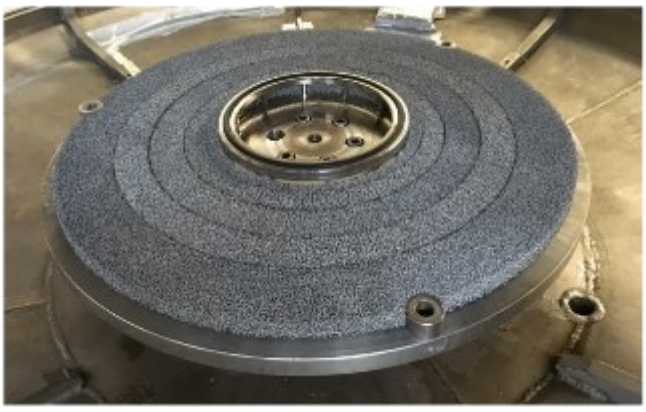

Figure 3.3: Chromium-Nickel metal foam NCX1116 cut into five rings.

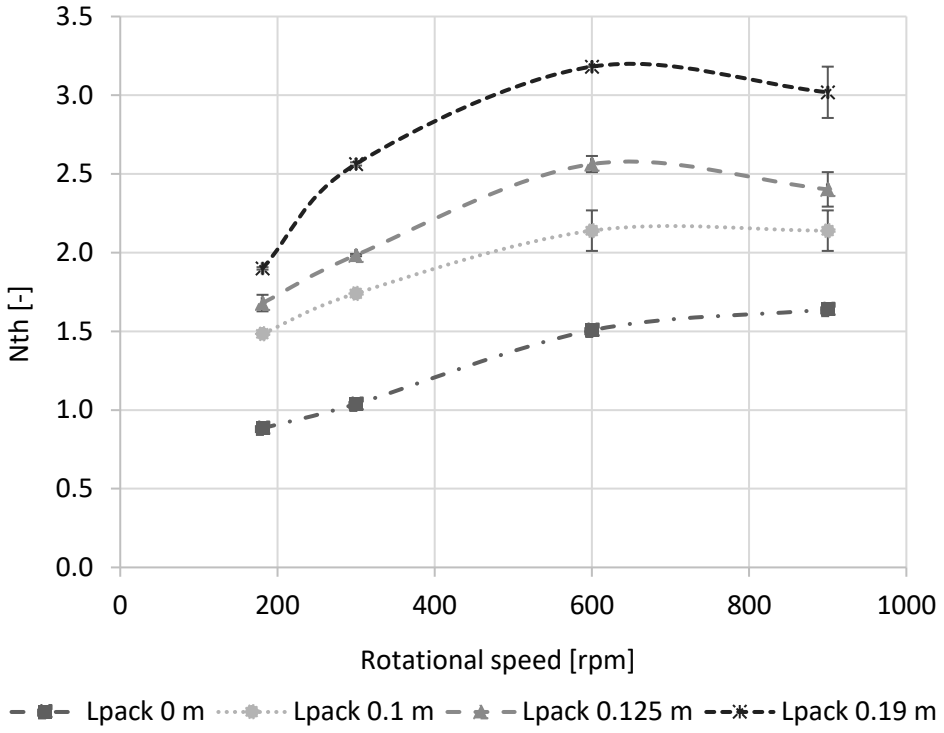

Figure 3.4: Effect of different radial packing lengths on the separation efficiency of metal foam NCX1116 at an F-factor of 2.1 $Pa^{0.5}$ and 400 mm OD rotor [61].

Figure 3.4 shows the total number of theoretical stages achieved in the RPB for different packing lengths. The separation efficiency increases with rotational speed and reaches a maximum for all packing lengths investigated. Furthermore, larger radial packing lengths lead to higher separation efficiencies; the maximum value of about 3.2 theoretical stages is achieved for the full metal foam (L_{pack} 0.19 m) at 600 rpm with flat fan nozzles. Larger radial packing lengths mean larger packing volume inside the rotor, providing a larger surface area for the mass transfer and thereby increasing the overall separation efficiency. Even though mass transfer improves with longer radial packing lengths, it is possible to achieve the same separation efficiency in some cases with less, or even without, packing by increasing the rotational speed. For example, in Figure 3.4, the separation efficiency of 1.5 theoretical stages can be achieved with each rotor configuration at different rotational speeds. For a radial packing length of 0.19 m, this efficiency can be achieved at a rotational speed of about 100 rpm; for the smaller radial packing length of 0.1 m, the required rotational speed is around 200 rpm,

whereas for the empty rotor, a speed of 600 rpm is needed. These results also demonstrate one of RPB's promising advantages: its operational flexibility. The results indicate that, in some rotor configurations, the same separation efficiency can be achieved with a small amount of packing by spinning faster.

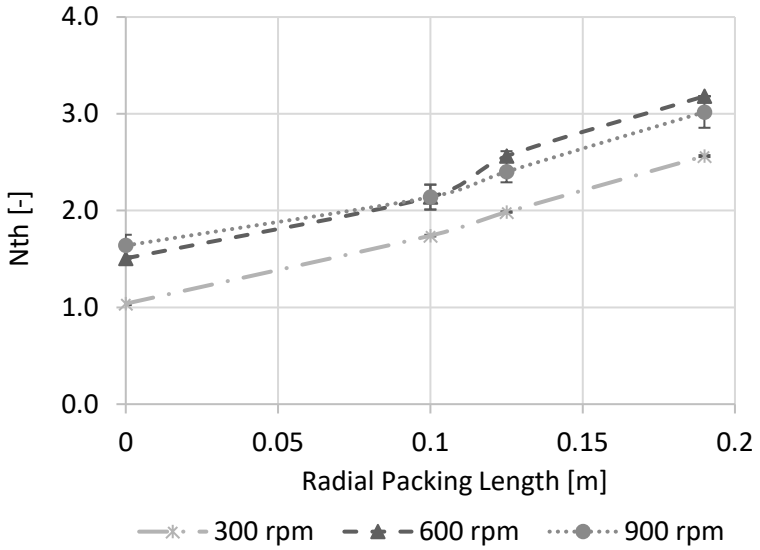

Figure 3.5: Dependence of the number of theoretical stages on radial packing length at different rotational speeds for a 400 mm OD rotor at an F-factor of 2.1 $Pa^{0.5}$

Figure 3.5 illustrates how the radial packing length affects the separation efficiency at 600 rpm. Adding the packing to an empty rotor improves the separation efficiency by 40%. Moreover, increasing the packing length by almost 100% further improves the number of theoretical stages by 50%, i.e., with a radial packing length of 0.1 m, 2.1 Nth are achieved. With a radial packing length of 0.19 m, almost 3.2 Nth is achieved. Similarly, suppose a similar evaluation is done at 300 rpm. In that case, the results indicate that the inner few centimeters of the packing contribute more effectively to overall mass transfer, and at higher rotational speed (e.g., 600 rpm), the outer area of the packing is more effective for separation. On the one hand, increasing the radial packing length, increasing the cross-sectional area, decreasing the liquid load, and non-uniform liquid distribution seem to make the outer part of the packing less effective than expected [80]. On the other hand, the initial liquid accumulation and deceleration of liquid at the inner side of the packing, especially at higher rotational speed, might be the reason for poor packing performance. There is room to improve the packing design to prevent loss of separation

performance due to liquid maldistribution throughout the packing, as also addressed in Section 3.4.

3.2.2. Effect of Rotor Diameter

To understand the fundamentals of mass transfer in a conventional RPB packing, experiments were conducted with and without packing at two rotor diameters (400 mm and 600 mm) and at varying rotational speeds. Figure 3.6 shows the results of separation efficiency for Rotor-1 (400 mm) and Rotor-2 (600 mm) for knit mesh packing and empty rotor at an F-factor of 2.8 $Pa^{0.5}$. In the case of an empty rotor, increasing the rotor diameter leads to two further effects, i.e.,

a. increase in the rotor geometrical surface area for mass transfer,

b. reduction in the cavity zone area.

The cavity zone is the area between the outer edge of the rotor plates and the casing wall. For an empty rotor, the cavity zone area reduces by almost 15% for Rotor-2; however, the increase in the packing zone area is much higher (c.f. Table 3.4), therefore, the overall separation efficiency of Rotor-2 is almost one theoretical stage higher than Rotor-1. The better separation is expected to come from the larger surface area since the Rotor-2 has nearly 2.4 times the geometrical surface area as Rotor-1 (c.f. Table 3.4) and shows a separation improvement in terms of Nth of 36 – 83% depending on the rotational speed. Similarly, increasing the rotor diameter in the case of knit-mesh packing is expected to have a similar effect. The larger rotor diameters provide larger packing surface areas for mass transfer; therefore, Rotor-2 has also shown better separation, as shown in Figure 3.6 (right). For knit mesh packing, Rotor-2 provides almost 3 times more packing surface area (c.f. Table 3.3) than Rotor-1; however, the improvement in the Nth values is only up to 39% at an F-factor of 2.1 $Pa^{0.5}$ and approx. 16% at an F-factor of 2.8 $Pa^{0.5}$ shows that simply increasing the rotor length of conventional RPB packings does not necessarily increase the separation efficiency proportionally. The effect is more pronounced with knit mesh packing, most likely due to non-uniform winding, indicating the need for a uniform packing design rather than simply increasing packing volume to achieve higher separation efficiencies. Moreover, mass transfer results from small-scale RPB experiments must be used with caution when extrapolated to large-scale units.

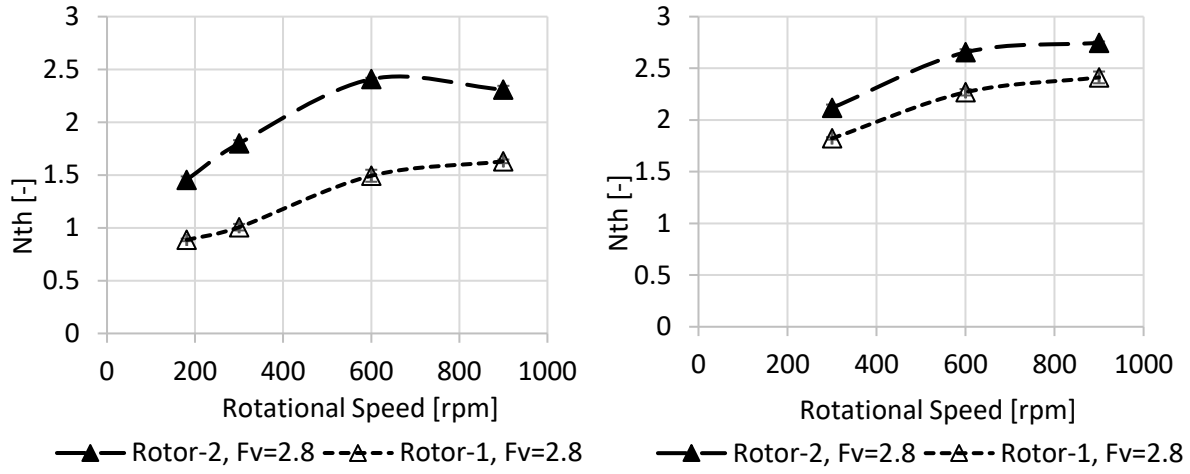

Figure 3.6: Effect of rotor outer diameter on the separation efficiency of RPB with empty rotor (left) and knit mesh packing (right).

The separation efficiency of the empty rotor is better than expected compared to the packed rotor, most likely because the inner support ring atomizes the liquid jets into tiny droplets, further increasing the surface area. Although atomization cannot be estimated readily, it is logical to assume that the influence will be more substantial without packing due to the extended free path length. However, in a packed rotor, the droplets will accumulate at the inner packing surface. As the packing surface area and vapor-liquid loads change nonuniformly along the radial length of the rotor, the additional surface area resulting from an increased rotor diameter cannot be used effectively. As with conventional columns, a redistribution of the liquid may improve separation efficiency. A detailed assessment of the packing performance along the radial packing length for empty and packed rotors is described in Chapter 4.

Table 3.3: Estimated geometrical surface area of the rotors, packing, and casing of the RPB investigated.

	Geometrical surface area (m^2)		
	Rotor (R)	Casing* (C)	Packing (P)
	$2\pi\ ({r_o}^2 - {r_i}^2)$	$\frac{3}{2}\pi\ {r_c}^2 + 2\pi r_c h_c$	$2\pi\ ({r_{o,p}}^2 - {r_{i,p}}^2) h_p a_p$
Rotor-1	0.11	1.16	2.27
Rotor-2	0.27	1.16	6.31

*The casing of the RPB investigated is a non-standard shape; therefore, a combination of two standard shapes is used to estimate the geometrical surface area of the casing. Details are given in Appendix A-3, Figure 10.2.

Table 3.4: Characterization of the geometrical surface area of the RPB investigated.

Zones of RPB and geometrical surface area (m^2)			
	Cavity Zone (C – R)	Packing Zone (P + R)	
		Empty rotor	Packed rotor
Rotor-1	1.05	0.11	2.38
Rotor-2	0.896	0.27	6.58

3.2.3. Effect of Packing Type

Two packing types (foam and knit mesh) were compared at two F-factors in the RPB, based on their estimated theoretical number of stages (Nth). As apparent from the illustration of the number of theoretical stages in Figure 3.7, the metal foam performs better at higher F-factors than the knit mesh. Nth values for both packing types are in a similar range, with Nth about 1 higher for an F-factor of 2.8 $Pa^{0.5}$, comparing metal foam to mesh. Both packing types show an increase in the Nth values with increasing rotational speed, before they start to decrease or remain constant at around 600 rpm, depending on the F-factor. This increase is qualitatively consistent with publications [11,90] that reported counter-current deaeration and distillation, respectively. Although knit mesh has a higher specific surface area (Table 3.1) than metal foam, the non-uniformities arising while winding the mesh onto the rotor seem to cause the non-uniformities in the liquid distribution. Handling of knit mesh is more difficult than the metal foam packing since knit mesh packing has to be wound on the inner support ring manually, which might introduce some non-uniformities due to slight variations in the winding force, which might be pronounced with increasing diameter of the rotor, and hence resulting in separation efficiency loss.

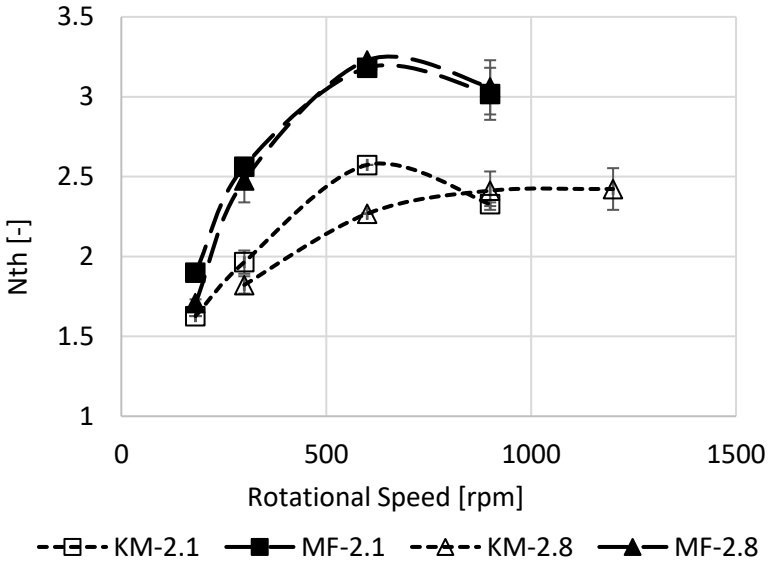

Figure 3.7: Comparison of knit mesh (KM) separation efficiency and metal foam (MF) packing. Rotor-1, F-factor, Fv = 2.1 $Pa^{0.5}$ and 2.8 $Pa^{0.5}$. Details of packing properties are given in Table 3.1. Error bars represent the standard deviation.

3.3. Influence of Operating Parameters

3.3.1. Rotational Speed and Vapor Load (Operating ranges)

The distillation operation limits of RPBs are shown in the following section. It is important to note that the limits depend on various factors, like distributor type, packing type, and rotational speed. The operational limit investigated for a particular setup may not be applicable to other setups/internals [66]. In the current study, the investigated setups are shown in Table 3.5, and the results are displayed in Figure 3.8.

Table 3.5: Investigated set-ups for the distillation operation limits in RPB

Rotor	Packing type	Distributor	F-factor [$Pa^{0.5}$]
Rotor-1	Metal foam (MF)	Flat fan nozzles 406 (Lechler)	1.2, 2.1, 2.8
	Knit mesh (KM)	Flat fan nozzles 406 (Lechler)	1.2, 2.1, 2.8
Rotor-2	Knit mesh	Flat fan nozzles 406 (Lechler)	1.2, 2.1, 2.8

An optimum rotational speed is required for each F-factor investigated to achieve maximum separation efficiency under the given conditions. More intense vapor-liquid contact is needed to process higher vapor-liquid loads in an RPB at a given separation efficiency, which can be achieved by increasing the rotational speed. As shown in Figure 3.8, the higher the F-factor, the higher the optimum rotational speed, after which the separation efficiency is either constant or slightly decreases with further increase in rotational speed [53]. For example, for an F-factor of 2.1 $Pa^{0.5}$, a rotational speed of 600 rpm is needed for both metal foam packing and knit mesh packing to achieve maximum separation efficiency under the given operating conditions. For an F-factor of 1.2 $Pa^{0.5}$, a rotational speed of 300 rpm is sufficient, as further increasing it does not improve separation [11,53]. Furthermore, in the investigated experimental set-up, flooding was observed for knit-mesh packing at F-factors of 1.2 $Pa^{0.5}$ for rotational speeds < 100 rpm and 2.1 $Pa^{0.5}$ and 2.8 $Pa^{0.5}$ for rotational speeds < 200 rpm. Knit mesh performs better at lower

vapor-liquid loads, while metal foam provides higher separation at higher vapor-liquid loads at a constant rotational speed.

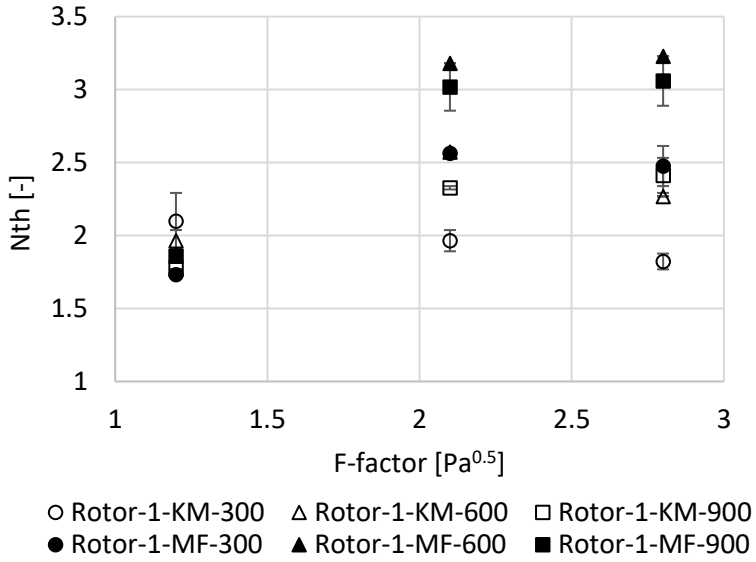

Figure 3.8: Operational ranges of RPB packed with knit mesh (KM) and metal foam (MF) packing. 300, 600, and 900 represent the rotational speed (rpm). Rotor-1: 400 mm outer diameter, 10 mm axial height.

Comparing the operational limits of Rotor-1 (Figure 3.8) and Rotor-2 (Figure 3.9), it can be concluded that for the smaller Rotor-1 (OD = 400 mm), changing the vapor-liquid loads immediately demands a change of the rotational speed; however, Rotor-2 (OD = 600 mm) can maintain the separation efficiency for a broader range of vapor-liquid loads at the same rotational speed. The larger radial dimension provides a greater effective contact area and a longer flow path, resulting in a more gradual variation of local fluid velocities and centrifugal acceleration. Consequently, increasing the rotor diameter improves operational flexibility and reduces the coupling between throughput and rotational speed. The broader operating envelope observed for Rotor-2 indicates a lower sensitivity of separation efficiency to variations in vapor and liquid loads, thereby enhancing process robustness. This behavior is particularly advantageous for scale-up and industrial applications, where feed rates are often subject to fluctuations and stable operation over a wide operating range is desired.

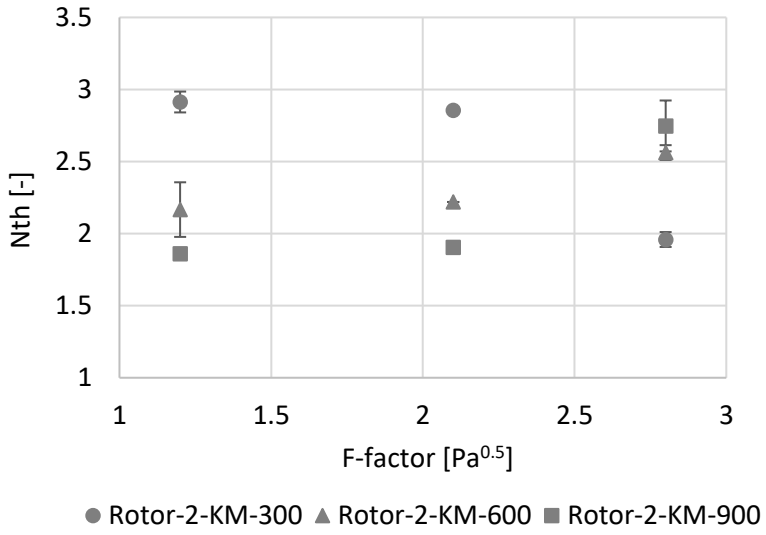

Figure 3.9: Operational ranges of RPB packed with knit mesh (KM) packing. 300, 600, and 900 represent the rotational speed (rpm). Rotor-2: 600 mm outer diameter, 10 mm axial height.

In conventional RPB packings such as metal foam and knit mesh, non-homogeneous liquid distribution and nonlinear changes in fluid loading with radius make scale-up of the packing very challenging. Therefore, based on experience gained from testing conventional RPB packings and to facilitate the scale-up of RPB packing, a new packing is developed and presented in the following section.

3.4. Development of Zickzack Packing Design

The concept of Zickzack (ZZ) packing was developed by combining the RZB structure with a single-block packing. The packing design is developed to provide uniform liquid distribution and better wetting conditions, especially on the outer side of the packing, compared to conventional RPB packings, such as foams and wire meshes.

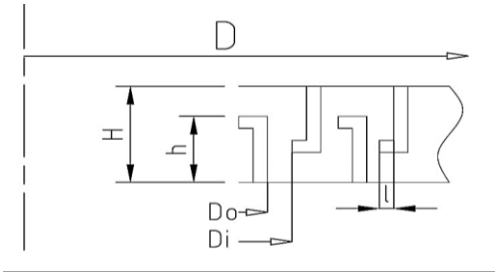

Figure 3.10: Zickzack packing cross-section sketch.

The initial design of the ZZ packing is illustrated in cross-section in Figure 3.10 and Figure 3.11. Like the RZB, the Zickzack packing enforces a zig-zag path of the gas and the liquid through the rotor, resulting in a higher liquid hold-up for gas-liquid contacting. However, unlike the RZB, in which the upper baffles are fixed to the static disc, while the lower baffles are mounted to the rotating disc, Zickzack packing is rotating at the same angular speed. Furthermore, the baffles in each stage have no holes (perforations in the vertical wall as described by Wang et al. [27]), so the liquid is transferred between stages by overflow. A horizontal protrusion on the top of each stage is introduced as an additional feature to maintain a minimum hold-up on the different stages. The total holdup can be calculated as the sum of the minimum holdup and the volume contributed by liquid curvature, depending on the rotational speed. However, as described by Lubarda (2013) [92], the curvature will flatten to a point where it can be neglected under the condition that the rotation-induced Bond number, Equation (3.3)

$$\mathrm{Bo}_{\omega} = \frac{\rho_l D^3 \omega^2}{8\sigma_{lv}} > 20. \qquad 3.3$$

Where Bo is the bond number, ρ_l is the liquid density, ω is the angular speed, D is the radial length, σ_{lv} is the vapor-liquid surface tension. Another essential feature of the Zickzack design is that the structure can be tailored to keep the F-factor almost constant, counteracting mass transfer performance loss with increasing packing radius. Therefore, the distance between consecutive baffles is adjusted to preserve the same free cross-sectional area. The corresponding positions of the baffles can be determined by Equation (3.4), in which Do_j is the outer diameter of baffle j and Di_{j+1} is the inner diameter of the next baffle. A tailored packing

structure can be designed for a wide range of flow rates, enabling operation under optimal conditions.

$$\frac{\left(\mathrm{Do}_{j+1}^2 - \mathrm{Di}_j^2\right) \cdot \pi}{4} = \mathrm{const.} \qquad 3.4$$

For the current study, two prototype packing structures with an inner diameter of 146 mm, an outer diameter of 356 mm, and a height of 8 mm have been designed, differing in free cross-sectional area and thus in the number of baffles (Table 3.6). It is important to note that for RZB and ZZ packing, the F-factor can be defined in two ways: (1) F-factor at the eye of the rotor, ($F_{eye,}$ = F-factor used in this chapter), and (2) F-factor at the free cross-sectional area between two adjacent baffles, $F_{packing}$. These F-factors can be estimated using Equations (3.5) and (3.6) respectively. F_{eye} is calculated based on the cylindrical surface area ($A_c = 2\pi r_i h$) at the inner radius of the rotor (aka eye of the rotor) and $F_{packing}$ is calculated based on the free cross-sectional area between the two adjacent baffles ($A_{free} = \pi \cdot ({r_{o,j}}^2 - {r_{i,j+1}}^2$). $\rho_{v,out}$is the vapor density and $\dot{m}_{v,out}$is the vapor mass flow rate at the vapor outlet of the RPB.

$$\mathrm{F}_{eye} = \mathrm{F-factor} = \frac{\dot{\mathrm{m}}_{\mathrm{v,out}}}{\rho_{\mathrm{v,out}}\, \mathrm{A_c}} \sqrt{\rho_{\mathrm{v,out}}} \qquad 3.5$$

$$\mathrm{F}_{packing} = \frac{\dot{\mathrm{m}}_{\mathrm{v,out}}}{\rho_{\mathrm{v,out}}\, \mathrm{A_{free}}} \sqrt{\rho_{\mathrm{v,out}}} \qquad 3.6$$

These packing designs were produced using a previously developed additive manufacturing approach [93], as classical subtractive manufacturing methods cannot be readily applied. In contrast to the previously applied Direct Light Processing (DLP) approach, a stereolithography (SLA) printer was used to employ another photopolymerization process. Here, a photosensitive liquid polymer (resin) is selectively exposed to UV laser light to form a very thin solid layer upon layer (usually 0.05-0.15 mm thick) to create the 3D part. The most important advantages of SLA over DLP are its larger build size, the smooth surface of the printed object, and the large variety of photopolymers. In this study, the packing was fabricated on a Formlabs 3D printer (Form 2) with a build size of 150×150×200 mm^3. The layer thickness was set to 0.1 mm per the manufacturer's recommendations, and Formlabs Hi-temp resin was selected, which has a deflection temperature of up to 238 °and moderate chemical resistance [94]. Since the build size is still not large enough to manufacture the packing in one piece, it was divided into 9

pieces and bonded with Technicoll 9464 2-component epoxy adhesive, resistant to high temperatures and alcohols [95].

Table 3.6: Zickzack packing basic parameters

	Zickzack 25	**Zickzack 38**
Baffle height - h_b [mm]	5.5	5.5
Protrusion length – l [mm]	1	1
Free cross-sectional area – A_{free} [mm^2]	1888.6	1401.4
Number of baffles [-]	25	38
Radial packing length – r_o - r_i [mm]	105	105
F-factor at the eye - F_{eye} [$Pa^{0.5}$]	0.6	0.6
F-factor annular packing space - $F_{packing}$ [$Pa^{0.5}$]*	1.6	2.1

Figure 3.11 illustrates the CAD model of a single packing piece with 38 baffles and the annular packing obtained by combining the nine single elements. To improve the mechanical stability of the packing, 72 radial rods and 186 vertical rods were added inside the structure. Further cut-outs on the sides are integrated to position and interlock adjacent pieces.

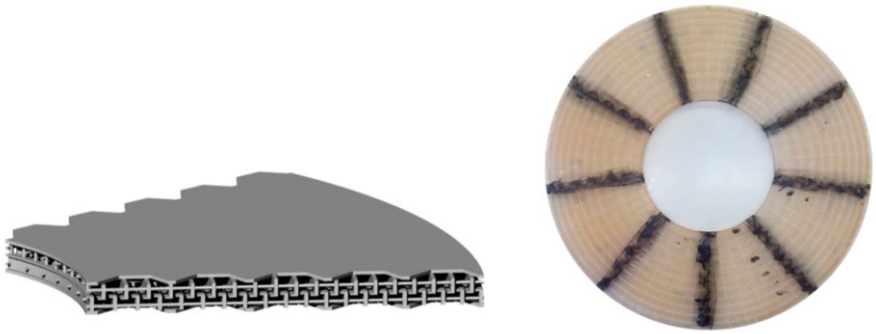

Figure 3.11: CAD model of the Zickzack packing piece and a photo of the bonded ZZ packing.

3.4.1. Performance Evaluation of the Advanced Zickzack Packing Design

The same experimental procedure was used to test the performance of the Zickzack packing as used for knit mesh and metal foams. While there are many design possibilities for Zickzack packing, the performance of two variants, ZZ-25 and ZZ-38, is initially evaluated. As given in Table 3.6, ZZ-25 has almost 25 baffles, and ZZ-38 has 38 baffles. Figure 3.12 shows that ZZ-25 provided better mass transfer performance, which is attributed to its larger free cross-sectional area for vapor-liquid contacting. A narrower annular gap in ZZ-38 leads to higher velocity and F-factor (Table 3.6). These results agree with the literature on RZB [96] and other classical packings [1], which show that increasing the F-factor beyond a specific value leads to poorer performance [96].

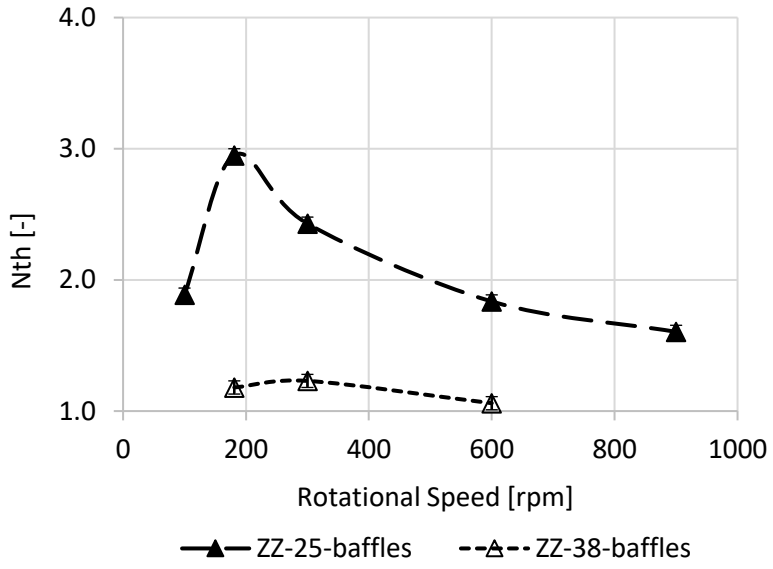

Figure 3.12: Mass transfer of two versions of Zick-Zack packing (ZZ-38) and ZZ-25; Rotor-2, F-factor = 0.6 $Pa^{0.5}$ [43].

A comparison of the hydrodynamic and mass transfer performance of ZZ-25 packing and knit mesh is shown in Figure 3.13. During the development of Zickzack packing, the available reboiler could provide a maximum F-factor of 0.6 $Pa^{0.5,}$ and at this F-factor, knit mesh packing showed better mass transfer performance compared to metal foam packing (Appendix A-4, Figure 10.3); therefore, knit mesh is used for comparing the performance of ZZ packing. The slightly superior mass transfer performance of the ZZ packing might be associated with its

more homogeneous hydrodynamics. The mass transfer inside the ZZ packing is further analyzed based on the temperature measurements described in Chapter 4 [86]. It should be noted that the results shown in Figure 3.12 and Figure 3.13 were obtained using the initial ZZ packing described by Qammar et al. (2019) [43]. The improved design by Loll et al. (2022) [48] might have achieved higher performance by avoiding liquid and gas bypasses in the spaces between the packing and rotor walls. Nevertheless, the results indicate that ZZ packing has the potential to provide more uniform hydrodynamic and mass transfer conditions than conventional packing types. Kruber et al. (2020) proposed an optimization-based design methodology for RPBs with Zickzack packing, combining a superstructure approach with an equilibrium-stage model. The framework provides a suitable basis for future optimization of Zickzack packing geometries and RPB design through improved hydrodynamic and mass transfer models [97].

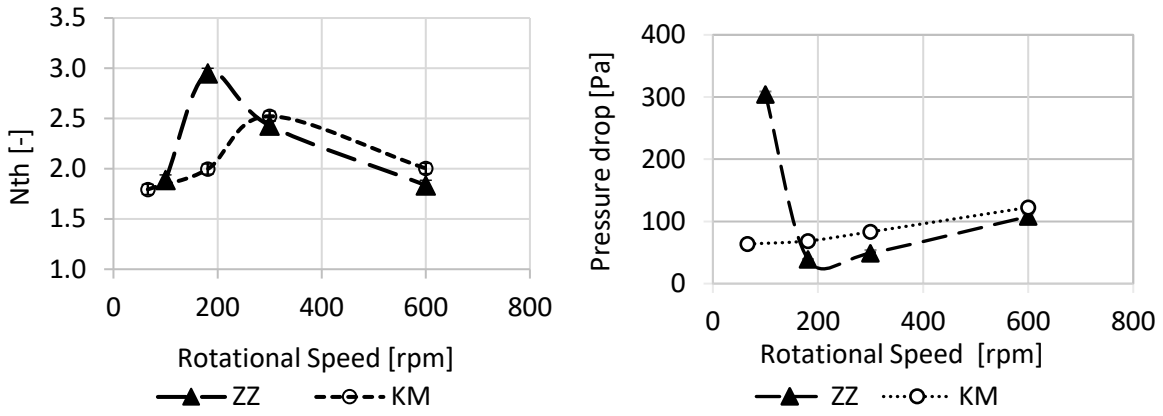

Figure 3.13: Mass transfer and hydrodynamic comparison of Zick-Zack (ZZ-38) packing with knit mesh (KM); Rotor-2, F-factor = 0.6 $Pa^{0.5}$ [43].

3.4.2. Comparison with Reported Literature

In light of the preceding analysis, the experimentally determined separation performance is further examined, along with the reported literature results for distillation experiments with similar systems and different types of packing. Table 3.7 lists the design and operation specifications of the investigated split packing and RZB. Based on the reported data, the maximum separation efficiency at F_{eye} of 0.6 $Pa^{0.5}$ (equivalent to $F_{packing}$ = 1.6 $Pa^{0.5}$) was selected as a reference for comparison since separation efficiency is a function of rotational

speed. For RZB, Wang et al. (2019) [96] investigated mass transfer and hydrodynamic performance of eleven different baffle structures for ethanol dehydration in RZB. Among these baffle design options, data at a $F_{packing}$ of 1.6 $Pa^{0.5}$ are available for three baffle structures: R-3, R-8, and R-9. R-3 is a standard baffle structure for RZB, whereas R-8 and R-9 are advanced forms of baffle structures with a few layers of metal gauze packing mounted on the baffle. R-3 and R-9 are chosen for comparison, as R-3 is the characteristic baffle design of an RZB and, among the advanced baffle designs, R-9 shows better mass transfer performance [96].

Similar to a conventional column, the ATU-NTU concept (section 2.3.3) can be used to compare and evaluate the separation efficiency of conventional RPB packing, which incorporates a non-constant cross-sectional area of the packing along the rotor. However, in the case of RZB and ZZ packing, the HETP concept can also be used for comparison, as the baffles are designed to keep the area between adjacent baffles constant. As already shown, the empty rotor and casing also contribute to the mass transfer in an RPB (Figure 3.4); therefore, besides the HETP value that is based on the reported separation efficiency for the respective RPB, a refined HETP value is determined that considers a maximum casing contribution equivalent to one theoretical stage for the reported mass transfer results and is calculated according to Equation (3.7)

$$\mathrm{HETP\_refined} = \frac{(r_o - r_i)_{packing}}{N_{th} - 1}. \qquad 3.7$$

The comparison of the HETP values resulting from the current study (based on N_{th} in Figure 3.13) and the literature data (Table 3.7) is illustrated in Figure 3.14. From Figure 3.13, the maximum Nth value for ZZ packing is 2.95. Excluding the casing contribution, using Equation (3.6), an HETP value of 5.3 cm is found for the Zickzack packing. As RZB is widely used for continuous distillation in Asia and has several reported advantages (section 2.2.2), it is reasonable to compare ZZ packing with RZB. As shown in Figure 3.14, the performance of ZZ packing is comparable to that of the two RZB variants mentioned. Although pressure drop is not the focus of this study, for comparison, the pressure drop of the above-mentioned RZB variants varies from approximately 138 Pa to 158 Pa per theoretical stage [96], and the pressure drop of ZZ packing is approximately 14 Pa per theoretical stage (Figure 3.12, right). Thus, the

initial experimental results for the Zickzack packing indicate that a separation efficiency comparable to that of an RZB can be obtained at a significantly reduced pressure drop.

Table 3.7: Design and operation specifications of the compared packing (split packing, metal foam) and rotor types (RZB).

Reference	Packing Specifications	Test system conditions	F-factor [$Pa^{0.5}$]	HETP [m]
Mondal et al., 2011 (Split Packing) [8]	d_i = 0.6 m; d_o = 0.31 m h = 0.027 m a_p = 280 $m^2 m^{-3}$	Methanol-ethanol Total reflux 101.325 kPa	0.36 – 0.6 (F_{eye})	0.029 – 0.15
Wang et al., 2019 (RZB) [96]	d_i = 0.11 m; d_o = 0.28 m h = 0.06 m; Rotor R-3, R-9	Ethanol-water Total reflux 101.325 kPa	0.4 – 3.6 ($F_{packing}$)	0.028 – 0.08

Note: Values are estimated from the reported literature data [1,8,96]

3.5. Comparison with Conventional Column

Traditionally, conventional distillation columns have been used in industry for at least two centuries; it would be reasonable to compare the performance of the RPB with that of a conventional column to illustrate better the advantages offered by RPB and RZB. To compare the resulting HETP values with conventional column data, a random packing, a Raschig super ring metal (RSRM), and an industrially used structured packing, HOLPACK, taken from Darakchiev and Semkov (2008), are considered [98]. The experimental data originate from the binary distillation of an ethanol-water mixture under total reflux conditions in a column with an inner diameter of 0.213 m and a packing height of 2.8 m [98]. As shown in Figure 3.14, a

reduction in the HETP value of 4 – 10 fold can be achieved with an RPB under the investigated operating conditions. Moreover, the packing volume required in the RPB or RZB would be much lower than that in the column [27,28], which opens the possibility of using specialized packing for certain processes despite its high cost. Considering the initially proposed potential for process intensification, quantified by Ramshaw and Mallinson (1983) [50] as a reduction of 10– 100-fold in HETP, it has to be concluded that the current and literature results are relatively close to the lower end of this ambitious range [1,8,22,96]. Based on the literature, split packing and RZB can achieve a reduction of 7 – 10 fold in HETP compared to conventional packed columns [22,98].

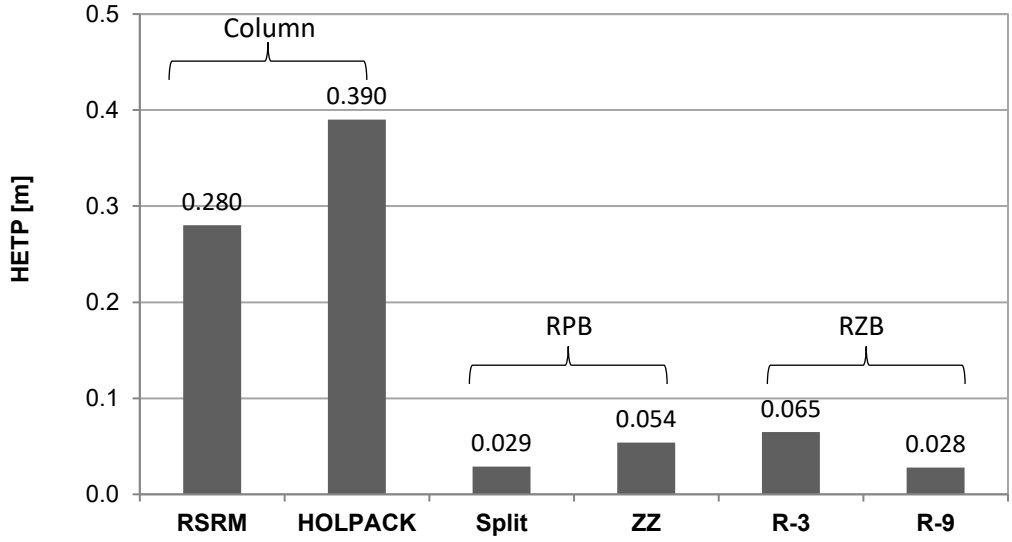

Figure 3.14: Comparison of HETP values of the conventional distillation column with different packing and rotor types of an RPB/RZB; F-factor = 0.6 $Pa^{0.5}$ and $F_{packing}$ = 1.6 $Pa^{0.5}$. ZZ is the Zickzack packing for RPBs, and R-3 and R-9 are rotor variants for RZB [43]. The test mixture is ethanol-water for the column, ZZ, R-3, and R-9, and methanol-ethanol for split packing. Equation (3.6) calculates the HETP values for RPB and RZB.

3.6. Summary

In this chapter, results of an experimental approach for the development of packing design for distillation operation in RPBs are presented, where initially the properties and mass transfer performance of different conventional RPB packings are compared under varying operational

and design parameters in a single-rotor RPB under total reflux conditions. Analysis of the experimental results shows the limitations of conventional RPB packings, such as poor liquid distribution and varying vapor-liquid loadings throughout the packing. Based on these insights, a more uniform packing is developed, tested, and compared with conventional RPB packings and distillation columns for the ethanol-water test system. Important insights from the chapter are given below.

The detailed analysis of mass transfer contributions in the packing and casing shows a clear need to differentiate them for reliable quantification of the overall RPB performance. Metal foam packings provide superior handling compared to knitted mesh due to their rigid form. Furthermore, it is shown that liquid dispersion within a rotating empty rotor can significantly contribute to the mass transfer rate. However, the additional surface area provided by the metal foam packing further increases the Nth value. The scale-up in terms of improved mass transfer performance has also been further evaluated through investigations of varying radial packing lengths. It was shown that the increased packing volume associated with the larger radial packing length improves overall mass transfer to a limited extent, underscoring the need for packing design improvements or liquid redistribution. The newly developed Zickzack packing provides comparable separation efficiency to RZB with about 10 times lower pressure drop and has the potential to reduce the HETP value by approximately 7-fold compared to conventional packed columns. Yet, there is significant potential to optimize the Zickzack packing design by modifying the packing height, baffles, and weir, as well as their geometries. It is also important to evaluate mass transfer performance at larger radial depths and vapor and liquid flow rates, which is essential for providing reliable data for process and equipment design.

Chapter 4 Temperature Profile Investigations in RPBs

Previously, different design variations of conventional RPB packings were used (e.g., varying the radial packing length and without packing) to estimate the mass transfer contribution of the packing. This chapter presents a novel temperature measurement technique that enables assessment of the packing temperature profile and separation performance without altering the packing design. Investigating the temperature profile in an RPB poses many challenges compared to conventional columns, due to the rotating parts. This chapter presents the details of the telemetry setup, the experimental results achieved, and the challenges.

Parts of Chapter 4 are Published in:

U. Hampel, M. Schubert, A. Döß, J. Sohr, V. Vishwakarma, J.-U. Repke, S.J. Gerke, H. Leuner, M. Rädle, V. Kapoustina, L. Schmitt, M. Grünewald, J.H. Brinkmann, D. Plate, E.Y. Kenig, N. Lutters, L. Bolenz, F. Buckmann, D. Toye, W. Arlt, T. Linder, R. Hoffmann, H. Klein, S. Rehfeldt, T. Winkler, H.-J. Bart, D. Wirz, J. Schulz, S. Scholl, W. Augustin, K. Jasch, F. Schlüter, N. Schwerdtfeger, S. Jahnke, A. Jupke, C. Kabatnik, A.S. Braeuer, M. D'Auria, T. Runowski, M.F. Casal, K. Becker, A.-L. David, A. Górak, M. Skiborowski, K. Groß, **H. Qammar**, Recent Advances in Experimental Techniques for Flow and Mass Transfer Analyses in Thermal Separation Systems, Chem. Ing. Tech. 92 (2020) 926–948. https://doi.org/10.1002/cite.202000076

Qammar, H.: Rotating Packed Beds in Distillation: Binary Distillation, in: M. Skiborowski, A. Górak (Eds.), Process Intensification, De Gruyter, 2022, pp. 159–188. https://doi.org/10.1515/9783110724998-006

H. Qammar, T. Pyka, J. Koop, A. Górak, G. Schembecker, Radial Temperature Profile Measurements to Understand Mass Transfer in Rotating Packed Bed Distillation, Ind. Eng. Chem. Res. (2023).

https://doi.org/10.1021/acs.iecr.3c01068

4.1. Fundamentals

Temperature profiles provide helpful information in interpreting the operation of distillation columns. Conventional distillation column temperature profiles (Figure 4.1) can be measured relatively easily and are often considered suitable tools for estimating separation and troubleshooting distillation columns [99]. Similarly, temperature data from the rotor of an RPB would provide insights into aspects such as evaluating the separation performance of different internals, understanding mass transfer in the packing under varying operating conditions, and designing an efficient packing.

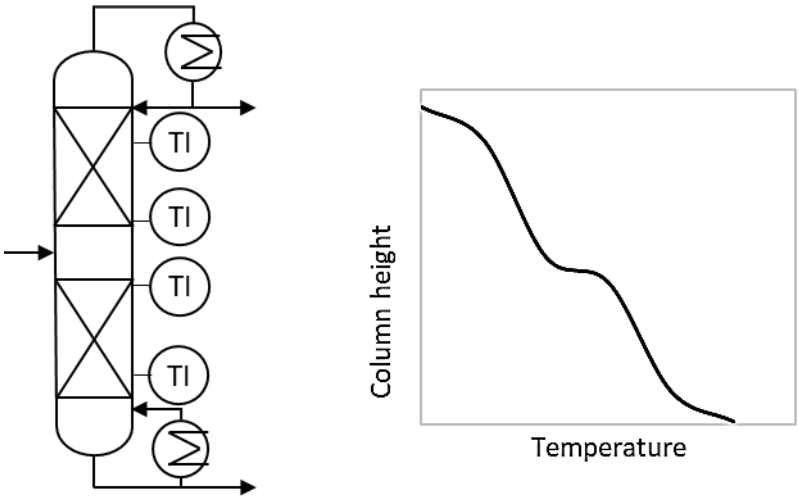

Figure 4.1: Schematic of a conventional distillation column and temperature profile.

The experimental setup used for temperature measurements along the rotor to characterize the temperature profile in the packing of an RPB and the casing separately is shown in Figure 4.2. This work aims to understand the mass transfer contribution of different sections/zones in an RPB for different rotor configurations, and not to achieve the maximum separation efficiency in an RPB. Figure 4.2 shows an overview of the sensor positions and the process flow of distillation in RPB. A few assumptions need to be considered to establish the basis of the work. First, two mass transfer zones are defined: the casing (aka cavity zone) and the packing. Mass transfer performance is represented by the number of theoretical stages (Nth). The temperature measurements of T1 and T12 sensors (Figure 4.2) are used to calculate the packing Nth. The

casing Nth is calculated by subtracting the packing contribution from the total Nth achieved in an RPB. Total Nth is calculated based on the samples withdrawn from the top and the bottom of the RPB. Following the studies on the characterization of mass transfer zones, the packing zone is further divided into an end zone (the initial few centimeters of the packing at the inner side of the rotor) and a bulk zone (the rest of the packing after the end zone) [55,100,101]. Therefore, a deeper analysis of the temperature/composition profile in the end and bulk zones is carried out after the initial characterization. For that purpose, temperature measurements from T1 to T12 are used.

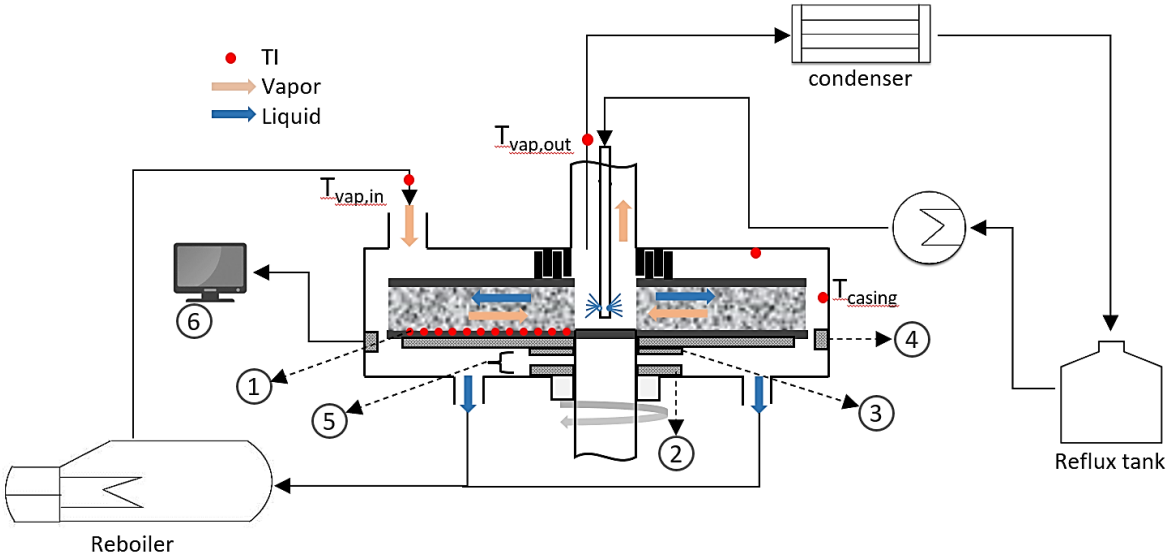

Figure 4.2: Process flow diagram of the distillation in RPB with rotor telemetry set-up. $T_{vap,in}$, $T_{vap,out}$, and T_{casing} are the thermocouples at the vapor inlet, vapor outlet, and casing. 1: T1 – T12 are the PT1000 temperature sensors mounted on the rotor, 2: Primary/Induction coil powered externally, 3: Secondary coil mounted on a steel plate with transmitters and PT1000 sensors, 4: Antenna for signal transmission connected with an external receiver, 5: Non-contact energy supply by inductive coupling, 6: Receiver display [61,102].

4.2. Materials and Methods

4.2.1. Experimental Setup

Figure 4.3 and Figure 4.4 illustrate the telemetry setup and internal components used for the distillation experiments. Details of the general RPB setup used for distillation experiments are given in section 3.1.1. In this section, details of the telemetry setup are explained. There are 24 positions on the rotor to mount the temperature sensors. In total, there are 12 PT1000 sensors (accuracy class A = $\pm(0.15\,°C + 0.002|T|)$ mounted on the rotor in a spiral to avoid the influence of a sensor on the proximate sensor, as shown in Figure 4.4. Screw-in fittings with PTFE insulation mount PT1000 sensors on the rotor to minimize heat conduction effects on sensor readings. The sensors are positioned 3 –4 mm above the rotor surface. Each set of four sensors is connected to a transmitter enclosed in a PEEK housing, which protects it from environmental conditions. Signals were transmitted at 1–2 ms intervals. All three transmitters are connected to the secondary coil that is inductively powered by the primary coil, as shown in Figure 4.2 and Figure 4.3. The primary coil/induction coil is powered externally. The secondary coil and transmitters are mounted on the lower side of the bottom rotor plate, and the primary coil (also called the induction coil) is fixed on the bottom of the RPB casing such that both coils are 5 – 6 mm apart. Two antennas in a PEEK housing are mounted inside the RPB casing to receive signals from the sensors. The antennas are connected to a receiver mounted outside the RPB via a cable. The receiver shown in Figure 4.4 features a 2.83-inch OLED display that displays the temperature sensor readings for each rotor position. The setup allows continuous online measurement of temperature profiles along the rotor.

The design specifications of the RPB, rotor, and packing are listed in Table 4.1. The design specification of the rotor telemetry system is given in Table 4.2. For the experimental investigation, three types of rotor setups were used: (1) with knit mesh packing, (2) without any packing, i.e., empty rotor, and (3) with advanced Zickzack (ZZ) packing (Figure 4.5) [43]. The details of the ZZ packing are given in section 3.4 [43]. As presented in section 3.4 [43], the developed ZZ prototype has a higher separation efficiency than the conventional RPB packing types [43]. Experiments were carried out using the telemetry setup described above to evaluate the radial separation efficiency of the ZZ packing. Twelve holes were drilled in the ZZ packing, and temperature sensors were assembled similarly to those in the knit mesh packing. The only

exception is that for ZZ packing, no liquid distributor is required as the packing is designed to distribute the liquid on its own under the applied centrifugal force.

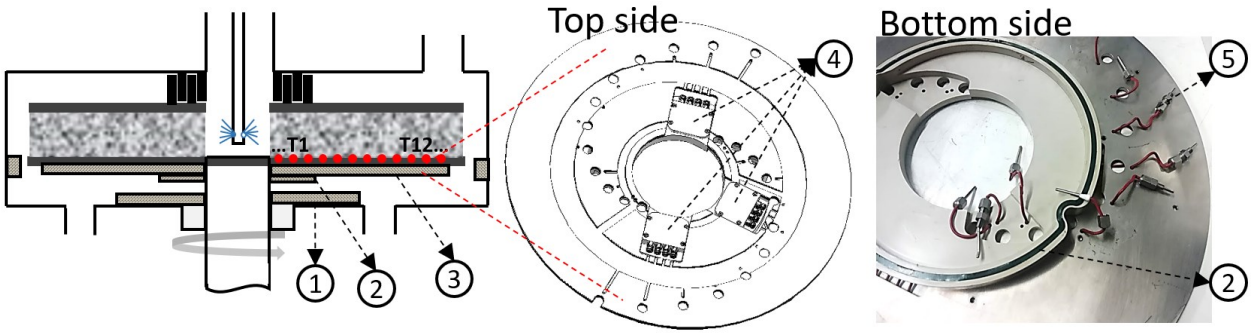

Figure 4.3: Details of the telemetry system mounted on the rotor. Schematic of an RPB (left), top side of the steel plate mounted on the lower rotor plate using screw fittings (middle), bottom side of the steel plate (right). 1: Primary/Induction coil, 2: secondary coil, 3: Steel plate containing the secondary coil, three transmitters, twelve PT1000 sensors, 4: three transmitters connected with the secondary coil, 5: PT1000 temperature sensors. Each transmitter is connected to four sensors. (Reprinted with permission from [103])

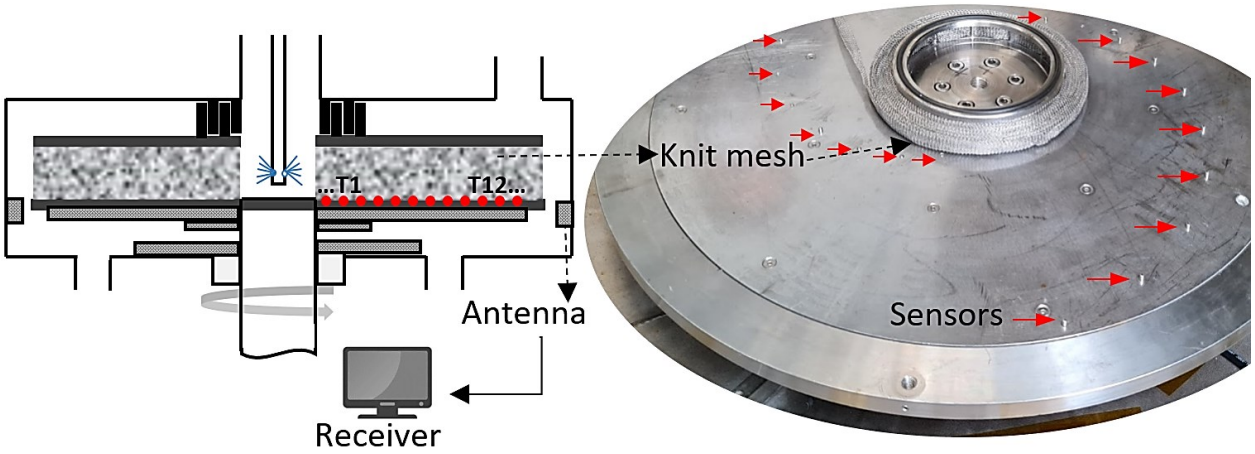

Figure 4.4: Arrangement of packing and sensor positions on the lower rotor plate. Red arrows show some possibilities of placing temperature sensors on the rotor. A few of the sensors are hidden under the packing. (Reprinted with permission from [103])

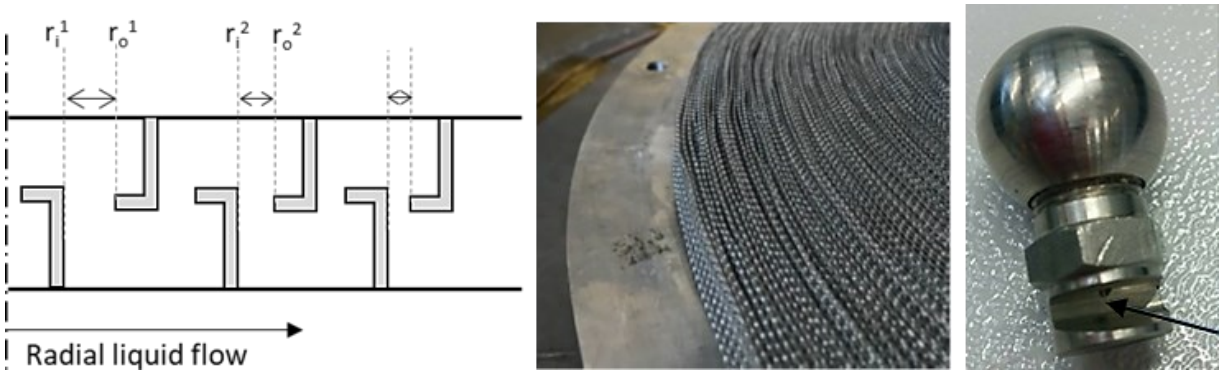

Figure 4.5: Zickzack packing (left), knit mesh packing (middle), and flat fan nozzles with 1 mm holes used as a liquid distributor (right) for the distillation experiments. (Reprinted with permission from [103])

Table 4.1: Design specifications of the RPB and the internals investigated.

RPB and Internals	
Specification	Dimension
RPB casing inner diameter	860 mm
RPB casing inner height (approx.)	129 mm
Rotor outer diameter	600 mm
Packing inner and outer diameter	d_i = 146 mm, d_o = 560 – 580 mm
Axial height of packing	h = 10 mm
Packing material	Metal knit mesh, ε = 85%, a_p = 3082 m^2m^{-3}, $Ø_{wire}$ = 0.2 mm
Liquid distributor	Flat flan nozzle, 3 nozzles with 1 hole each, $Ø_{hole}$ = 1 mm, 120° apart, 90° spray angle

Table 4.2: Specification of the rotor telemetry system

Rotor telemetry	
Specification	Dimension
Operating temperature range [°C]	-40 – +125
Housing material (Antenna, transmitter, induction coils)	PEEK
PT1000 maximum error [K]	± 0.3
The radial position of PT1000 sensors on the rotor [mm]	87.1, 102.5, 117.8, 133, 148, 162, 177.8, 192.5, 207.9, 222.6, 237.5, 252.5

4.2.2. Experimental Procedure

All experiments were conducted using a 10 wt.% ethanol-water mixture in the reboiler at 1 bar absolute pressure and under total reflux conditions. First, a feed mixture containing 10 wt.% ethanol in water was prepared and pumped into the reboiler (Figure 4.2). Nitrogen was supplied to the entire plant to ensure safe operation. The rotational speed of the RPB was fixed to a value between 300 rpm and 1200 rpm. The power of the electrically heated reboiler was set to attain an F-factor of 2.1 $Pa^{0.5}$ at the eye of the rotor. The vapor stream from the reboiler enters the RPB from the vapor inlet, flows through the packing from the outer to the inner radius (Figure 4.2), and leaves the RPB through the eye of the rotor. The vapor stream exiting the RPB was condensed in the overhead condenser, and the condensate was collected in the reflux tank. The reflux pump flow was controlled by maintaining a constant liquid mass in the reflux tank. Three flat fan nozzles are used as a liquid distributor at the eye of the rotor.

An eye ring or packing support with 89% free area is used as shown in Figure 4.4. Online measurement of the liquid reflux flow rate and density is performed using a Coriolis mass flow meter (Siemens SITRANS FC300 with MASS6000 transmitter, accuracy ±0.1%). A steady state was assumed when two criteria were met: (1) the density change of the reflux liquid was less

than 0.0005 g cm^{-3} over 10 minutes, and (2) the temperature change of PT1000 sensors on the rotor was less than 0.3 °C over 10 minutes. The temperature readings were recorded, and liquid samples were taken from the reflux and the bottom stream of the RPB once a steady state was achieved. A density meter (Mettler Toledo-Densito 30 PX, accuracy ±0.001 g cm^{-3}) was used to analyze the liquid samples according to their ethanol content. After start-up, 2 – 2.5 h were required to achieve steady-state operation, and then approximately 30 minutes to reach a new steady-state operation after changing the rotational speed. Each experimental run was carried out twice. During the first run, the rotational speed increased stepwise from 300 rpm to 1200 rpm. Subsequently, the cycle was completed by reducing the rotational speed stepwise in the same intervals. The standard error of the measured data and the error propagation are calculated using random errors and the measurement accuracy of the measuring devices.

4.3. Calculation of Theoretical Stages Using Temperature Measurements

An analytic description of the vapor-liquid equilibrium (VLE) curve calculates the number of theoretical stages (Nth) achieved in the RPB. Since ethanol-water is a non-ideal system, the relative volatility (α) changes with the liquid composition. An empirical approach proposed by Li et al. (2014) [40] was used to correlate the α of the ethanol-water system with the liquid composition (x) by a composite function and five empirical constants (a-e). Details of the calculation and constants are already explained in section 3.1.3 [43].

To explain the calculation method for theoretical stages, it is assumed that the temperature readings correspond to the vapor-phase temperature. Therefore, the temperature measurements estimate vapor composition from the T-x,y data as shown in Figure 4.6. The temperature and composition data were obtained from Aspen Plus® V8.8 (NRTL property method with the APV88 VLE-IG database) (Appendix A-5, Table 10.2). The equilibrium vapor composition is calculated using the method in section 3.1.3. Finally, using the VLE diagram for the ethanol-water system and the total reflux criterion (x = y), the number of theoretical stages was calculated iteratively between two vapor compositions. For ease of understanding, a graphical demonstration is shown in Figure 4.6.

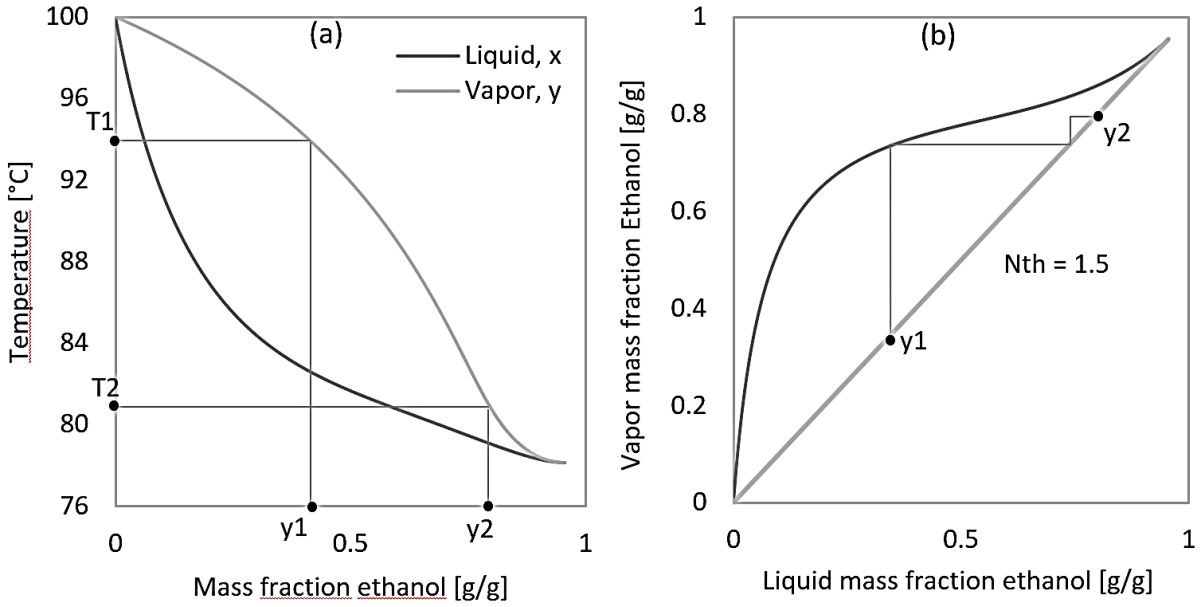

Figure 4.6: (a) Temperature and composition data of the ethanol-water system at 1.01325 bar, (b) VLE diagram of the ethanol-water system at 1.01325 bar.

By placing sensors along the radial length of the packing and using the temperature measurements and the above method, the number of theoretical stages in the packing can be calculated. For example, one sensor on the outer side of the rotor (ro) shows a temperature of 94°C (T1), and the other sensor on the inner side of the rotor (ri) shows a temperature of 81°C (T2). The goal is to find the number of theoretical stages between ro and ri. The vapor composition corresponding to these temperatures can be estimated using the T-x,y diagram (Figure 4.6, (a)). The number of theoretical stages can be calculated using the estimated vapor compositions and the x,y diagram (Figure 4.6, (b)). Instead of using the diagram, another way is to use the method in section 3.1.3. i.e., using Equation (3.2) to calculate the relative volatility (α) with the compositions from the T-x,y diagram, and then using Equation (3.1) to calculate the equilibrium vapor composition and repeating the steps until the composition y2 is reached.

Additionally, in section 4.3.4, the local Nth represented in Figure 4.12, Figure 4.13, and Figure 4.14 is estimated from a regressed temperature profile. A regressed temperature profile is found by fitting a model to the original temperature measurements based on the following assumptions:

a. The temperature of the vapor mixture entering the rotor decreases from the outer to the inner side, i.e., the rotor and packing cannot pollute a vapor mixture (no negative Nth values).

Therefore, some outlying temperature data points are filtered to meet this criterion while preserving the shape of the original temperature profile. The regression coefficient value (R-squared value) is greater than 0.7. Using these criteria, a linear temperature profile fits an empty rotor, and a second-order polynomial temperature profile fits a packed rotor. The fitted temperature profile estimates the vapor or liquid composition from the ethanol-water system's T-x,y equilibrium data. Using Equation (3.2), the equilibrium composition at the regressed temperature is estimated; using Equation (3.1), the relative volatility is calculated; and the number of theoretical stages is iteratively determined. Additional details on the fitted model and filtered temperature data points can be found in Appendix A-7, Table 10.4, and Figure 10.5.

b. Since it can not be determined whether the sensors are measuring the vapor phase temperature or the liquid phase temperature, although vapor is the continuous phase and the liquid holdup rapidly decreases a few centimeters after the start of the packing, the possibility that liquid droplets might influence the vapor temperature or that some sensors might be covered with liquid can not be avoided entirely in the current analysis. Therefore, both conservative estimates are considered one after another.

4.3.1. Overall Composition Profile in an RPB

Figure 4.7 shows an overall view of the change in vapor composition in an RPB at 600 rpm. The temperature sensors at the vapor inlet and outlet represent the vapor composition at the RPB inlet and outlet, respectively, and the temperature sensors T1–T12 are used to determine the radial composition profile in the rotor. Due to a technical error, measurements for T10 –T12 were not displayed for knit-mesh packing during the experiment. At first, it appears that most of the mass transfer occurs in the casing, as the change in vapor composition from the vapor inlet to T12 is larger than that from T1 to T12. However, this observation might be misleading since the ethanol-water system is non-ideal and has varying α values. A significant concentration change can be reached at low ethanol content with only one theoretical stage (see Figure 4.6). Therefore, mass transfer efficiency is calculated in terms of Nth to better understand the mass transfer fundamentals, as represented in Figure 4.8 and Figure 4.9.

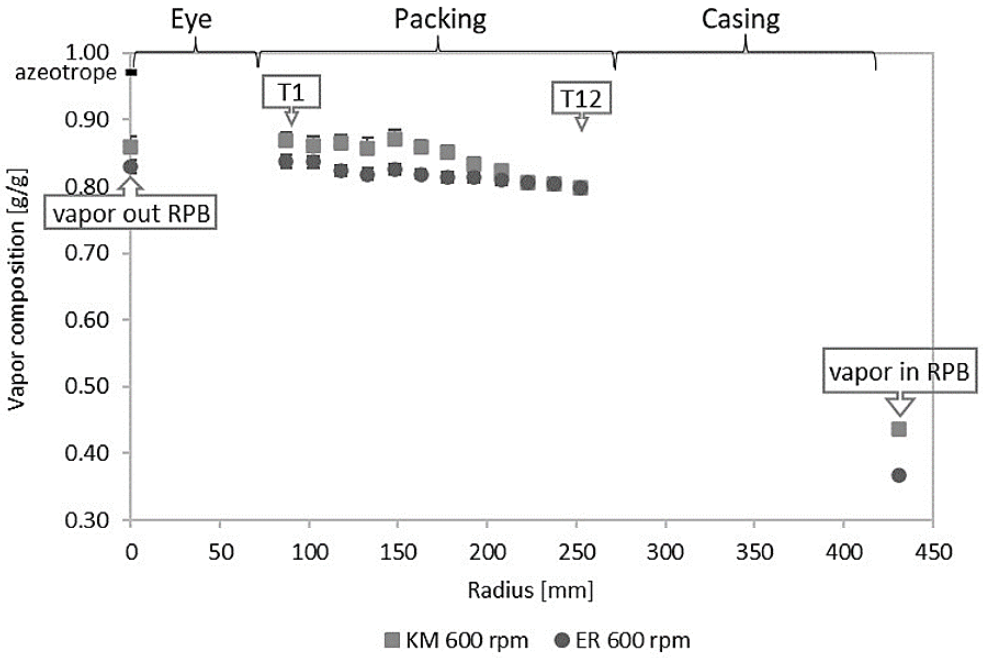

Figure 4.7: Overall change in vapor composition in RPB from vapor inlet to vapor outlet for knit mesh (KM) and empty rotor (ER) at 600 rpm and 2.1 $Pa^{0.5}$ F-factor.

4.3.2. Contribution of Packing and Casing to the Overall Mass Transfer

Figure 4.8 and Figure 4.9 display the separation efficiency of an RPB based on temperature measurements on a rotor equipped with knit mesh packing and an empty rotor, respectively. In Figure 4.8, the total separation in an RPB is mainly governed by the separation in the rotor as the packing Nth is always higher than the casing Nth, as indicated in our previous investigations [43,104]. The results of temperature measurements at the rotor suggest that, as rotational speed increases, the packing separation efficiency decreases, while the casing separation efficiency reaches a maximum. Similar results were also observed by Guo et al. (2014) [73] and Sang et al. (2017) [105]. The packing contribution at maximum separation efficiency for knit mesh packing is 2.1 Nth, and the maximum casing contribution is almost equivalent to one theoretical stage to the overall mass transfer in the RPB. Although the separation efficiency of a packed rotor can be increased by using other types of packing, liquid distributors, etc., the goal of this work was not to find the maximum separation efficiency in an RPB.

These results align with theoretical considerations derived from the correlations of Burns et al. (2000) [82] for liquid holdup and also with the liquid holdup measurements using gamma-ray

tomography by Groß et al. (2019) [80], which indicate that the liquid holdup in the packing decreases significantly with increasing rotational speed. At the maximum separation efficiency, the contribution of the packed rotor is approximately 78%. However, depending on the rotational speed, the packing contribution varies from 56% to 78%, and the casing contribution ranges from 22% to 44%. Mass transfer in the casing (aka cavity zone) may result from flying liquid droplets leaving the rotor, striking the casing walls, and either rebounding or running down the casing. Sang et al. (2017) [101] conducted an experimental study and concluded that film mass transfer on the casing wall and the rebound of the droplets after striking the wall contribute more to the mass transfer in the cavity zone as compared to the flying droplets toward the casing wall. Therefore, the mass transfer in the casing can be equally significant as that inside the packing, depending on the dimensions of the packing and the casing, as well as the rotational speed. Qammar et al. (2019) [43] showed similar results for smaller F-factors of 0.6 $Pa^{0.5}$. In Figure 4.9, the contribution of the empty rotor is smaller than the casing contribution, indicating that mass transfer resulting from the flying droplets in the casing and these droplets striking the casing walls and running down contributes more to the mass transfer than the film mass transfer on the empty rotor plate [104]. The overall separation efficiency of a rotor equipped with knit mesh is almost 0.7 theoretical stages better than that of an empty rotor. However, adding packing material lowers the rotational speed at which maximum separation efficiency is reached. These results can be supported by the investigations reported by Lukin et al. (2021) [104], which show that the total wetted surface area of the empty rotor (without packing) and the casing is approximately in the range of 69 – 88% of the surface area generated in an RPB when the packing is used [104]. Therefore, conventional RPB packings must be further improved to fully utilize their high specific surface areas. Hacking et al., 2020 [106] experimentally demonstrated the use of redistribution rings for RPBs to mitigate the liquid maldistribution in an RPB independent of the type of packing used [106].

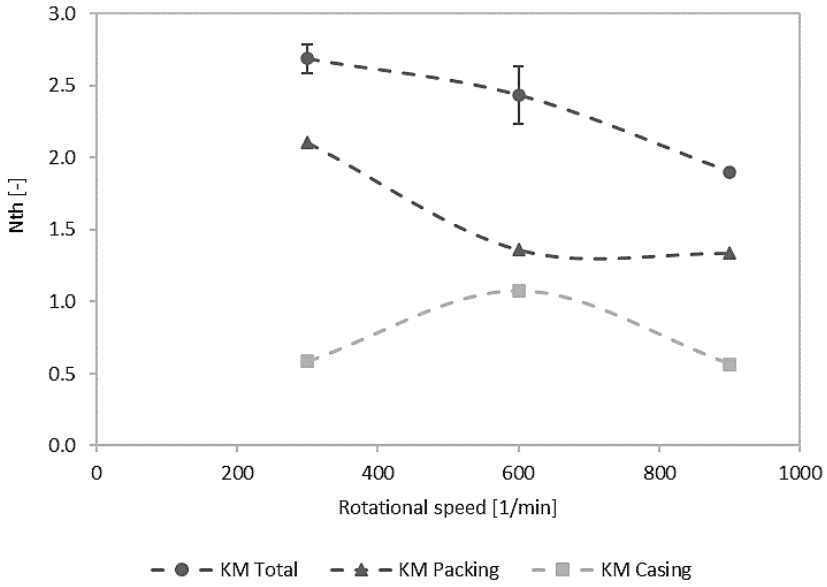

Figure 4.8: Mass transfer distribution in terms of the number of theoretical stages (Nth) between packing and casing in an RPB with knit mesh packing (KM) at an F-factor of 2.1 $Pa^{0.5}$.

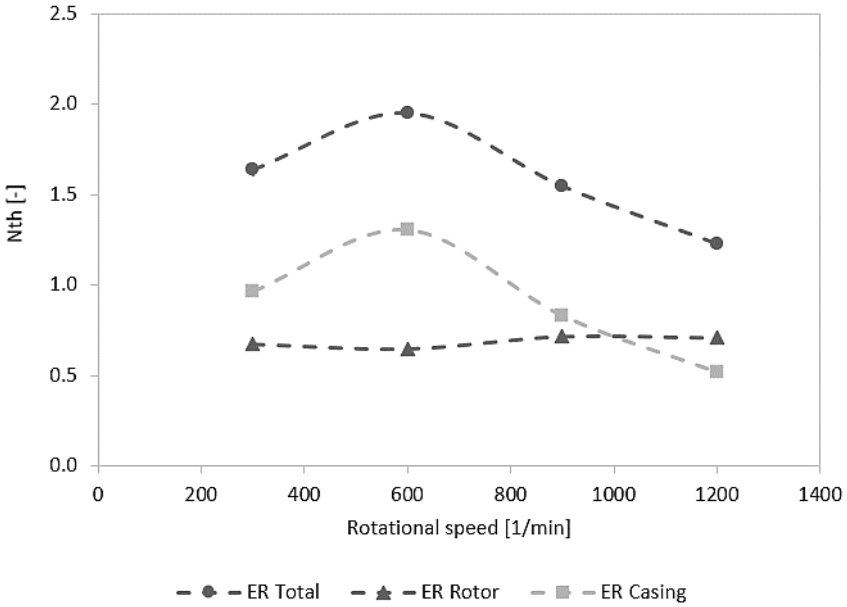

Figure 4.9: Mass transfer distribution in terms of the number of theoretical stages (Nth) between packing and casing in an RPB with the empty rotor (ER) at an F-factor of 2.1 $Pa^{0.5}$.

4.3.3. Radial Temperature Profile in Packed and Empty Rotor

Figure 4.10 displays the measured temperature profiles of an empty rotor (T1–T12). The radial temperature profile in the empty rotor roughly follows a straight line when plotted against radial position, with a nearly identical slope across different rotational speeds. Figure 4.10 illustrates that the temperature at 600 rpm is generally lower throughout the rotor than at other rotational speeds. That also explains the highest separation efficiency at 600 rpm (see Figure 4.9). However, the casing's contribution at 600 rpm is also significant, as the vapors entering from the outer side of the rotor already have the highest vapor composition compared to other rotational speeds. The rotor's temperature profile helps explain the overall product purity at different rotational speeds: 300 rpm, 600 rpm, 900 rpm, and 1200 rpm. Qammar et al. (2018) [86] explained that an optimal rotational speed exists for each rotor configuration, resulting in maximum separation efficiency. In the current case of an empty rotor, 600 rpm is the optimal rotational speed. At that operating point, a balance is reached between the beneficial effects of higher turbulence at higher rotational speed and the loss of liquid hold-up or liquid maldistribution.

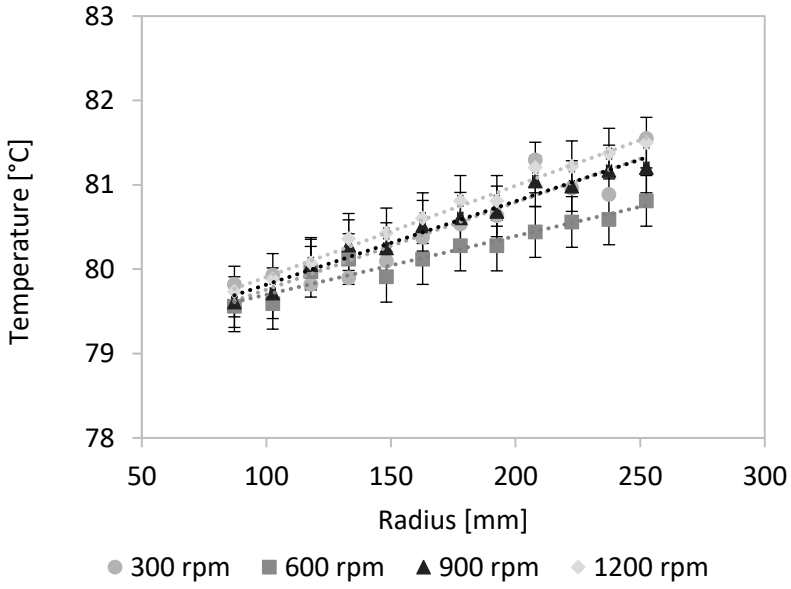

Figure 4.10: Measured temperature profile (raw data) along the empty rotor (ER) rotor at an F-factor of 2.1 $Pa^{0.5}$. (Reprinted with permission from [103])

The temperature profile of the rotor with knit mesh packing is shown in Figure 4.11. As depicted in Figure 4.8, 300 rpm yields the maximum number of theoretical stages (Nth), and the temperature profile at 300 rpm is also at the bottom, indicating the highest ethanol composition. In contrast to the empty rotor, the temperature profile across the radius is not linear. It is almost constant near the rotor's eye and becomes steeper in the outer rotor regions. The data points do not precisely fit the curves for one or more reasons, such as liquid maldistribution causing dry or wet spots on the sensors or some sensors being covered by the liquid, thereby not representing the true vapor temperature; inaccuracies in the measurements; etc. Data points are filtered according to the criteria described in Section 4.3 to estimate the number of theoretical stages in the packing and enable a reasonable analysis of the results.

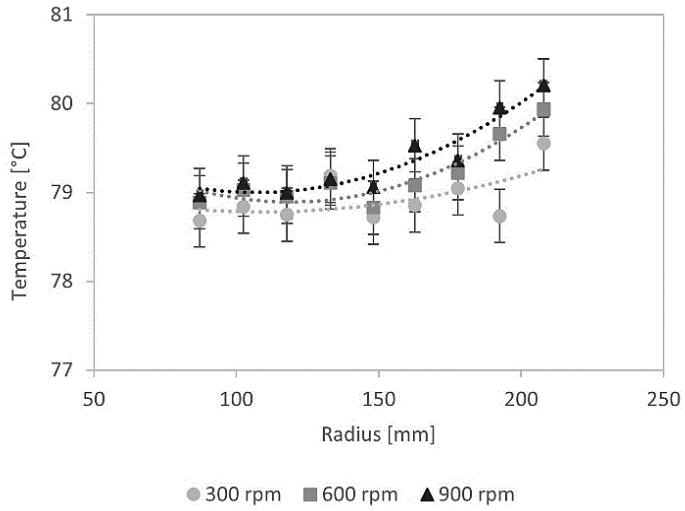

Figure 4.11: Temperature profile along the knit mesh (KM) packing at an F-factor of 2.1 $Pa^{0.5}$. The data points represent the raw measured data.

4.3.4. Change in the Separation Efficiency Along the Radial Packing Length

The results of the temperature measurements in Figure 4.10 and Figure 4.11 can be transformed into separation efficiencies (in terms of Nth) in the same way as in Section 4.3.3. As a result, Figure 4.12 represents the radial change in the mass transfer performance inside an RPB packing. In Figure 4.12, the Nth values increase with increasing radial length, most likely due to the more uniform liquid distribution that might have been established a few centimeters after entering the packing [80]. As the packing radius increases, the liquid load per unit packing area decreases,

potentially leading to liquid maldistribution and dry spots in the packing, thereby reducing the packing's separation performance despite an increase in specific surface area.

The separation efficiency curves along the radius in Figure 4.12 roughly follow the course of radial liquid holdup measurements by Yang et al. (2015) [83] for wire mesh by Groß et al. (2019) [80] for metal foam packing. The authors showed that the liquid holdup initially increases over the first few millimeters of the packing and then decreases with radial position [83]. The initial increase in the liquid holdup can be attributed to the packing catching the liquid as reported by Yang et al. (2015) [83], and decelerating the liquid on contact with the packing, as reported by Groß et al. (2019) [80]. As mentioned in section 4.3, it is not confirmed whether the temperature sensors measure vapor or liquid-phase temperatures; therefore, both assumptions are considered, and the Nth curves are plotted. The trends of the Nth_{Vapor} and Nth_{Liquid} curves are similar. Nth_Liquid is showing slightly higher values. Comparing the separation efficiency at 300 rpm and 900 rpm, the inner half of the rotor performs better at the lower speed, most likely because the packing at 300 rpm more effectively captures the liquid. These results are supported by the radial liquid holdup profile in packing [80], where the liquid holdup at 300 rpm is higher at the inner radius than at other higher rotational speeds [80]. From Figure 4.12, the outer half of the rotor gives a slightly higher separation efficiency (local Nth_{Vapor}) at 900 rpm compared to 300 rpm, most likely due to higher centrifugal forces causing higher turbulence and higher velocities leading to smaller droplets and/or thinner films and hence more rigorous mass transfer as also reported by Yang et al., 2015 [83] that higher rotational speeds improve the liquid distribution. Nevertheless, considering the measurement errors, a concrete conclusion cannot be drawn, as the separation efficiency of the outer half of the rotor is nearly the same for the investigated rotational speeds.

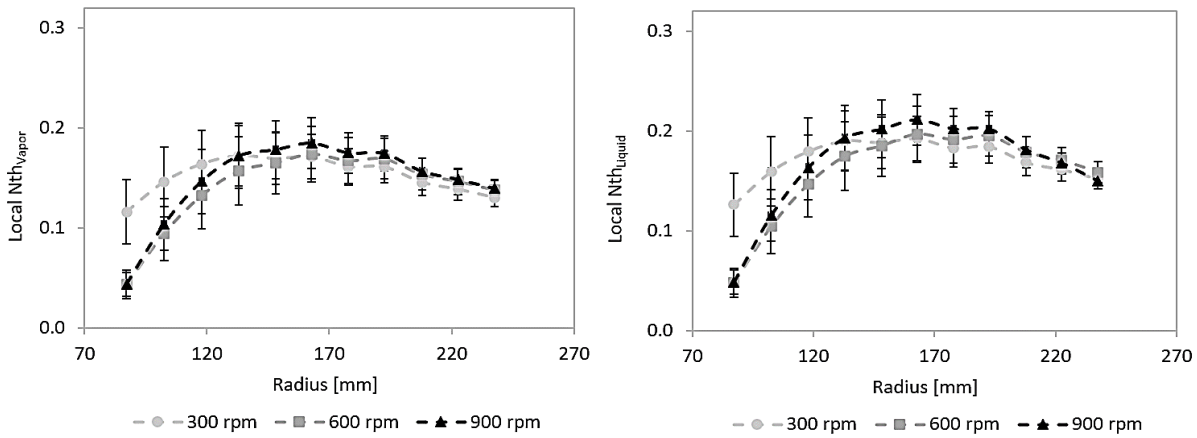

Figure 4.12: Radial change in the packing mass transfer efficiency as a function of rotational speed in an RPB with knit mesh packing (KM). Nth_{Vapor} (left) assumes the vapor phase temperature, and Nth_{Liquid} (right) assumes the liquid phase temperature is measured.

Similarly, the radial change in mass transfer efficiency for an empty rotor is displayed in Figure 4.13. The trends of the Nth_{Vapor} and Nth_{Liquid} curves are similar, with slightly higher Nth values when the sensors are assumed to measure liquid temperature. In contrast to the packed rotor, the mass transfer efficiency continuously decreases from the inner to the outer side of the rotor. The higher Nth at the start of the rotor may result from liquid spray from the flat fan nozzle hitting the support ring at the eye of the rotor, further breaking down into smaller droplets and creating more mass transfer area. As those droplets travel along the rotor, they hit the top or bottom plate and form a film. As stated above, the decreasing liquid loads on the outer side of the rotor and liquid maldistribution could be the reason for poor performance at the outer part of the rotor. Comparing Figure 4.12 and Figure 4.13, the inner half of the empty rotor performs better than the inner half of the packed rotor, most likely due to the difference in the initial liquid accumulation and distribution, as explained above. These results show the importance of uniform initial liquid distribution for higher separation efficiency and the need for liquid redistribution within the packing, as is commonly done in a conventional column. Pyka et al. (2023) introduced a novel liquid distributor for an RPB, the rotating baffle distributor (RBD) [44]. Comparing overall separation efficiency in an RPB, the authors showed that RBD is one theoretical stage superior to the conventional liquid distributor (full-jet nozzles) and also helps address the liquid distribution problem in multi-rotor RPBs.

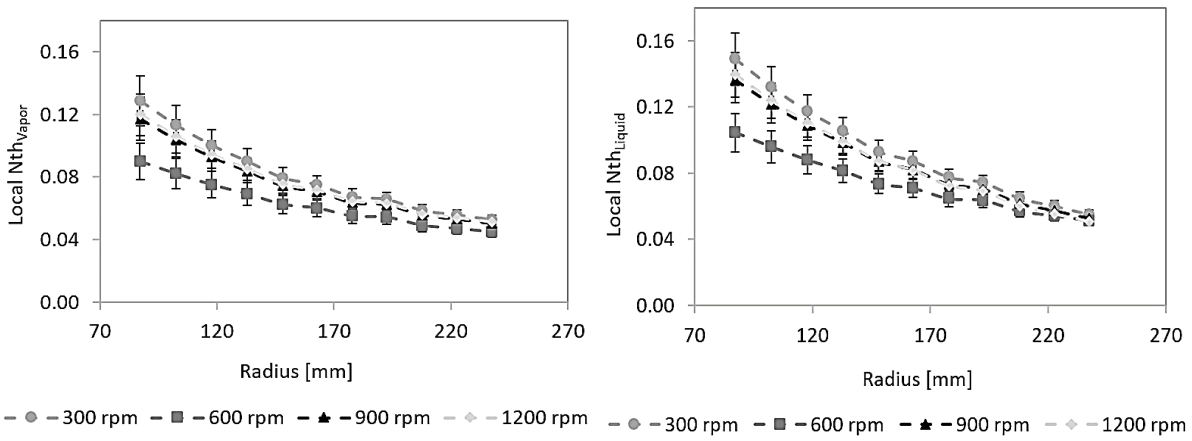

Figure 4.13: Radial change in the rotor mass transfer efficiency as a function of rotational speed in an RPB for the empty rotor (ER). Nth assumes that the vapor-phase temperature (left) and the liquid-phase temperature (right) are measured.

Figure 4.14 shows the overall and local separation efficiency of a Zickzack (ZZ) packing in an RPB. It should be noted that the results shown in Figure 4.14 were obtained using the initial design of ZZ packing described by Qammar et al. (2019) [43]. The improved design by Loll et al. (2022) [48] might have demonstrated higher performance by avoiding liquid and gas bypasses in the spaces between the packing and rotor walls. Nevertheless, the results will allow testing the hypothesis that ZZ packing provides more uniform hydrodynamic and mass-transfer conditions than conventional packing types.

The ZZ packing was tested at an F-factor of 0.3 $Pa^{0.5}$ and a rotational speed up to 600 rpm, considering its mechanical stability under high temperatures, chemical systems, and centrifugal forces. Figure 4.14 shows that, like the knit mesh packing, the Nth values of ZZ packing decrease with increasing rotational speed after a specific value. In contrast to knit mesh packing, the radial separation efficiency of a ZZ packing is almost constant at 600 rpm across the radial position, most likely due to a more uniform initial liquid distribution and more homogeneous hydrodynamic conditions within the packing. The loss of separation efficiency observed in the initial few centimeters of the knit mesh packing due to liquid accumulation and deceleration is not observed in ZZ packing, demonstrating the advantage of ZZ packing over conventional packing types for RPB. Moreover, the uniform radial separation profile will help effectively scale the packing from the lab to the industrial scale. The slight dip in the radial separation profile at

300 rpm in Figure 4.14 might be due to liquid bypassing through holes or gaps in the ZZ packing [48]. Overall, ZZ packing showed promising results by improving liquid distribution and holdup. Further design improvements in the ZZ packing will enable a quantitative comparison among different packings and address scalability and liquid maldistribution problems in conventional RPB packing types.

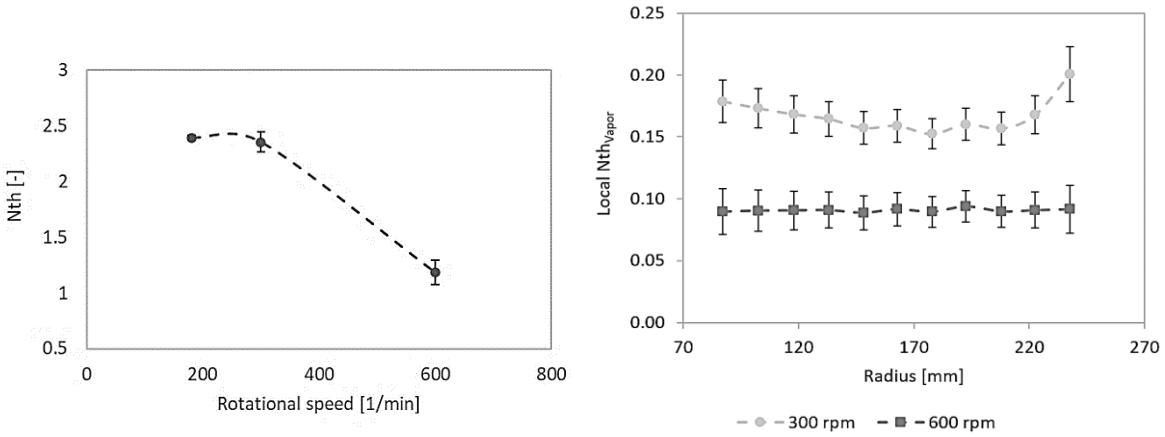

Figure 4.14: Total separation efficiency of ZZ packing in an RPB (left), and radial change in the mass transfer efficiency as a function of rotational speed (right) at an F-factor of 0.3 $Pa^{0.5}$.

4.4. Contribution of Mass Transfer Zones

As explained earlier, many authors divide the RPB into three zones: the cavity zone, the bulk zone, and the end zone [55,100,105]. There are a few experimental and visual studies [55,100,105] (predicted with physical or chemisorption of CO_2) showing that the initial few centimeters of packing contribute most to overall mass transfer in an RPB (end zone) compared to the rest of the packing (bulk zone). Most of the experiments supporting the high contribution of the end zone were conducted by adding packing layers in steps and varying the rotational speed and the initial liquid velocity. High-speed cameras were used to record changes in the tangential angle of the liquid droplets. According to the authors, the change in the tangential angle of liquid droplets is greatest at the end zone. All experiments were conducted with packing installed and a height-to-packing-radius ratio greater than 0.1.

The current case study (height-to-packing radius = 0.03) found that the entire packing, including the middle and outer parts, also known as the bulk zone, contributes comparably to overall mass

transfer. The difference in experimental results and interpretation depends on how the experiments are conducted and interpreted. Moreover, the operating and design conditions of the RPBs differ across these studies; therefore, a general conclusion about the contribution of the mass transfer zones cannot be drawn. Nevertheless, the results of the temperature measurements can be supported by the experimental results shown in section 3.2.1 [61,86] using a metal foam with varying packing length and an empty rotor with the same F-factor and RPB design. The results showed that even with no packing, there is a certain amount of separation in an RPB, which leads to the observation that there might not be a significant contribution of the end zone to the overall mass transfer; instead, it might be the result of mass transfer on empty rotor plates and the mass transfer in the casing as also supported by the wetted area observations made by Lukin et al., 2021 [104] in an RPB (height to packing radius = 0.2) with and without packing.

Table 4.3 [61] indicates that almost half of the separation is achieved even without packing compared to the separation with a packing length of 0.19 m. If a few centimeters of the packing are added to the empty rotor, then it only increases the Nth by half a stage, and so on. These observations support the results shown in Figure 4.12 and Figure 4.13. Moreover, the mass transfer correlations obtained during absorption experiments might not be valid for distillation in all cases, so care must be taken when using these correlations and when normalizing and averaging the packing and casing separation efficiency. For reliable scaling-up of packings, it is essential to differentiate between the separation efficiency of packing and non-packing elements; therefore, the actual separation efficiency of a packing should be calculated as the difference between the separation efficiency of a packed rotor and the empty rotor.

Table 4.3: Overall separation efficiency of metal foam at 600 rpm, 400 mm OD rotor, and 2.1 $Pa^{0.5}$ F-factor. Values are estimated from the data reported in [61].

Number of theoretical stages at 600 rpm				
Radial packing length	0 m	0.1 m	0.125 m	0.19 m
Nth	1.5	2.1	2.6	3.2

4.5. Summary

In this chapter, a measuring method was presented to determine the radial temperature profile in the packing of an RPB. A complete overview of the total RPB performance and the radial local separation performance along the rotor was determined, and the contributions of the packing and the casing were evaluated for different packing types, along with the empty rotor, for the first time. The results show that the packing's contribution is 56–78% of the total separation efficiency achieved in an RPB, depending on the rotational speed. Adding packing to the empty rotor enhances the total separation and reduces the rotational speed at which maximum separation performance is achieved.

Radial temperature measurements allow calculation of separation efficiencies along the packing radius. The results of knit mesh packing showed a maximum separation efficiency at the middle of the rotor at higher rotational speeds, while no conclusive results could be deduced for lower rotational speeds. The temperature measurements help determine which parts of the packing can be further improved to enhance separation performance. The qualitative comparison of the radial separation efficiency of additively manufactured Zickzack packing with that of conventional knit mesh packing showed that Zickzack provides higher separation efficiency at the rotor inner radius, most likely due to uniform liquid distribution and holdup. Moreover, it tended to maintain a constant separation throughout the packing. However, care should be taken when interpreting temperature measurement results, as they depend on the accuracy of the sensors and the evaluation method. Nevertheless, the results indicate that the scale-up of packing requires differentiating the separation efficiency of the packing elements from that of the non-packing elements. Those novel insights pave the way for mass transfer correlations, which are common in distillation columns, bringing distillation in RPBs one step closer to industrial application.

As it is one of the first studies on RPBs, there is room to improve the measurement method by building an experimental database. Further investigations with other test mixtures, packing types, liquid distributors, and experimental validation of the assumptions regarding the measured phase and the absence of backmixing will help to refine the interpretation of the results. This would provide greater confidence in the calculated radial separation efficiencies and the resulting understanding of mass transfer within the rotor.

Chapter 5 Mass Transfer Modeling

This chapter presents the rate-based approach to discuss the experimental results of mass transfer in an RPB. Furthermore, available literature correlations are used to estimate the vapor-side volumetric mass transfer coefficient from the current experimental data, and their limitations are addressed to expand their applicability to changing operational and equipment conditions.

Parts of Chapter 5 are published in:

Qammar, H.: Rotating Packed Beds in Distillation: Binary Distillation, in: M. Skiborowski, A. Górak (Eds.), Process Intensification, De Gruyter, 2022, pp. 159–188.

https://doi.org/10.1515/9783110724998-006

H. Qammar, T. Pyka, J. Koop, A. Górak, G. Schembecker, Radial Temperature Profile Measurements to Understand Mass Transfer in Rotating Packed Bed Distillation, Ind. Eng. Chem. Res. (2023).

https://doi.org/10.1021/acs.iecr.3c01068

5.1. Mass Transfer Rate

The number of theoretical stages is suitable for more general estimations or thermodynamic feasibility. Using the number of theoretical stages is a quick and simple method for predicting mass transfer performance in many separation processes; however, it also has limitations. For example, it mainly relies on thermodynamic data and does not consider apparatus-specific features, packing geometries, or other complex hydrodynamic conditions often needed for scaling the apparatuses. The rate-based approach is more suitable for calculating mass transfer as a combination of the mass transfer coefficient and driving force. The calculation of the mass transfer coefficient considers packing geometry, hydraulics, or surface area. The following section will use this approach to describe the mass transfer in the RPB more effectively.

5.2. Experimental Mass Transfer Coefficient

The ATU-NTU approach by Kelleher and Fair (1996) [1], described in Section 2.3.3, is used to calculate the overall volumetric mass transfer coefficient, $K_G a$ (s^{-1}). For the local $k_g a$, the ATU-NTU approach is applied over differential radial segments of the packing where yi and yo are estimated from local temperature measurements, and the characteristic volume corresponds only to the packing segment. For ease of readability, the Equations presented in Chapter 2 are restated.

$$NTU_g = \int_{y_i}^{y_o} \frac{dy_E}{(y^{eq} - y)} \tag{5.1}$$

$$\pi({r_o}^2 - {r_i}^2) = ATU \cdot NTU \tag{5.2}$$

$$K_G a = \frac{\dot{m}_g}{\rho_g \cdot h \cdot ATU_g} \tag{5.3}$$

The NTU values are estimated using Equation (5.1) with a shortcut method based on C-Routines in MATLAB, which numerically integrates the residue curve to obtain the area under the graph and, therefore, the integral for the total reflux boundaries (x = y) [107]. The method uses the ode45 MATLAB solver and property data from the NRTL model exported from Aspen Plus® V8.8. The function calculates the area under the graph between the starting value, yi, and the final value, yo, where yi and yo are the ethanol vapor molar fractions measured at the inlet and

outlet of the RPB, respectively (for the case of overall mass transfer coefficient, $K_G a$). The NTU values are taken from the data point and calculated using the routines. The NRTL property method is selected according to Hadrich and Kechaou (2010) [108], who identified the NRTL model as the best at fitting equilibrium data for the ethanol-water system, with a root-mean-square (RMS) deviation of 0.4%. Using the NTU values, ATU values are calculated using Equation (5.2), and the respective $K_G a$ (s^{-1}) is calculated using Equation (5.3).

Many publications estimate the $K_G a$ value using the radial dimensions (r_i,r_o) of the packing only, while the concentrations are measured at the inlet and outlet of the whole RPB, thereby assuming that mass transfer takes place only in the packing and neglecting the non-packing related contribution to the mass transfer. It may lead to an overestimation of the mass transfer coefficient when the total mass transfer of an RPB is accounted for only within the packing volume. As already shown in Chapter 4 using the temperature measurements, depending upon operational and design parameters, there are significant contributions from the non-packing related elements of the RPB; therefore, in the following section, the approach suggested by Groß et al. [67] for the calculation of the overall volumetric mass transfer coefficient is adapted. According to this approach, for the calculation of $K_G a$ value of a packed rotor, casing, and packing volume is used (C+P), and for the calculation of $K_G a$ value of an empty rotor (ER) casing and rotor volume is used (C+R), as also shown in Chapter 3, Table 3.3. The resulting values are given in Table 5.1.

Table 5.1: Geometrical surface area of different rotor configurations of Rotor-1 to calculate $K_G a$.

	Geometrical surface area (m^2)		
	Rotor (R)	Casing (C)	Packing (P)
	$2\pi\ ({r_o}^2 - {r_i}^2)$	$\frac{3}{2}\pi\ {r_c}^2 + 2\pi r_c h_c$	$2\pi\ ({r_{o,p}}^2 - {r_{i,p}}^2) h_p a_p$
	C+R		**C+P**
Knit mesh	-		3.44
Full metal foam	-		2.13
Empty rotor	1.27		-

From the experimental database investigated, mass transfer coefficient values for three rotor configurations (empty rotor, knit mesh, and metal foam with varying packing length) are shown in Figure 5.1. These rotor configurations are chosen as they are the most commonly used packing types. It is important to note that in the current section, first, an overall volumetric mass transfer coefficient is shown for the whole RPB ($K_G a$) considering a combination of surface area of rotor, casing, and packing according to rotor configuration, and later, a local volumetric mass transfer coefficient is shown that is related to the packing only, local $k_g a$, (s^{-1}).

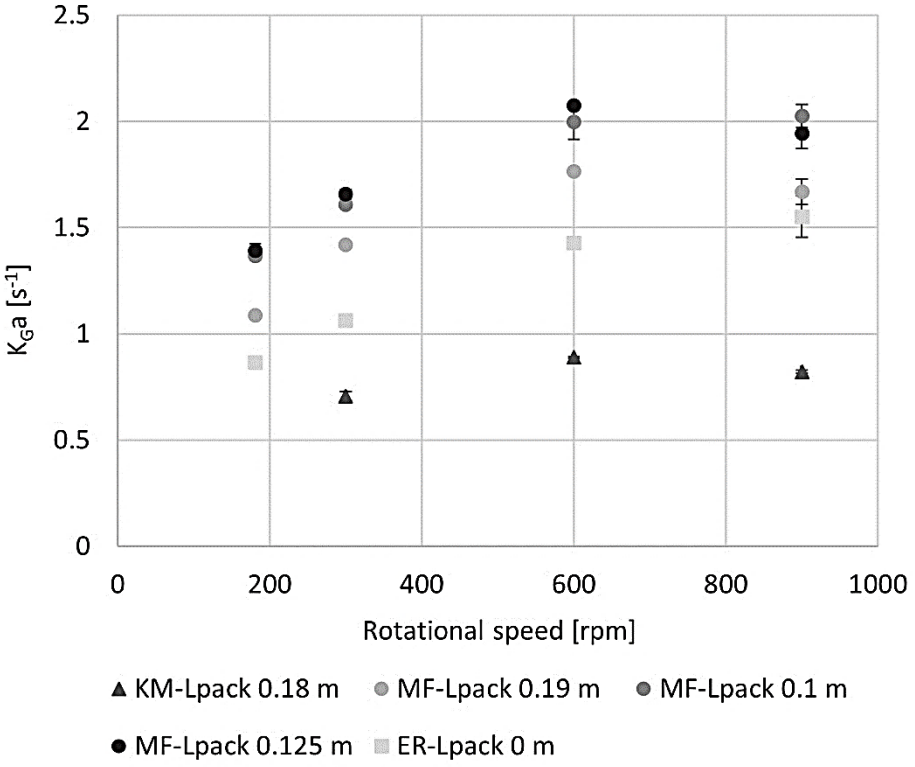

Figure 5.1: Comparison of the different experimental K_Ga value for the RPB equipped with knit mesh and metal foam. F-factor 2.1 $Pa^{0.5}$, Rotor-1: OD 0.4 m, knit mesh (KM) $OD_{packing}$ 0.18 m, Metal foam (MF) $OD_{packing}$ 0.1 m, 0.125 m, 0.19 m, respectively. ER denotes empty rotor. Error bars depict the standard deviation.

Figure 5.1 shows the overall volumetric mass transfer coefficient for different rotor configurations in the RPB. Although the Nth values for the larger radial packing length of the metal foam are higher, they yield a lower K_Ga, indicating that the effective mass transfer behavior varies with packing length and radius. This trend could be due to geometric changes along the radius, especially the increasing cross-sectional area and the increasing centrifugal acceleration at the rotor's outer edge, which directly and significantly influence the vapor and liquid velocities and the liquid distribution. Moreover, the contribution of the non-packing-related elements, i.e., end effects, might be more pronounced with a small packing length. Ultimately, these changing conditions lead to varying mass transfer behavior along the rotor.

Considering the approximately 7-fold increase in the metal foam packing volume with a radial length of 0.19 m compared to the metal foam packing with a radial length of 0.1 m, the increase in the Nth values is 50% (Figure 3.4), whereas the mass transfer coefficient in the RPB decreases by 12 – 21 % (depending upon the rotational speed) of the one resulting for the radial packing length of 0.1 m. Therefore, a correction for the specific dimensions of the RPB is required when extrapolating the results of small-scale RPB to large-scale units. The relative constancy or decrease in $K_G a$ value above a certain rotational speed (also called the optimal rotational speed) is supported by tomographic evaluations by Groß et al. [80], which show that high rotational speeds can lead to maldistribution and a reduced overall liquid hold-up within the packing, potentially causing dry spots and thereby limiting further improvements in mass transfer. The longer packing length shows better separation efficiency (Nth) than the shorter packing length, whereas the $K_G a$ results show the opposite. The $K_G a$ is relatively smaller for the larger packing size. These investigations reveal that the added packing volume at higher diameters is used less effectively; however, it still contributes to overall mass transfer. Moreover, the $K_G a$ values for the knit mesh packing are the worst of all the packings investigated at the given conditions, indicating that the outer parts of the packing do not contribute efficiently to overall mass transfer improvement, despite a significant increase in packing volume.

The conclusion drawn above regarding the non-linear effect of varying packing lengths on the mass transfer coefficient can be rechecked with another technique, i.e., the temperature measurements presented in Chapter 4. The temperature measurements in the packing can be used to estimate the inlet and outlet concentrations of a packing element from the T-x,y data. Hence, the mass transfer coefficient in the packing can be calculated using the same procedure described above, with Equations (5.1)–(5.3). To differentiate the mass transfer coefficient in the RPB from the packing mass transfer coefficient, the latter is denoted as ``local $k_g a''$ (s^{-1}). Results of local $k_g a$ for knit mesh packing are shown in Figure 5.2. Since the overall shape of the separation efficiency curves remains similar whether the liquid or vapor phase temperature is measured (Figure 4.12), only the gas-side volumetric mass transfer coefficient is plotted. The local mass transfer coefficient trends show similar behavior as the local Nth curve in Figure 4.12, i.e., for 300 rpm, the mass transfer coefficient seems to be constant at the inner side of the packing before it declines towards the outer side of the packing, whereas a maximum exists for 600 rpm and 900 rpm. The sharp decline in the mass transfer coefficient towards the outer radius might indicate

that the larger surface area in the outer rotor is not utilized effectively, which supports the above conclusions from the metal foam with varying packing lengths and highlights the need for more efficient packing design.

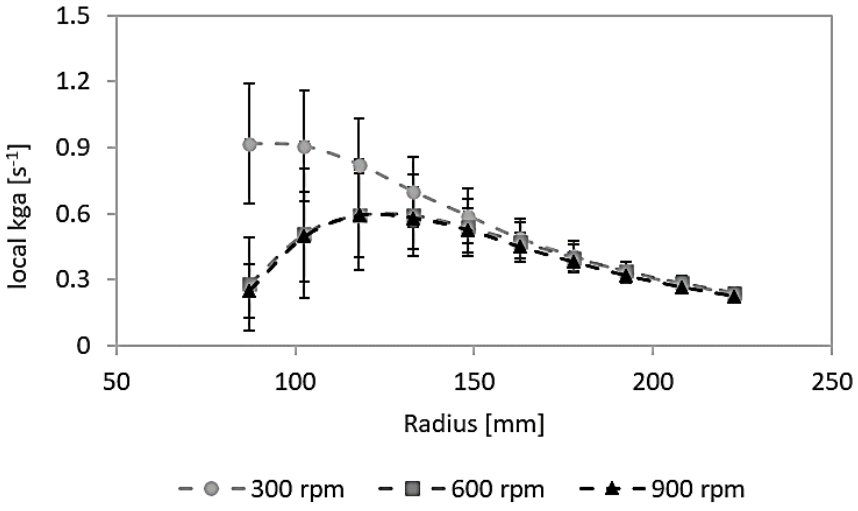

Figure 5.2: Radial change in the local mass transfer coefficient ($k_g a$) as a function of rotational speed in an RPB with knit mesh packing (KM) at 2.1 $Pa^{0.5}$ F-factor. $k_g a$ assumes that the sensors measure vapor phase temperature. (Reprinted with permission from [103])

5.3. Simulated Mass Transfer Coefficient

A mathematical correlation presents an image of reality. Most available modeling approaches provide insights into the effect of various parameters on mass transfer coefficients. In the case of RPB, there is limited knowledge and correlations purely for distillation. In this section, the correlation proposed by Mondal et al. [8] is used along with the improvements suggested by Sudhoff et al. [54] and Gross et al. [67] to estimate the mass transfer coefficient.

As explained in section 2.3.3, Mondal et al. (2012) [8] proposed a correlation for correlating the overall volumetric mass transfer coefficient with both the vapor load and the rotational speed, Equation (5.4):

$$K_G a = c_1 \, (F_{factor})^{\,c_2} \, (\omega^2 \, r_{avg})^{c_3} \qquad 5.4$$

Based on the average packing radius (r_{avg}), K_Ga and $\omega^2 r_{avg}$ represent the overall volumetric mass transfer coefficient and the centrifugal acceleration, respectively. The experimental values of K_Ga were estimated from Equation (5.3), and the constants c_1, c_2, and c_3 were found by fitting K_Ga to Equation (5.4) by non-linear regression.

The original correlation of Mondal et al. [8] could predict 75% of the experimental data in this work with an error range of ±30%, as shown in Figure 5.3. The correlation predicts the current experimental data with an average standard deviation of ±0.19 in the K_Ga-value. The correlation is overpredicting the K_Ga values primarily for knit mesh packing, although the correlation was initially developed for stainless steel wire mesh annular packing with an average packing surface area of 280 m^2m^{-3} and for the methanol-ethanol test system. However, the current experimental work uses stainless steel wire mesh with an average packing surface area of 2700 m^2 m^{-3}. It indicates that the correlation might need to consider packing-specific parameters and system independence.

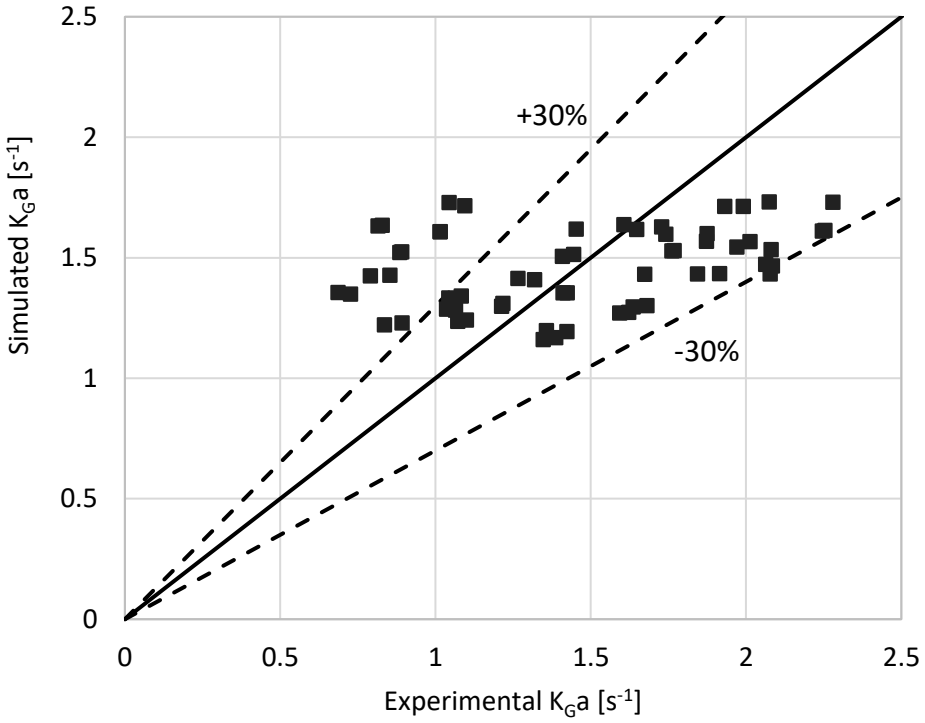

Figure 5.3: Parity plot for simulated K_Ga-value using the Mondal et al. model (Equation 5.4) and the experimental K_Ga -value for Knit Mesh (KM), Metal Foam (MF), and Empty Rotor (ER). Rotor-1: OD 0.4 m, F-factor: 2.1 $Pa^{0.5}$ and 2.8 $Pa^{0.5}$. c_1 = 0.73, c_2=0.23, c_3=0.08.

Sudhoff et al. [54] suggested the use of integrated centrifugal acceleration ($a_{c,int}$) as shown in Equation (5.5), instead of using average centrifugal accelaration ($a_{c,avg}$) to take the rotor volume into account since two completely different rotors may have the same mean centrifugal acceleration. The limitation with this approach is that it still does not incorporate the effects of casing or different packing geometries. In this regard, the approach suggested by Groß et al. [67] is used as shown in section 5.2 and Table 5.1.

$$a_{c,int} = \int_{0}^{2\pi} \int_{ri}^{ro} a_c r \, dr \, d\varphi \tag{5.5}$$

Furthermore, an equivalence is developed to use a system-independent description according to Sudhoff [54] by using the ratio of the relative volatility of the current chemical system (α) to the relative volatility of the reference chemical system (α_{ref}), Equation (5.6). 1.79 is the average relative volatility value for the methanol-ethanol system (Appendix A-8, Table 10.5) and is considered a reference value [88].

$$K_G a = c_1 \frac{\alpha}{\alpha_{ref}} (F_{factor})^{c_2} (a_{c,int})^{c_3} \tag{5.6}$$

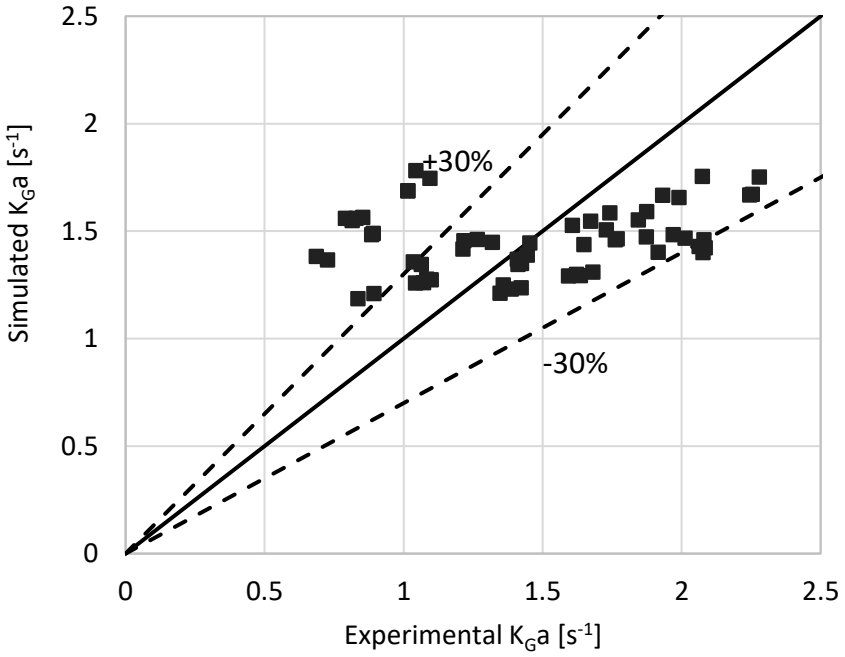

Figure 5.4: Parity plot for simulated K_Ga-value using the Mondal et al. model with modification as per Equation 5.5 [54] and the experimental K_Ga for KM, MF, and ER. Rotor-1: OD 400 mm, F-factor: 2.1 $Pa^{0.5}$ and 2.8 $Pa^{0.5}$. c_1 = 0.86, c_2=0.56, c_3=0.05.

With the modifications suggested in the literature, the K_Ga model still overpredicts the K_Ga values beyond the ±30% error margin (Figure 5.4). It indicates that the effects of rotational speed and F-factor are not uniform across the vapor-side mass transfer coefficient for different packing types and lengths. Table 5.2 shows the individual values of constants fitted for each packing type/rotor configuration separately, and the resulting correlation can predict the experimental K_Ga value within a ±20% error range (Figure 5.5).

Table 5.2: Regression constants of Equation (5.4) for different rotor configurations of RPB.

	L_{pack} [m]	C_1	C_2	C_3
Empty Rotor (ER)	0	0.23	0.92	0.17
Knit Mesh (KM)	0.18	0.23	0.81	0.09
Metal Foam (MF)	0.19	0.33	0.95	0.13
Metal Foam (MF)	0.125, 0.1	0.65	0.64	0.11

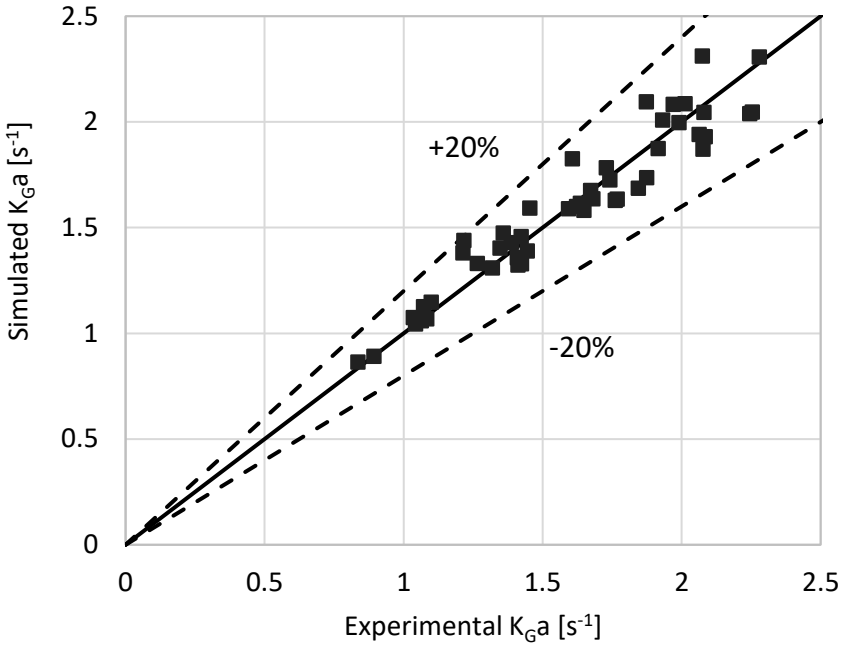

Figure 5.5: Parity plot for simulated $K_G a$-value using Equation 5.5 with modification as per Equation 5.6, with constants fitting for each configuration, and the experimental $K_G a$ -value for Knit Mesh (KM), Metal Foam (MF), and Empty Rotor (ER). Rotor-1: OD 400 mm, F-factor: 2.1 $Pa^{0.5}$ and 2.8 $Pa^{0.5}$.

The influence of the F-factor appears to be more prominent on the overall volumetric mass transfer coefficient than centrifugal acceleration (Table 5.2). Moreover, the mass transfer coefficient values for metal foam are more strongly influenced by centrifugal acceleration than those for knit mesh. Similarly, comparing metal foam with varying packing length, the F-factor has a greater influence on $K_G a$ values at larger packing lengths. The improvement in the estimation of $K_G a$ by individually fitting the constants for each packing type and packing length, which indicates that incorporating the packing-related parameters into the correlations will result in a more realistic estimation of the mass transfer coefficient.

Chapter 6 Key Design and Operation Findings for Distillation in RPBs

The chapters on mass transfer (Chapter 3), temperature profile (Chapter 4), and modeling (Chapter 5) serve as a reference for establishing scaling and operational key learnings for distillation in RPBs. Figure 6.1 summarizes the design and operation parameters investigated in this work.

6.1. Overview of Parameters Investigated in this Work

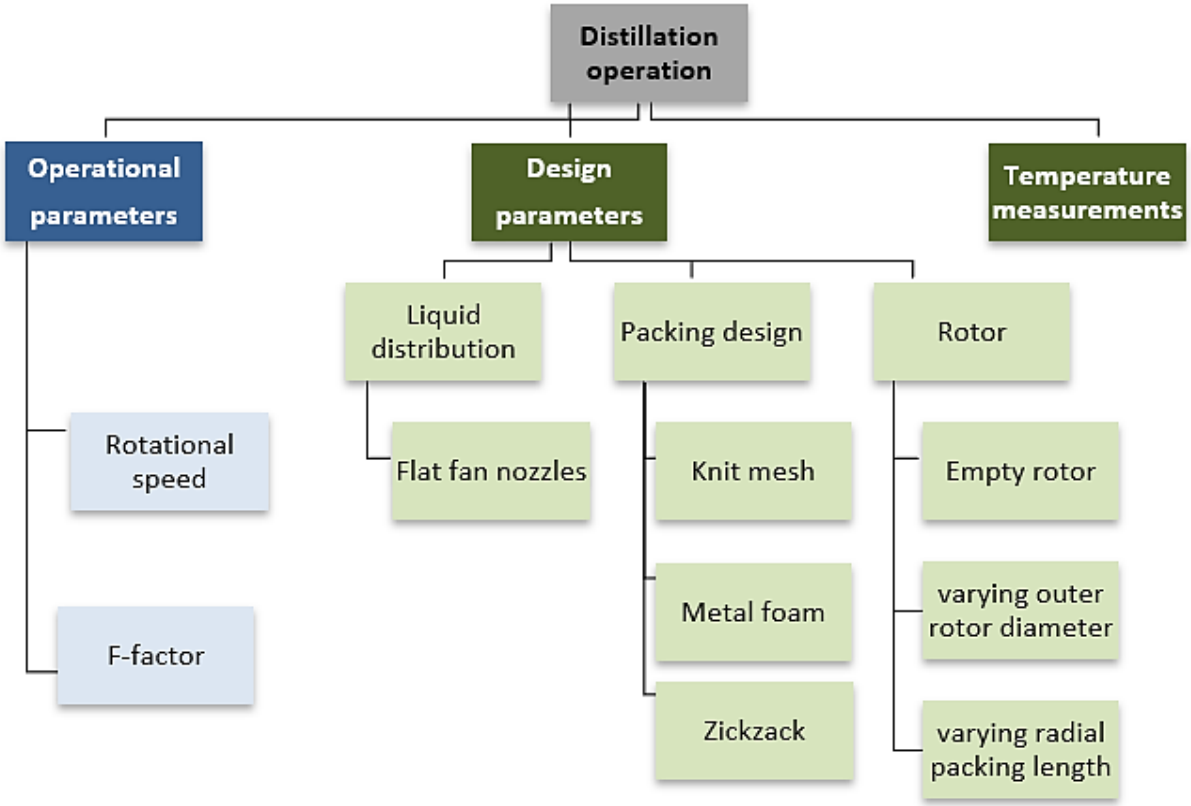

Figure 6.1: Overview of operational and design parameters investigated in RPB

The mass transfer investigations for distillation in RPBs are summarised in Table 6.1 based on the experiments performed with:

(1) chemical system: Ethanol-water
(2) total reflux conditions at 1.01 bar pressure
(3) nozzle type: flat fan nozzles,
(4) packing types: metal knit mesh, metal foam, Zickzack packing, and empty rotor,
(5) packing axial height: 0.01 m,
(6) F-factor at the inner packing radius: 1.2 – 2.8 $Pa^{0.5}$
(7) Rotational speed: 181 min^{-1} – 900 min^{-1}

Table 6.1: Summary of the mass transfer investigations in RPB

OPERATIONAL PARAMETERS	
Rotational speed	**Literature Results** • Generally, it is found that the separation efficiency (measured in terms of the number of theoretical stages, Nth, or overall volumetric mass transfer coefficient, $K_G a$) increases with increasing rotational speed. • At higher rotational speeds, some authors report a flattening effect [1,67,84] while others report a slight decrease [14,27,53] in separation efficiency as rotational speed increases further. • Increasing rotational speed widens the operating range of RPB for vapor and liquid loads. The operating ranges depend on various RPB internals, like distributor and packing types [66]. **Experimental Results [43,86]** • Experimental investigations showed that increasing the rotational speed increases the separation efficiency to the optimal rotational speed, n_{optm} (which gives the maximum Nth for a given rotor configuration). Increasing the rotational speed above n_{optm} either slightly reduces separation efficiency or has no effect, depending on the rotor configuration. • For an empty rotor (rotating disks without packing), n_{optm} is generally higher than for a rotor with packing. In addition, the separation efficiency curve almost flattens after n_{optm}. • For rotors packed with knit mesh or metal foam, increasing the rotational speed beyond noptm does not increase the separation efficiency; rather, the detrimental effect is slightly pronounced beyond n_{optm}. • Increasing the F-factor to 2.8 Pa0.5 shifts the optimum rotational speed from 300 to 900 rpm; i.e., the higher the F-factor, the higher the n_{optm}.

	Summary ➢ RPBs offer greater flexibility than conventional columns. Depending on the rotor configuration, the rotational speed can be adjusted to influence separation efficiency and the operating range. In a separation task, choices could be made between a higher rotational speed with minimal to no packing and a lower rotational speed with greater packing volume in the rotor.
Vapor/Liquid flow rates (F-factor)	**Literature Results** • The separation efficiency (Nth) increases with increasing F-factor to a certain extent for a given rotational speed, with a constant Nth/HETP value after a specific value of F-factor [8]. • Some authors report a detrimental effect on separation efficiency when the F-factor is increased after a specific value [1,27]. These results are similar to conventional columns, which often dictate the column's operating limit. However, RPB offers to extend this operating limit by increasing the rotational speed. **Experimental Results** For a pilot-scale RPB, and with the above-mentioned experimental set-up and conditions, the following limits are observed: • At lower rotational speeds of up to 300 rpm, the separation efficiency (Nth values) decreases by increasing the F-factor from 2.1 $Pa^{0.5}$ to 2.8 $Pa^{0.5}$ for all rotor configurations. • At higher rotational speeds (600 rpm and above), the following is observed: o Rotor-1 (0.4 m OD): ▪ An empty rotor offers a very slight increase in Nth values with increasing F-factor until it becomes constant. A maximum of

	1.6 theoretical stages is achieved at 900 rpm with an F-factor of up to 2.8 $Pa^{0.5}$ ▪ Knit mesh packing shows an increase in Nth values up to an F-factor of 2.1 $Pa^{0.5}$. Further increasing the F-factor shows a slight decrease or flattening of the trend for 600 rpm and 900 rpm, respectively. A maximum of 2.6 Nth is achieved at 600 rpm and 2.1 $Pa^{0.5}$ F-factor. Moreover, entrainment is observed at 2.8 $Pa^{0.5}$ for rotational speeds less than 300 rpm. ▪ Metal foam shows a similar trend to knit mesh packing; however, only flattening of the Nth curve is observed with further increase in the F-factor to more than 2.1 $Pa^{0.5}$. A maximum of almost 3.2 theoretical stages is acquired at 600 rpm and F-factors of 2.1 $Pa^{0.5}$ and 2.8 $Pa^{0.5}$. o Rotor-2 (0.6 m OD): ▪ An empty rotor shows a clear increase in Nth values with increasing F-factor. Under the investigated conditions, the limit/flattening was not observed in the Nth values as the F-factor increased. A maximum of 2.4 theoretical stages is achieved at 600 rpm and 900 rpm at an F-factor of up to 2.8 Pa0.5, with an increasing tendency beyond 2.8 $Pa^{0.5}$. ▪ Knit mesh packing shows an increase in Nth values with increasing F-factor, especially from 2.1 $Pa^{0.5}$ to 2.8 $Pa^{0.5}$ at the same rotational speed. A maximum of 2.8 Nth is achieved. **Summary** ➢ Increasing F-factor or vapor/liquid load can be processed in RPBs efficiently using one or a combination of the following operational and design parameters: (1) higher rotational speed and/or (2) using another packing type, for instance, metal foam instead of knit mesh.

DESIGN PARAMETERS	
Radial packing length, rotor outer diameter	**Literature Results** Most of the results available are from absorption/desorption studies. The radial packing length significantly influences the mass transfer coefficient, and the change is nonlinear [67,84]. A smaller packed bed showed a higher mass transfer coefficient value [84]. **Experimental Results [61]** • For an empty rotor, increasing the rotor surface area by 2.4 times improves the separation efficiency (Nth) by almost 83% at lower rotational speeds (300 rpm) and by nearly 36% at higher rotational speeds (900 rpm). The percentage improvement mentioned above is an average value of all the investigated F-factors. • For a rotor with knit mesh packing, increasing the packing's geometrical surface area by three times increases the Nth values by only 16%, indicating the need for packing design improvement. • For a rotor packed with metal foam, increasing the radial packing length by almost 100% increases the Nth values from 41% to nearly 50%, depending upon rotational speed. Increasing the packing area for mass transfer at lower rotational speeds is more significant for separation efficiency. The impact of increased packing/rotor surface area weakens with increasing rotational speed. • The mass transfer coefficient decreases nonlinearly with increasing radial packing length in metal foam. **Summary** ➢ A trade-off exists between the rotor size and the rotational speed. The rotor size should be chosen as large as necessary to meet the purity constraints and as small as possible to minimize power consumption.

Packing type	**Literature Results** There is a lack of experimental studies comparing conventional RPB packing types under similar design and operating conditions. Loll et al. showed in a deaeration study comparable mass transfer performance of metal foam packing with double-sealed Zickzack packing at a liquid flow rate of 0.48 m^3/h and a slightly higher mass transfer coefficient (higher by a value of 0.3 – 0.5 s^{-1}) of double-sealed Zickzack packing at higher rotational speed (> 900 rpm) and a liquid flow rate of 0.96 m^3/h [48]. The advantage of double-sealed Zickzack packing comes at the cost of a slightly higher pressure drop. Another deaeration study showed comparable performance between metal foam and knit mesh packing at lower liquid flow rates (0.48 m3/h); however, metal foam performed slightly better at higher liquid flow rates (0.96 m^3/h) [109]. **Experimental Results [43]** • Knit mesh provides slightly better separation efficiency at lower vapor-liquid loads (F-factor 1.2 $Pa^{0.5}$) than the metal foam. • Metal foam offers significantly higher separation efficiency than knit mesh at F-factors higher than 2 $Pa^{0.5}$. • The handling and reproducibility of experimental results with metal foam are more straightforward than with knit mesh. • Similar to the design of a Rotating zigzag bed (RZB)[3], an innovative packing design, Zickzack packing, was developed in this study for RPBs. Based on initial prototype test runs, the Zickzack packing with L-shaped baffles demonstrated a separation efficiency approximately 0.3–0.4 theoretical stages higher than that achieved with knit mesh packing. Compared with RZB, a similar separation efficiency can be achieved with a pressure drop that is almost 10 times lower. • In addition, the design of Zickzack packing might facilitate the development of scale-up rules, given its flexibility in maintaining a constant cross-sectional area between the baffles. An HETP value of 5.3

	cm was determined from the experimental investigations, resulting in a 7– 10-fold reduction in size compared to conventional columns packed with Raschig super ring metal and HOLPACK. **Summary** ➢ The packing design plays an essential role in determining the separation efficiency. Conventional knit mesh packing provides higher separation efficiency than metal foams at lower F-factors; however, metal foams are superior for mass transfer at higher F-factors. Extending the packing depth of conventional packing types does not maintain separation performance as measured by HETP or Nth. Zickzack packings or similar packing designs with constant cross-sectional area are likely better for developing reliable design rules for RPB packings. Other than that, a multi-rotor could be an option for scaling RPBs.
Mass transfer distribution (Temperature measurements, Rotor telemetry)	**Literature Results** A physical absorption study showed that the end-zone contributes the most to the total mass transfer [55]. A distillation study with metal foam showed that the casing contribution was equivalent to 0.86 theoretical stages and that mass transfer rates decreased with increasing radial position, i.e., the outer regions of the packing showed lower separation efficiency [87]. Moreover, varying radial packing length does not affect the local separation performance inside the packing [110]. **Experimental Results [103]** • The rotor telemetry proves that the total mass transfer in an RPB does not occur only in the rotating packing; instead, the overall mass transfer in an RPB is the sum of mass transfer in different sections (casing and packing) of the RPB.

	• Investigations with temperature sensors along the rotor indicate that the packing contribution accounts for 56–78% of the total mass transfer in an RPB, depending on the rotational speed. • Results of knit mesh packing with rotor telemetry showed a maximum local separation efficiency at the middle of the rotor at higher rotational speeds, with a slight decrease towards the rotor outer radius. For lower rotational speeds, considering the error margins, the local separation efficiency appears to be almost constant along the radial length of the packing. • The calculation of the local mass transfer coefficient, $k_g a$, in the rotor shows an almost constant value along the radial packing length (taking error margins into account) with a slight decrease in $k_g a$ towards the outer packing radius. • Increasing the rotational speed does not appear to improve the local separation efficiency of the rotor/packing; instead, a declining trend is observed. • The qualitative comparison of the radial separation efficiency of Zickzack packing with the knit mesh packing showed that Zickzack provides higher separation efficiency at the inner radius of the rotor. It appears to maintain a constant separation throughout the packing, thereby supporting the hypothesis that improved packing design, providing homogeneous conditions, is necessary for easy scaling up. • The casing (or cavity zone) of the RPB is found to contribute almost a maximum of one theoretical stage to the total separation efficiency found in an RPB. **Summary** ➢ Packing scale-up must be done carefully. At an optimal rotational speed, excluding the casing contribution to the overall mass transfer and assuming homogeneous hydrodynamic conditions in the packing, might help develop a more reliable scale-up and design rule for the packing.

Supporting Information

[1] T. Kelleher, J.R. Fair, Distillation studies in a high-gravity contactor, (1996).

[8] A. Mondal, A. Pramanik, A. Bhowal, S. Datta, Distillation studies in rotating packed bed with split packing, (2012).

[14] G.E. Cortes Garcia, J. van der Schaaf, A.A. Kiss, A review on process intensification in HiGee distillation, J. Chem. Technol. Biotechnol. 92 (2017) 1136–1156.

[27] G.Q. Wang, O.G. Xu, Z.C. Xu, J.B. Ji, New HIGEE-Rotating Zigzag Bed and Its Mass Transfer Performance, (2008).

[28] G.Q. Wang, Z.C. Xu, Y.L. Yu, J.B. Ji, Performance of a rotating zigzag bed—A new HIGEE: (2008).

[43] H. Qammar, K. Gładyszewski, A. Górak, M. Skiborowski, Towards the Development of Advanced Packing Design for Distillation in Rotating Packed Beds, (2019).

[53] Y. Luo, G.-W. Chu, H.-K. Zou, Y. Xiang, L. Shao, J.-F. Chen, Characteristics of a two-stage counter-current rotating packed bed for continuous distillation, (2012).

[61] H. Qammar, Rotating Packed Beds in Distillation: Binary Distillation, in: M. Skiborowski, A. Górak (Eds.), (2022).

[66] K. Neumann, S. Hunold, K. Groß, A. Górak, Experimental investigations on the upper operating limit in rotating packed beds, (2017).

[67] K. Groß, M. de Beer, S. Dohrn, M. Skiborowski, Scale-Up of the Radial Packing Length in Rotating Packed Beds for Deaeration Processes, (2020).

[11] M. Hilpert, G.U. Calvillo Aranda, J.-U. Repke, Experimental analysis and rate-based stage modeling of multicomponent distillation in a Rotating Packed Bed, (2021).

[84] Y.S. Chen, C.C. Lin, H.S. Liu, Mass Transfer in a Rotating Packed Bed with Various Radii of the Bed, (2005).

[85] R. Loll, L. Nordhausen, A. Bieberle, M. Schubert, T. Pyka, J. Koop, C. Held, G. Schembecker, Analysis of Flow Patterns in Structured Zickzack Packings for Rotating Packed Beds Using γ-Ray Computed Tomography, (2023).

[86] H. Qammar, F. Hecht, M. Skiborowski, A. Górak, Experimental Investigation and Design of Rotating Packed Beds for Distillation, (2018).

[103] H. Qammar, T. Pyka, J. Koop, A. Górak, G. Schembecker, Radial Temperature Profile Measurements to Understand Mass Transfer in Rotating Packed Bed Distillation, (2023).

[109] K.M. Groß, Deaeration in Rotating Packed Beds, PH.D. thesis, (2021).

[110] A. Ressemann, M. Illner, J.U. Repke, Local Separation Performance for Distillation Processes in Rotating Packed Beds: Transferability and Applicability, (2024).

Chapter 7 Conclusion

The use of centrifugal forces has proven promising, providing process intensification in separation processes to address current challenges in the chemical and biochemical industries. In this regard, RPB technology has been gaining interest; however, there is limited knowledge, especially regarding distillation in RPBs, due to the operation's complexity, and very few studies have been found on this topic. Issues such as the performance evaluation and comparison of conventional packing types with a consistent experimental setup and conditions, limitations of traditional RPB packings, limited knowledge of local mass transfer inside the packing, and scaling of RPB packings are not adequately addressed in the literature. Therefore, this work addresses this gap and evaluates RPBs for distillation. The chapters of this work addressed the results of the experimental investigations regarding the mass transfer performance of various packings, local radial temperature profile and local mass transfer performance, operating range, packing design, and modeling of mass transfer, and eventually, a database is built for the comparison of different rotor configurations and compared to the conventional distillation column to evaluate the potential of RPBs for distillation. This study is expected to serve as a basis for future developments in this field. The summary of the different chapters of this work is presented in the following paragraphs.

Firstly, the experimental setup was built to investigate different rotor configurations (internals) and their influence on separation efficiency. The ethanol-water system, one of the most widely used systems for distillation in RPBs, was investigated as part of a mass transfer study. The highest F-factor of up to 2.8 $Pa^{0.5}$ could be investigated, which is a commonly used load range for column packings. The flexibility of RPB operation was demonstrated by varying vapor loads (F-factor) and adjusting the rotational speed to meet specifications, illustrating the degree of freedom in RPB that can be used to accommodate operational changes quickly.

Secondly, experimental data were generated using a consistent RPB design and operation to compare the separation efficiency of metal foam and knit mesh. The results helped develop an innovative packing design, known as zickzack packing. Metal foam is found to be superior in terms of handling and separation efficiency at higher vapor loads. The test runs on the zickzack prototype showed an improved performance due to better liquid redistribution and more

homogeneous hydrodynamic conditions. The empty rotor showed a high mass transfer performance; however, applying knit mesh or metal foam packing also contributed significantly to the overall mass transfer.

Thirdly, packing scale-up experiments with different packing lengths and rotor outer diameters revealed a non-linear relationship between separation efficiency and rotor length, indicating that care must be taken when scaling the packing. Comparison with conventional columns showed that RPBs could reduce equipment size by 7–10 times, based on the current study.

To support the packing scaling, the investigations using rotor telemetry, one of the first studies of its kind in RPBs, were conducted, which enabled the estimation of local mass transfer inside the packing and revealed the contribution of the packing and casing to the total mass transfer in an RPB. These investigations offer insights into the packing necessary for establishing consistent mass transfer along the rotor and utilizing the increasing packing volume on the outer side of the rotor more effectively. The qualitative analysis of zickzack packing and knit mesh packing using rotor telemetry revealed that improving packing design facilitates more homogeneous and consistent mass transfer throughout the radial length of the packing, whereas knit mesh showed a maximum near the middle of the rotor.

Finally, the experimental evaluation of the overall vapor-side volumetric mass transfer coefficient with varying radial lengths of metal foam showed that the mass transfer coefficient is variable and not constant along the radial packing length. The mass transfer performance can be estimated using Mondal et al.'s modified mass transfer correlation [8], with an estimated error of approximately ±30%. Although the original correlation of Mondal et al. [8] was further developed by Sudhoff et al. [54] by incorporating the independence of the chemical test system and rotor volume, the correlation still requires consideration of packing-specific properties for a more realistic estimation.

Chapter 8 Outlook

This work makes a substantial contribution to the fundamental understanding of distillation in RPBs. The significant outcomes of the investigations are summarized in Chapter 6. They support RPB operation for distillation. An investigation of different rotor configurations and a first step towards estimating local mass transfer in the packing using rotor telemetry was conducted in this thesis. Nonetheless, promising avenues for future study remain.

The experimental database could be expanded further, including

- other standard chemical systems like ethanol-propanol, chlorobenzene-ethylbenzene,
- other types of liquid distributors,
- dedicated experiments with newly developed zickzack packing to quantitatively evaluate the mass transfer improvement potential,
- experiments using rotor telemetry with other packing types like metal foam, Zickzack,
- multirotor operation to help scale up RPB for distillation.

Furthermore, by expanding the database, the mass transfer correlation can be improved by incorporating packing- and casing-specific parameters and validating the results via dedicated experiments. Further validation of the assumption of no backmixing and the promising applications of RPB, such as handling heat-sensitive and fouling or dirty fluids, would help promote this technology in the chemical industry.

Chapter 9 References

[1] T. Kelleher, J.R. Fair, Distillation studies in a high-gravity contactor, Ind. Eng. Chem. Res. 35 (1996) 4646–4655.

[2] H.-S. Liu, C.-C. Lin, S.-C. Wu, H.-W. Hsu, Characteristics of a Rotating Packed Bed, Ind. Eng. Chem. Res. 35 (1996) 3590–3596.

[3] National Research Council (U.S.), ebrary, Inc, Separation technologies for the industries of the future, Publication NMAB 487-3, National Academy Press, Washington, D.C., 1998.

[4] X.P. Li, Y.Z. Liu, Z.Q. Li, X. Wang, Continuous Distillation Experiment with Rotating Packed Bed, Chin. J. Chem. Eng. 16 (2008) 656–662.

[5] J.V.S. Nascimento, T.M.K. Ravagnani, J.A.F.R. Pereira, Experimental study of a rotating packed bed distillation column, Braz. J. Chem. Eng. 26 (2009) 219–226.

[6] M. Jobson, Chapter 6 - Energy Considerations in Distillation, in: A. Górak, E. Sorensen (Eds.), Distillation, Academic Press, Boston, 2014, pp. 225–270.

[7] P. Lutze, R. Gani, J.M. Woodley, Process Intensification: A Perspective on Process Synthesis, Elsevier BV, 2010.

[8] A. Mondal, A. Pramanik, A. Bhowal, S. Datta, Distillation studies in rotating packed bed with split packing, Chem. Eng. Res. Des. 90 (2012) 453–457.

[9] H. Zhao, L. Shao, J.-F. Chen, High-gravity process intensification technology and application, Chem. Eng. J. 156 (2010) 588–593.

[10] D. Zhang, P. Y. Zhang, H. K. Zou, G. W. Chu, W. Wu, Z. W. Zhu, L. Shao, J. F. Chen, Application of HIGEE process intensification technology in synthesis of petroleum sulfonate surfactant, Chemical Engineering and Processing: Process Intensification 49 (2010) 508–513.

[11] M. Hilpert, G.U. Calvillo Aranda, J.-U. Repke, Experimental analysis and rate-based stage modeling of multicomponent distillation in a Rotating Packed Bed, Chemical Engineering and Processing - Process Intensification (2021) 108651.

[12] M. Hilpert, J.-U. Repke, Experimental Investigation and Correlation of Liquid-Side Mass Transfer in Pilot-Scale Rotating Packed Beds, Ind. Eng. Chem. Res. 60 (2021) 5251–5263.

[13] G.Q. Wang, Z.C. Xu, J.B. Ji, Progress on Higee distillation—Introduction to a new device and its industrial applications, Chem. Eng. Res. Des. 89 (2011) 1434–1442.

[14] G.E. Cortes Garcia, J. van der Schaaf, A.A. Kiss, A review on process intensification in HiGee distillation, J. Chem. Technol. Biotechnol. 92 (2017) 1136–1156.

[15] D.P. Rao, A. Bhowal, P.S. Goswami, Process Intensification in Rotating Packed Beds (HIGEE): An Appraisal, Ind. Eng. Chem. Res. 43 (2004) 1150–1162.

[16] L. Agarwal, V. Pavani, D.P. Rao, N. Kaistha, Process intensification in HiGee absorption and distillation: Design procedure and applications, Ind. Eng. Chem. Res. 49 (2010) 10046–10058.

[17] D.P. Rao, The Story of "HIGEE", Indian Chem. Eng. 57 (2015) 282–299.

[18] K. Neumann, K. Gladyszewski, K. Groß, H. Qammar, D. Wenzel, A. Górak, M. Skiborowski, A guide on the industrial application of rotating packed beds, Chem. Eng. Res. Des. 134 (2018) 443–462.

[19] Podbielniak W. J., US2004011, 1935.

[20] W. Pilo, W. Dahlbeck, Apparatus for intimate contacting of two fluid media having different specific weight: US81919159A (1960).

[21] C. Ramshaw, R.H. Mallinson, US 4283255, 1981.

[22] C.C. Lin, T.J. Ho, W.T. Liu, Distillation in a rotating packed bed, J. Chem. Eng. Jpn. 35 (2002) 1298–1304.

[23] K. Neumann, S. Hunold, M. de Beer, M. Skiborowski, A. Górak, Mass Transfer Studies in a Pilot Scale RPB with Different Packing Diameters, Ind. Eng. Chem. Res. 57 (2018) 2258–2266.

[24] Y. Luo, G. Chu, L. Sang, H. Zou, Y. Xiang, J. Chen, A two-stage blade-packing rotating packed bed for intensification of continuous distillation, Chin. J. Chem. Eng. 24 (2016) 109–115.

[25] C.-C. Lin, Y.-C. Lin, K.-S. Chien, VOCs absorption in rotating packed beds equipped with blade packings, J. Ind. Eng. Chem. 15 (2009) 813–818.

[26] X.P. Li, Y.Z. Liu, Characteristics of Fin Baffle Packing Used in Rotating Packed Bed, Chin. J. Chem. Eng. 18 (2010) 55–60.

[27] G.Q. Wang, O.G. Xu, Z.C. Xu, J.B. Ji, New HIGEE-Rotating Zigzag Bed and Its Mass Transfer Performance, Ind. Eng. Chem. Res. 47 (2008) 8840–8846.

[28] G.Q. Wang, Z.C. Xu, Y.L. Yu, J.B. Ji, Performance of a rotating zigzag bed—A new HIGEE: Process Intensification, Chem. Eng. Process. 47 (2008) 2131–2139.

[29] Y.M. Li, Y. Yuli, Z. Xuli, X. Lili, X. Liu, J.B. Ji, Rotating zigzag bed as trayed HIGEE and its power consumption, Asia-Pac. J. Chem. Eng (2012).

[30] A. Stankiewicz, T. van Gerven, G. Stefanidis, The fundamentals of process intensification, Wiley-VCH Verlag GmbH & Co, Weinheim, Germany, 2019.

[31] M. Skiborowski, A. Górak (Eds.), Process Intensification, De Gruyter, 2022.

[32] H.J. Teuteberg, G. Wiegelmann, Unsere tägliche Kost: Studien zur Geschichte d. Alltags, 2. Aufl. ed., Studien zur Geschichte des Alltags 6, Coppenrath, Münster, 1986.

[33] G.A. Bachmann, US544080A - Centrifugal filtering-machine, 1895, https://patents.google.com/patent/US544080A#citedBy, accessed 23 September 2024.

[34] A. Stankiewicz, J.A. Moulijn, Re-engineering the chemical processing plant: Process intensification, New York, 2004.

[35] A. Stankiewicz, J.A. Moulijn, Re-engineering the chemical processing plant: Process intensification, Chemical industries 98, M. Dekker, New York, 2003.

[36] C. Ramshaw, K. Arkley, PROCESS INTENSIFICATION BY MINIATURE MASS TRANSFER, Process Eng. 64 (1983).

[37] P. Lutze, A. Górak, Reactive and Membrane-Assisted Separations, De Gruyter Graduate, De Gruyter, Berlin, Boston, 2016.

[38] J.A. Moulijn, A. Stankiewicz, J. Grievink, A. Gorak, Process intensification and process system engineering: a friendly symbiosis, in: W. Marquardt, C. Pantelides (Eds.), Computer Aided Chemical Engineering 16th European Symposium on Computer Aided Process Engineering and 9th International Symposium on Process Systems Engineering, Elsevier, 2006, pp. 29–37.

[39] G.Q. Wang, Xu, Z.C., Ji, J.B., Progress on Higee distillation—Introduction to a new device and its industrial applications, Chem. Eng. Res. Des. 89 (2011) 1434–1442.

[40] Y. Li, X. Li, Y. Wang, Y. Chen, J. Ji, Y. Yu, Z. Xu, Distillation in a Counterflow Concentric-Ring Rotating Bed, Ind. Eng. Chem. Res. 53 (2014) 4821–4837.

[41] I. Lukin, K. Gładyszewski, M. Skiborowski, A. Górak, G. Schembecker, Aroma absorption in a rotating packed bed with a tailor-made archimedean spiral packing, Chemical Engineering Science 231 (2021) 116334.

[42] Y. Liu, D. Gu, C. Xu, G. Qi, W. Jiao, Mass transfer characteristics in a rotating packed bed with split packing, Chin. J. Chem. Eng. 23 (2015) 868–872.

[43] H. Qammar, K. Gładyszewski, A. Górak, M. Skiborowski, Towards the Development of Advanced Packing Design for Distillation in Rotating Packed Beds, Chem. Ing. Tech. 91 (2019) 1663–1673.

[44] T. Pyka, M. Brunert, J. Koop, A. Bieberle, C. Held, G. Schembecker, Novel Liquid Distributor Concept for Rotating Packed Beds, Ind. Eng. Chem. Res. 62 (2023) 5984–5994.

[45] T. Pyka, V. Backhaus, C. Held, G. Schembecker, Impact of Number of Rotors in Rotating Packed Beds on Separation Performance in Distillation, Ind. Eng. Chem. Res. 62 (2023) 19855–19861.

[46] Y.L. Yu, Z.C. Xu, G.Q. Wang, J.B. Ji, A New Type and High Efficiency Distillation Apparatus - Zigzag Rotating Bed, Bull. Science Techn. 01 (2008).

[47] Xu, Z. C., Ji, J. B., Wang, G., Li, X. H., Li, Y., Rotating Zigzag Bed Application in Extractive Distillation Process of THF-Methanol-Water System, Mod. Chem. Ind. (China) 32 (2012) 94–96.

[48] R. Loll, L. Runge, J. Koop, C. Held, G. Schembecker, Zickzack Packings for Deaeration in Rotating Packed Beds─Improved Rotor Design to Counter Bypass Flows, Ind. Eng. Chem. Res. 61 (2022) 11934–11946.

[49] Hangzhou Hecci Technology Co., Ltd, Distillation expert in the fine chemical and pharmaceutical industries: Manufacturer, https://www.globalsources.com/si/AS/Hangzhou-Hecci/6008850191753/Homepage.htm, accessed 13 July 2021.

[50] C. Ramshaw, 'HIGEE' Distillation - An Example of Process Intensification, Chem. Eng. (London) 389 (1983) 13–14.

[51] C. Ramshaw, The Opportunities for Explaoiting Centrifugal Fields, Printed in Great Britain, Heat Recovery Syst. CHP. 13 (1993) 493–513.

[52] A. Chandra, P.S. Goswami, D.P. Rao, Characteristics of Flow in a Rotating Packed Bed (HIGEE) with Split Packing, Ind. Eng. Chem. Res. 44 (2005) 4051–4060.

[53] Y. Luo, G.-W. Chu, H.-K. Zou, Y. Xiang, L. Shao, J.-F. Chen, Characteristics of a two-stage counter-current rotating packed bed for continuous distillation, Chemical Engineering and Processing - Process Intensification 52 (2012) 55–62.

[54] D. Sudhoff, M. Leimbrink, M. Schleinitz, A. Górak, P. Lutze, Modelling, design and flexibility analysis of rotating packed beds for distillation, Chemical Engineering Research and Design 94 (2015) 72–89.

[55] F. Guo, C. Zheng, K. Guo, Y. Feng, N.C. Gardner, Hydrodynamics and mass transfer in cross-flow rotating packed bed, Chem. Eng. Sci. 52 (1997) 3853–3859.

[56] C. Zheng, K. Guo, Y. Song, X. Zhou, D. Al, Z. Xin, N.C. Gardner, Industrial practice of HIGRAVITEC in water deaeration, 2nd International Conference on Process Intensification in Practice / applications and opportunities (1997) 273–288.

[57] J. Peel, C.R. Howarth, C. Ramshaw, Process Intensification: Higee Seawater Deaeration, Chem. Eng. Res. Des. 76 (1998) 585–593.

[58] Harbold, G., Park, J., Using the GasTran® Deaeration System to achieve low dissolved oxygen levels for superior line speed and product quality: a case study in carbonated soft drink bottling, 7th International Conference on Process Intensification (2008).

[59] D. Wenzel, N. Gerdes, M. Steinbrink, L.S. Ojeda, A. Górak, Liquid Distribution and Mixing in Rotating Packed Beds, Ind. Eng. Chem. Res. 58 (2019) 5919–5928.

[60] J. Chen, Y.Z. Liu, X.P. Li, Distillation process of methanol in rotating packed bed, Chem. Ind. Eng. Prog. 28 (2009) 1333.

[61] H. Qammar, Rotating Packed Beds in Distillation: Binary Distillation, in: M. Skiborowski, A. Górak (Eds.), Process Intensification, De Gruyter, 2022, pp. 159–188.

[62] Olajide Otitoju, Eni Oko, Meihong Wang, Modelling, scale-up and techno-economic assessment of rotating packed bed absorber for CO2 capture from a 250 MWe combined cycle gas turbine power plant, Applied Energy 335 (2023) 120747.

[63] Carbon clean, Introducing CycloneCC™: Effective, efficient carbon capture technology, 2021, https://www.carbonclean.com/insights/efficient-carbon-capture, accessed 23 January 2024.

[64] S.P. Singh, J.H. Wilson, R.M. Counce, A.J. Lucero, G.D. Reed, R.A. Ashworth, M.G. Elliott, Removal of volatile organic compounds from groundwater using a rotary air stripper, Ind. Eng. Chem. Res. 31 (1992) 574–580.

[65] K. Neumann, S. Hunold, M. Skiborowski, A. Górak, Dry Pressure Drop in Rotating Packed Beds—Systematic Experimental Studies, Ind. Eng. Chem. Res. 56 (2017) 12395–12405.

[66] K. Neumann, S. Hunold, K. Groß, A. Górak, Experimental investigations on the upper operating limit in rotating packed beds, Chem. Eng. Process. 121 (2017) 240–247.

[67] K. Groß, M. de Beer, S. Dohrn, M. Skiborowski, Scale-Up of the Radial Packing Length in Rotating Packed Beds for Deaeration Processes, Ind. Eng. Chem. Res. 59 (2020) 11042–11053.

[68] Gross Kai, Neumann Kolja, Skiborowski Mirko, Gorak Andrzej, Analyzing the operating limits in high gravity equipment, CHEMICAL ENGINEERING TRANSACTIONS 69 (2018) 661–666.

[69] K. Guo, J. Wen, Y. Zhao, Y. Wang, Z. Zhang, Z. Li, Z. Qian, Optimal packing of a rotating packed bed for H(2)S removal, Environmental science & technology 48 (2014) 6844–6849.

[70] T.-Y. Guo, K.-P. Cheng, L.-X. Wen, R. Andersson, J.-F. Chen, Three-Dimensional Simulation on Liquid Flow in a Rotating Packed Bed Reactor, Ind. Eng. Chem. Res. 56 (2017) 8169–8179.

[71] M.J. Lockett, Flooding of rotating structured packing and its application to conventional packed columns, Chem. Eng. Res. Des. 73 (1995) 379–384.

[72] M.J. Lockett, D.P. Rao, Evaluation of Higee for distillation, in: AIChE (Ed.), Annual Meeting 2006, 2006.

[73] K. Guo, Z. Zhang, H. Luo, J. Dang, Z. Qian, An Innovative Approach of the Effective Mass Transfer Area in the Rotating Packed Bed, Ind. Eng. Chem. Res. 53 (2014) 4052–4058.

[74] D.P. Rao, Distillation in Rotating Packed Beds, Hyderabad, India, January 25th, 2011.

[75] D. Sudhoff, K. Neumann, P. Lutze, An integrated design method for rotating packed beds for distillation, Computer Aided Chemical Engineering 33 (2014) 1303–1308.

[76] P. Sandilya, D.P. Rao, A. Sharma, G. Biswas, Gas-Phase Mass Transfer in a Centrifugal Contactor, Ind. Eng. Chem. Res. 40 (2001) 384–392.

[77] C.-C. Lin, T.-Y. Wei, W.-T. Liu, K.-P. Shen, Removal of VOCs from Gaseous Streams in a High-Voidage Rotating Packed Bed, J. Chem. Eng. Jpn. 37 (2004) 1471–1477.

[78] Y.-S. Chen, Correlations of Mass Transfer Coefficients in a Rotating Packed Bed, Ind. Eng. Chem. Res. 50 (2011) 1778–1785.

[79] T. Winkler, H. Klein, S. Rehfeldt, Experimental investigation of liquid maldistribution in random packed columns using temperature measurements, Chem. Eng. Sci. 249 (2022) 117350.

[80] K. Groß, A. Bieberle, K. Gladyszewski, M. Schubert, U. Hampel, M. Skiborowski, A. Górak, Analysis of Flow Patterns in High-Gravity Equipment Using Gamma-Ray Computed Tomography, Chem. Ing. Tech. 134 (2019) 443.

[81] J.R. Burns, C. Ramshaw, Process intensification: Visual study of liquid maldistribution in rotating packed beds, Chemical Engineering Science 51 (1996) 1347–1352.

[82] J.R. Burns, J.N. Jamil, C. Ramshaw, Process intensification: operating characteristics of rotating packed beds — determination of liquid hold-up for a high-voidage structured packing, Chem. Eng. Sci. 55 (2000) 2401–2415.

[83] Y. Yang, Y. Xiang, G. Chu, H. Zou, Y. Luo, M. Arowo, J.-F. Chen, A noninvasive X-ray technique for determination of liquid holdup in a rotating packed bed, Chem. Eng. Sci. 138 (2015) 244–255.

[84] Y.-S. Chen, C.-C. Lin, H.-S. Liu, Mass Transfer in a Rotating Packed Bed with Various Radii of the Bed, Ind. Eng. Chem. Res. 44 (2005) 7868–7875.

[85] R. Loll, L. Nordhausen, A. Bieberle, M. Schubert, T. Pyka, J. Koop, C. Held, G. Schembecker, Analysis of Flow Patterns in Structured Zickzack Packings for Rotating Packed Beds Using γ-Ray Computed Tomography, Ind. Eng. Chem. Res. (2023).

[86] H. Qammar, F. Hecht, M. Skiborowski, A. Górak, Experimental Investigation and Design of Rotating Packed Beds for Distillation, Chem. Eng. Trans. 69 (2018) 655–660.

[87] A. Ressemann, M. Illner, J.-U. Repke, A methodology for the analysis of distillation processes within rotating packed beds based on local temperature measurements, Chem. Eng. Res. Des. 193 (2023) 198–206.

[88] U. Onken, W. Arlt, Recommended test mixtures for distillation columns, 2nd ed. ed., The institution of Chemical Engineers, Warwickshire, 1990.

[89] T. Pyka, A. Ressemann, C. Held, G. Schembecker, J.-U. Repke, Impact of Vapor Bypasses on Separation Performance of Rotating Packed Beds in Distillation, Ind. Eng. Chem. Res. 62 (2023) 13274–13279.

[90] G.-W. Chu, X. Gao, Y. Luo, H.-K. Zou, L. Shao, J.-F. Chen, Distillation studies in a two-stage counter-current rotating packed bed, Sep. Purif. Technol. 102 (2013) 62–66.

[91] K. Neumann, Verlag Dr. Hut (München), Operating characteristics of rotating packed beds, Verlag Dr. Hut, München, 2018.

[92] V.A. Lubarda, The shape of a liquid surface in a uniformly rotating cylinder in the presence of surface tension, Acta Mech 224 (2013) 1365–1382.

[93] K. Gładyszewski, M. Skiborowski, Additive manufacturing of packings for rotating packed beds, Chem. Eng. Process. 127 (2018) 1–9.

[94] Foamlabs, HighTemp-DataSheet, https://formlabs.com/media/upload/HighTemp-DataSheet.pdf, accessed 2 April 2019.

[95] Technicoll®, Technical Data Sheet, https://www.technicoll.eu/fileadmin/media/Documents/Produktinformationen_englisch/PI_technicoll_9464__GB_.pdf, accessed 2 April 2019.

[96] G.Q. Wang, Z.J. Zhou, Y.M. Li, J.B. Ji, Qualitative relationships between structure and performance of rotating zigzag bed in distillation, Chemical Engineering and Processing - Process Intensification 135 (2019) 141–147.

[97] K.F. Kruber, H. Qammar, M. Skiborowski, Optimization-Based Design of Rotating Packed Beds with Zickzack Packings, Computer Aided Chemical Engineering 48 (2020) 997–1002.

[98] S. Darakchiev, K. Semkov, A Study on Modern High Effective Random Packings for Ethanol-Water Rectification, Chem. Eng. Technol. 31 (2008) 1039–1045.

[99] L.-M. Ränger, I.J. Halvorsen, T. Grützner, S. Skogestad, Understanding Temperature Profiles of Distillation Columns, Ind. Eng. Chem. Res. 63 (2024) 4533–4546.

[100] Le Sang, Y. Luo, G.-W. Chu, B.-C. Sun, L.-L. Zhang, J.-F. Chen, A three-zone mass transfer model for a rotating packed bed, AIChE J. 65 (2019).

[101] Le Sang, Y. Luo, G.-W. Chu, Y.-Z. Liu, X.-Z. Liu, J.-F. Chen, Modeling and experimental studies of mass transfer in the cavity zone of a rotating packed bed, Chemical Engineering Science 170 (2017) 355–364.

[102] U. Hampel, M. Schubert, A. Döß, J. Sohr, V. Vishwakarma, J.-U. Repke, S.J. Gerke, H. Leuner, M. Rädle, V. Kapoustina, L. Schmitt, M. Grünewald, J.H. Brinkmann, D. Plate, E.Y. Kenig, N. Lutters, L. Bolenz, F. Buckmann, D. Toye, W. Arlt, T. Linder, R. Hoffmann, H. Klein, S. Rehfeldt, T. Winkler, H.-J. Bart, D. Wirz, J. Schulz, S. Scholl, W. Augustin, K. Jasch, F. Schlüter, N. Schwerdtfeger, S. Jahnke, A. Jupke, C. Kabatnik, A.S. Braeuer, M. D'Auria, T. Runowski, M.F. Casal, K. Becker, A.-L. David, A. Górak, M. Skiborowski, K.

Groß, H. Qammar, Recent Advances in Experimental Techniques for Flow and Mass Transfer Analyses in Thermal Separation Systems, Chem. Ing. Tech. 92 (2020) 926–948.

[103] H. Qammar, T. Pyka, J. Koop, A. Górak, G. Schembecker, Radial Temperature Profile Measurements to Understand Mass Transfer in Rotating Packed Bed Distillation, Ind. Eng. Chem. Res. (2023).

[104] I. Lukin, L. Pietzka, I. Wingartz, G. Schembecker, Aroma absorption in rapeseed oil using rotating packed bed, Flavour Fragrance J. 36 (2021) 137–147.

[105] L. Sang, Y. Luo, G.-W. Chu, J.-P. Zhang, Y. Xiang, J.-F. Chen, Liquid flow pattern transition, droplet diameter and size distribution in the cavity zone of a rotating packed bed: A visual study, Chemical Engineering Science 158 (2017) 429–438.

[106] J.A. Hacking, N. Delsing, M.M. de Beer, J. van der Schaaf, Improving liquid distribution in a rotating packed bed, Chem. Eng. Process. 149 (2020) 107861.

[107] A. Verfahrenstechnik, Relevante Publikationen - RWTH AACHEN UNIVERSITY Aachener Verfahrenstechnik - Deutsch, 2001, https://www.avt.rwth-aachen.de/go/id/ipyo, accessed 19 September 2024.

[108] B. Hadrich, N. Kechaou, Identification of Best Model for Equilibrium Data of Ethanol-Water Mixture, Journal of Chemistry and Chemical Engineering 4 (2010).

[109] K.M. Groß, Deaeration in Rotating Packed Beds: Ph.D. thesis, 2021.

[110] A. Ressemann, M. Illner, J.-U. Repke, Local Separation Performance for Distillation Processes in Rotating Packed Beds: Transferability and Applicability, Ind. Eng. Chem. Res. 63 (2024) 13291–13307.

Chapter 10 Appendix

A-1: List of Dimensionless Numbers

Table 10.1: List of dimensionless numbers with their equations used in mass transfer correlations.

Dimensionless Group	Symbol	Equation
Schmidt number	Sc	$Sc = \frac{\mu}{\rho D}$
Grashof number	Gr	$Gr = \frac{d_p^3 \rho^2 a_c}{\mu^2}$
Reynolds number	Re	$Re = \frac{\rho d u}{\mu}$
Bond number	Bo	$BO = \frac{\Delta \rho g L^2}{\sigma}$

A-2: P&ID of Distillation in RPBs

A simplified P&ID of distillation in the RPB pilot plant that is equipped with various instruments for monitoring and control is shown in Figure 10.1. The liquid feed is heated in the reboiler that is equipped with a safety level switch (LS1). To prevent dry heating, the heater shuts off when the liquid level drops below approximately 35 L. The temperature of the vapors entering and leaving the RPB can be recorded with temperature sensors TIR1 and TIR2, respectively. The vapors leaving the RPB are condensed in a compact plate-type condenser C1 and collected in a buffer tank (B1). The reflux liquid is pumped back to the RPB via pump P1. FIR1 indicates the flow rate of the reflux liquid. Pumps Liquid leaving the RPB is collected in a buffer tank (B2) and pumped back to the reboiler via pump P2. FI2 indicates the flow of the liquid going back to the reboiler. P1 and P2 are automatically controlled in LabVIEW using set points for the mass of liquid in the buffer tank. PI1 is used to estimate the pressure drop in the RPB using a U-tube manometer. PI2 is an analog pressure gauge at the vapor inlet connected with a safety relief valve (limit 1.4 bar) to minimize pressure build-up in the system.

The plant's LabVIEW control system displays selected temperature readings as well as the reflux flow rate. In addition, the distillate and bottom pumps are operated through this interface. Figure 10.1a presents a screenshot of the control system. The left section shows the control panels for the two pumps, while the central area illustrates a process flow diagram with indicated temperatures, weights, and reflux rate. These parameters are also visualized in the monitoring charts on the right-hand side.

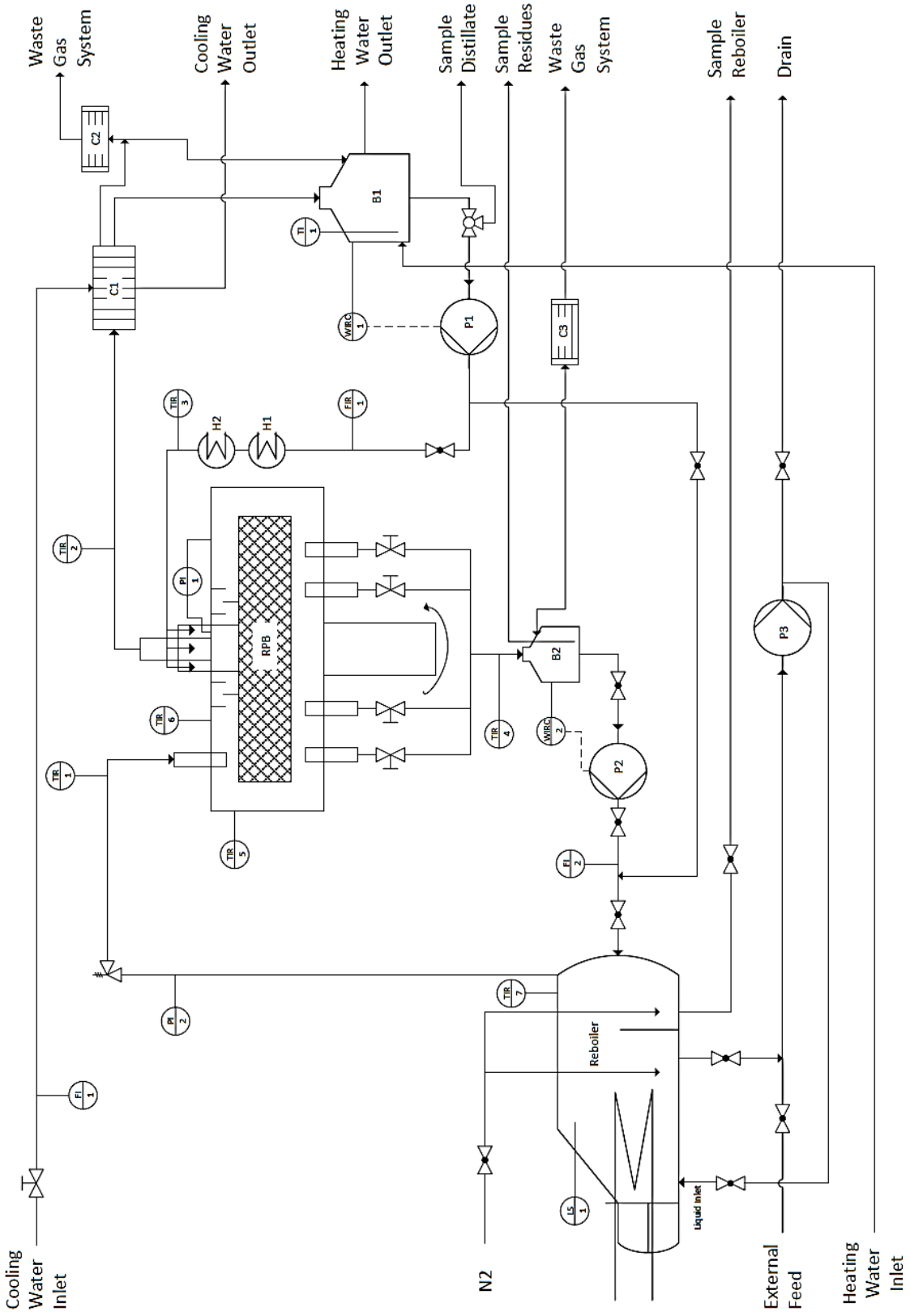

Figure 10.1: Process and Instrumentation diagram of RPB distillation pilot plant.

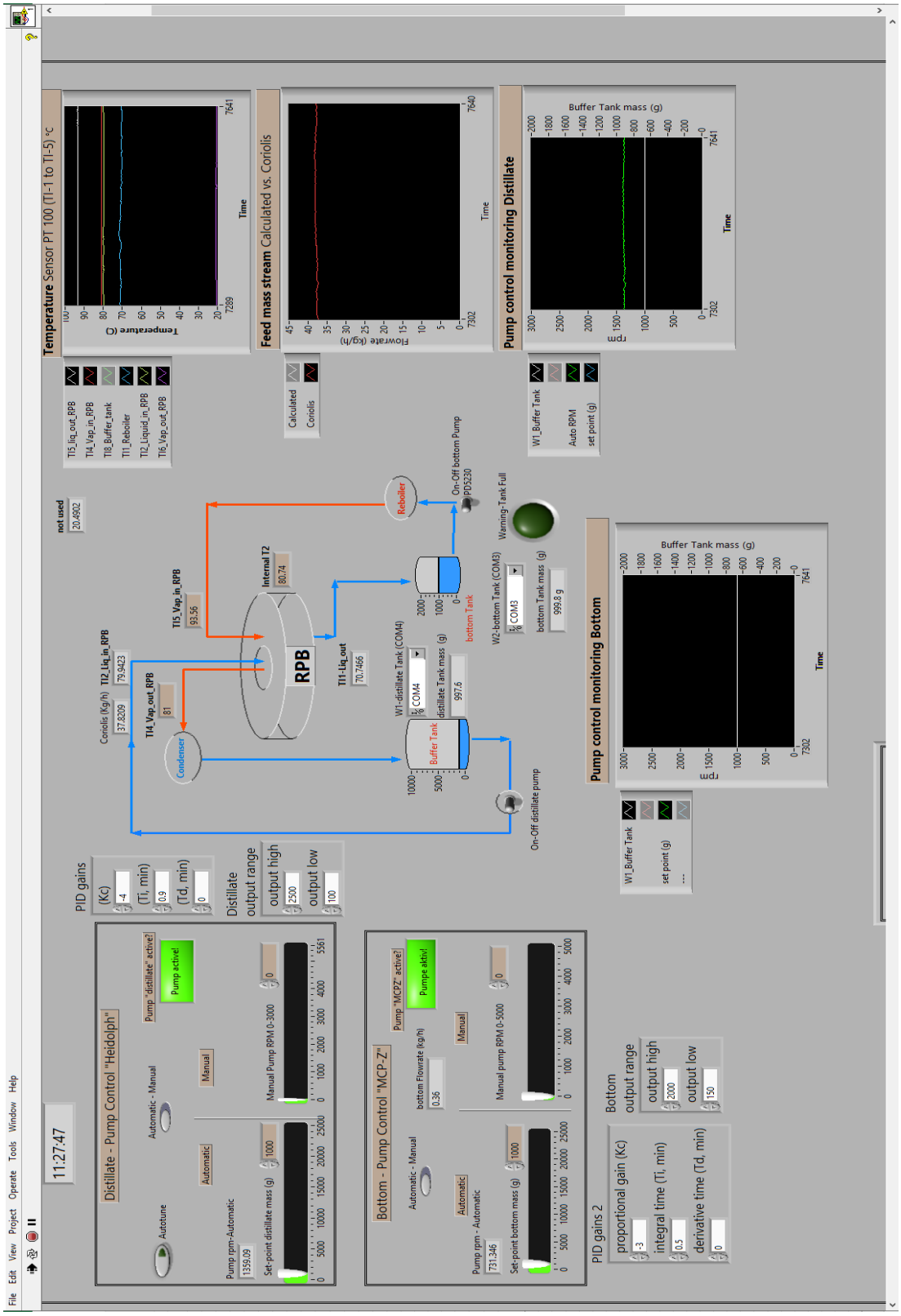

Figure 10.1a: Picture of the measurement & control interface (LabVIEW) during operation.

A-3: Calculation of Geometrical Surface Area of RPB Casing

The casing of the RPB investigated is a non-standard geometry; therefore, a combination of two standard shapes is used to estimate the geometrical surface area of the casing as mentioned below.

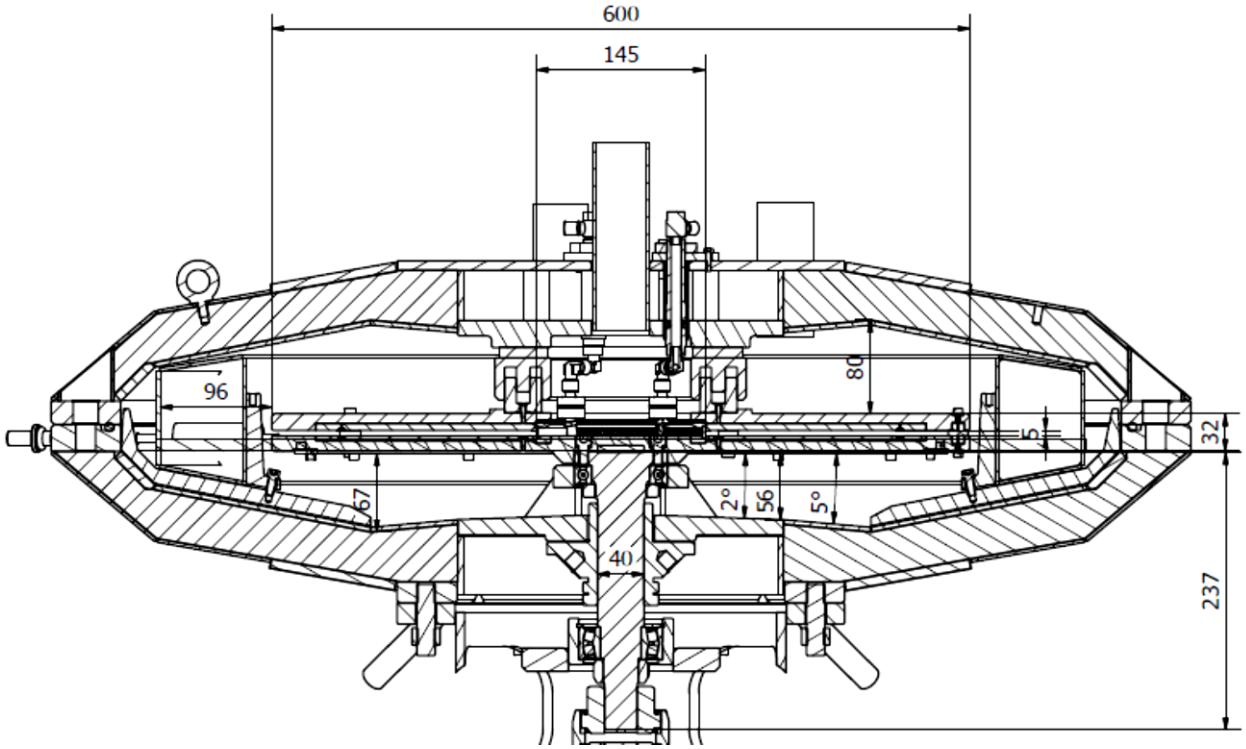

Figure 10.2: Schematic drawing of the RPB showing the geometrical measurements used for casing volume calculation. All the measurements are given in 'mm'.

1) One semi-circle on top, one semi-circle on the bottom, and a cylindrical shape in the middle

$$\frac{\pi d^2}{4} + \pi \cdot d \cdot h = 0.8\, m^2$$

Where d is the inner diameter of the casing and h is the inner axial height of the casing. h = 0.1 m, and d = 0.83 m

2) Cylindrical shape only

$$\frac{\pi d^2}{2} + \pi \cdot d \cdot h = 1.5\, m^2$$

where h = 80 mm + 32 mm + 56 mm = 168 mm and d = 830.5 mm

average casing volume = 1.16 m^2

A-4: Mass transfer of Conventional RPB Packing at an F-factor of 0.6 $Pa^{0.5}$

Initially, a reboiler with 5 kW capacity was available that could provide a maximum F-factor of 0.6 $Pa^{0.5}$. Therefore, a comparison of conventional RPB packing at low F-factor is shown below. Knit mesh showed better separation efficiency at a lower F-factor than metal foam, most likely due to the higher specific surface area of knit mesh packing.

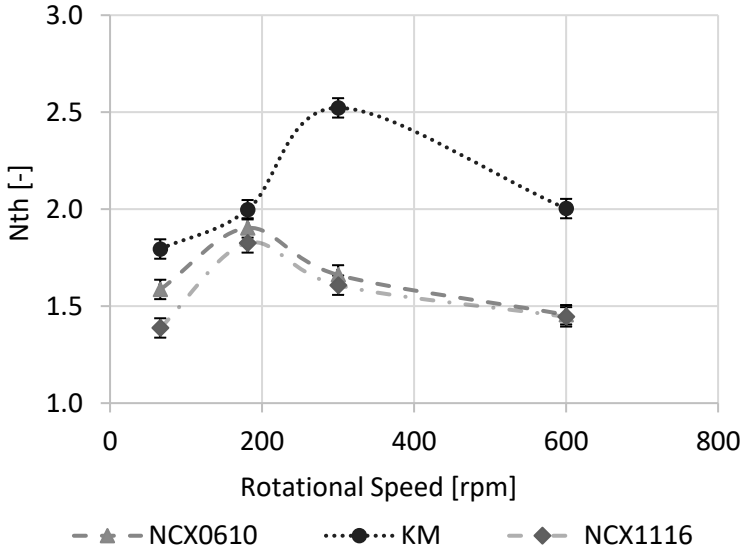

Figure 10.3: Mass transfer of conventional RPB packings; metal foam (NCX0610 and NCX1116) and knit mesh (KM); Rotor-2, F-factor = 0.6 $Pa^{0.5}$ [43].

A-5: Equilibrium Curve of Ethanol-Water Test System at 1.0133 bar Pressure

Equilibrium data for the ethanol-water test mixture used for the calculations in this work are shown below in Table 10.2. The NRTL model with the database APV88 VLE-IG is used in Aspen Plus® to generate the VLE data. In the table below, 'y' represents the ethanol vapor fraction (kg/kg), 'x' is the ethanol liquid fraction (kg/kg), and 'T' is the temperature of the mixture (°C).

Table 10.2: Equilibrium data of ethanol-water test system at 1.0133 bar pressure.

#	T	y, Ethanol	x, Ethanol	#	T	y, Ethanol	x, Ethanol
1	78.15	0.9551	0.955	479	81.90	0.7725	0.477
2	78.15	0.9543	0.954	480	81.91	0.7723	0.476
3	78.15	0.9534	0.953	481	81.92	0.7720	0.475
4	78.15	0.9525	0.952	482	81.93	0.7718	0.474
5	78.15	0.9517	0.951	483	81.94	0.7716	0.473
6	78.15	0.9508	0.950	484	81.95	0.7713	0.472
7	78.15	0.9499	0.949	485	81.96	0.7711	0.471
8	78.16	0.9491	0.948	486	81.97	0.7708	0.470
9	78.16	0.9482	0.947	487	81.98	0.7706	0.469
10	78.16	0.9474	0.946	488	81.99	0.7704	0.468
11	78.16	0.9466	0.945	489	82.00	0.7701	0.467
12	78.16	0.9457	0.944	490	82.01	0.7699	0.466
13	78.16	0.9449	0.943	491	82.03	0.7697	0.465
14	78.16	0.9441	0.942	492	82.04	0.7694	0.464
15	78.17	0.9432	0.941	493	82.05	0.7692	0.463
16	78.17	0.9424	0.940	494	82.06	0.7689	0.462
17	78.17	0.9416	0.939	495	82.07	0.7687	0.461
18	78.17	0.9408	0.938	496	82.08	0.7685	0.460
19	78.17	0.9400	0.937	497	82.09	0.7682	0.459
20	78.18	0.9392	0.936	498	82.10	0.7680	0.458
21	78.18	0.9384	0.935	499	82.11	0.7677	0.457
22	78.18	0.9376	0.934	500	82.12	0.7675	0.456
23	78.18	0.9368	0.933	501	82.13	0.7672	0.455
24	78.19	0.9360	0.932	502	82.14	0.7670	0.454
25	78.19	0.9353	0.931	503	82.16	0.7667	0.453
26	78.19	0.9345	0.930	504	82.17	0.7665	0.452
27	78.20	0.9337	0.929	505	82.18	0.7663	0.451
28	78.20	0.9329	0.928	506	82.19	0.7660	0.450
29	78.20	0.9322	0.927	507	82.20	0.7658	0.449
30	78.21	0.9314	0.926	508	82.21	0.7655	0.448

#	T [°C]	y, Ethanol	x, Ethanol	#	T [°C]	y, Ethanol	x, Ethanol
31	78.21	0.9307	0.925	509	82.22	0.7653	0.447
32	78.21	0.9299	0.924	510	82.23	0.7650	0.446
33	78.22	0.9292	0.923	511	82.24	0.7648	0.445
34	78.22	0.9284	0.922	512	82.26	0.7645	0.444
35	78.22	0.9277	0.921	513	82.27	0.7643	0.443
36	78.23	0.9269	0.920	514	82.28	0.7640	0.442
37	78.23	0.9262	0.919	515	82.29	0.7638	0.441
38	78.24	0.9255	0.918	516	82.30	0.7635	0.440
39	78.24	0.9247	0.917	517	82.31	0.7633	0.439
40	78.24	0.9240	0.916	518	82.32	0.7630	0.438
41	78.25	0.9233	0.915	519	82.33	0.7627	0.437
42	78.25	0.9226	0.914	520	82.35	0.7625	0.436
43	78.26	0.9219	0.913	521	82.36	0.7622	0.435
44	78.26	0.9212	0.912	522	82.37	0.7620	0.434
45	78.27	0.9205	0.911	523	82.38	0.7617	0.433
46	78.27	0.9198	0.910	524	82.39	0.7615	0.432
47	78.27	0.9191	0.909	525	82.40	0.7612	0.431
48	78.28	0.9184	0.908	526	82.42	0.7609	0.430
49	78.28	0.9177	0.907	527	82.43	0.7607	0.429
50	78.29	0.9170	0.906	528	82.44	0.7604	0.428
51	78.29	0.9163	0.905	529	82.45	0.7602	0.427
52	78.30	0.9156	0.904	530	82.46	0.7599	0.426
53	78.30	0.9149	0.903	531	82.48	0.7596	0.425
54	78.31	0.9143	0.902	532	82.49	0.7594	0.424
55	78.31	0.9136	0.901	533	82.50	0.7591	0.423
56	78.32	0.9129	0.900	534	82.51	0.7588	0.422
57	78.33	0.9123	0.899	535	82.52	0.7586	0.421
58	78.33	0.9116	0.898	536	82.54	0.7583	0.420
59	78.34	0.9110	0.897	537	82.55	0.7580	0.419
60	78.34	0.9103	0.896	538	82.56	0.7578	0.418
61	78.35	0.9096	0.895	539	82.57	0.7575	0.417
62	78.35	0.9090	0.894	540	82.58	0.7572	0.416
63	78.36	0.9084	0.893	541	82.60	0.7570	0.415
64	78.36	0.9077	0.892	542	82.61	0.7567	0.414
65	78.37	0.9071	0.891	543	82.62	0.7564	0.413
66	78.38	0.9064	0.890	544	82.63	0.7561	0.412
67	78.38	0.9058	0.889	545	82.65	0.7559	0.411
68	78.39	0.9052	0.888	546	82.66	0.7556	0.410
69	78.39	0.9046	0.887	547	82.67	0.7553	0.409
70	78.40	0.9039	0.886	548	82.68	0.7550	0.408
71	78.41	0.9033	0.885	549	82.70	0.7548	0.407

#	T [°C]	y, Ethanol	x, Ethanol	#	T [°C]	y, Ethanol	x, Ethanol
72	78.41	0.9027	0.884	550	82.71	0.7545	0.406
73	78.42	0.9021	0.883	551	82.72	0.7542	0.405
74	78.43	0.9015	0.882	552	82.74	0.7539	0.404
75	78.43	0.9009	0.881	553	82.75	0.7536	0.403
76	78.44	0.9003	0.880	554	82.76	0.7533	0.402
77	78.44	0.8997	0.879	555	82.77	0.7531	0.401
78	78.45	0.8991	0.878	556	82.79	0.7528	0.400
79	78.46	0.8985	0.877	557	82.80	0.7525	0.399
80	78.46	0.8979	0.876	558	82.81	0.7522	0.398
81	78.47	0.8973	0.875	559	82.83	0.7519	0.397
82	78.48	0.8967	0.874	560	82.84	0.7516	0.396
83	78.48	0.8961	0.873	561	82.85	0.7513	0.395
84	78.49	0.8955	0.872	562	82.87	0.7510	0.394
85	78.50	0.8949	0.871	563	82.88	0.7508	0.393
86	78.50	0.8944	0.870	564	82.89	0.7505	0.392
87	78.51	0.8938	0.869	565	82.91	0.7502	0.391
88	78.52	0.8932	0.868	566	82.92	0.7499	0.390
89	78.52	0.8927	0.867	567	82.93	0.7496	0.389
90	78.53	0.8921	0.866	568	82.95	0.7493	0.388
91	78.54	0.8915	0.865	569	82.96	0.7490	0.387
92	78.55	0.8910	0.864	570	82.98	0.7487	0.386
93	78.55	0.8904	0.863	571	82.99	0.7484	0.385
94	78.56	0.8898	0.862	572	83.00	0.7481	0.384
95	78.57	0.8893	0.861	573	83.02	0.7478	0.383
96	78.57	0.8887	0.860	574	83.03	0.7475	0.382
97	78.58	0.8882	0.859	575	83.04	0.7472	0.381
98	78.59	0.8877	0.858	576	83.06	0.7469	0.380
99	78.60	0.8871	0.857	577	83.07	0.7465	0.379
100	78.60	0.8866	0.856	578	83.09	0.7462	0.378
101	78.61	0.8860	0.855	579	83.10	0.7459	0.377
102	78.62	0.8855	0.854	580	83.12	0.7456	0.376
103	78.63	0.8850	0.853	581	83.13	0.7453	0.375
104	78.63	0.8844	0.852	582	83.14	0.7450	0.374
105	78.64	0.8839	0.851	583	83.16	0.7447	0.373
106	78.65	0.8834	0.850	584	83.17	0.7444	0.372
107	78.66	0.8829	0.849	585	83.19	0.7440	0.371
108	78.66	0.8823	0.848	586	83.20	0.7437	0.370
109	78.67	0.8818	0.847	587	83.22	0.7434	0.369
110	78.68	0.8813	0.846	588	83.23	0.7431	0.368
111	78.69	0.8808	0.845	589	83.25	0.7428	0.367
112	78.69	0.8803	0.844	590	83.26	0.7424	0.366

#	T [°C]	y, Ethanol	x, Ethanol	#	T [°C]	y, Ethanol	x, Ethanol
113	78.70	0.8798	0.843	591	83.28	0.7421	0.365
114	78.71	0.8793	0.842	592	83.29	0.7418	0.364
115	78.72	0.8788	0.841	593	83.31	0.7414	0.363
116	78.72	0.8783	0.840	594	83.32	0.7411	0.362
117	78.73	0.8778	0.839	595	83.34	0.7408	0.361
118	78.74	0.8773	0.838	596	83.35	0.7405	0.360
119	78.75	0.8768	0.837	597	83.37	0.7401	0.359
120	78.76	0.8763	0.836	598	83.38	0.7398	0.358
121	78.76	0.8758	0.835	599	83.40	0.7394	0.357
122	78.77	0.8753	0.834	600	83.41	0.7391	0.356
123	78.78	0.8748	0.833	601	83.43	0.7388	0.355
124	78.79	0.8743	0.832	602	83.44	0.7384	0.354
125	78.79	0.8739	0.831	603	83.46	0.7381	0.353
126	78.80	0.8734	0.830	604	83.47	0.7377	0.352
127	78.81	0.8729	0.829	605	83.49	0.7374	0.351
128	78.82	0.8724	0.828	606	83.51	0.7371	0.350
129	78.83	0.8720	0.827	607	83.52	0.7367	0.349
130	78.83	0.8715	0.826	608	83.54	0.7364	0.348
131	78.84	0.8710	0.825	609	83.55	0.7360	0.347
132	78.85	0.8706	0.824	610	83.57	0.7356	0.346
133	78.86	0.8701	0.823	611	83.59	0.7353	0.345
134	78.87	0.8696	0.822	612	83.60	0.7349	0.344
135	78.87	0.8692	0.821	613	83.62	0.7346	0.343
136	78.88	0.8687	0.820	614	83.64	0.7342	0.342
137	78.89	0.8682	0.819	615	83.65	0.7339	0.341
138	78.90	0.8678	0.818	616	83.67	0.7335	0.340
139	78.91	0.8673	0.817	617	83.68	0.7331	0.339
140	78.92	0.8669	0.816	618	83.70	0.7328	0.338
141	78.92	0.8664	0.815	619	83.72	0.7324	0.337
142	78.93	0.8660	0.814	620	83.74	0.7320	0.336
143	78.94	0.8656	0.813	621	83.75	0.7317	0.335
144	78.95	0.8651	0.812	622	83.77	0.7313	0.334
145	78.96	0.8647	0.811	623	83.79	0.7309	0.333
146	78.97	0.8642	0.810	624	83.80	0.7305	0.332
147	78.97	0.8638	0.809	625	83.82	0.7301	0.331
148	78.98	0.8634	0.808	626	83.84	0.7298	0.330
149	78.99	0.8629	0.807	627	83.85	0.7294	0.329
150	79.00	0.8625	0.806	628	83.87	0.7290	0.328
151	79.01	0.8621	0.805	629	83.89	0.7286	0.327
152	79.02	0.8616	0.804	630	83.91	0.7282	0.326
153	79.02	0.8612	0.803	631	83.92	0.7278	0.325

#	T [°C]	y, Ethanol	x, Ethanol	#	T [°C]	y, Ethanol	x, Ethanol
154	79.03	0.8608	0.802	632	83.94	0.7274	0.324
155	79.04	0.8604	0.801	633	83.96	0.7271	0.323
156	79.05	0.8600	0.800	634	83.98	0.7267	0.322
157	79.06	0.8595	0.799	635	84.00	0.7263	0.321
158	79.07	0.8591	0.798	636	84.01	0.7259	0.320
159	79.07	0.8587	0.797	637	84.03	0.7255	0.319
160	79.08	0.8583	0.796	638	84.05	0.7251	0.318
161	79.09	0.8579	0.795	639	84.07	0.7246	0.317
162	79.10	0.8575	0.794	640	84.09	0.7242	0.316
163	79.11	0.8571	0.793	641	84.11	0.7238	0.315
164	79.12	0.8567	0.792	642	84.12	0.7234	0.314
165	79.12	0.8563	0.791	643	84.14	0.7230	0.313
166	79.13	0.8559	0.790	644	84.16	0.7226	0.312
167	79.14	0.8554	0.789	645	84.18	0.7222	0.311
168	79.15	0.8551	0.788	646	84.20	0.7217	0.310
169	79.16	0.8547	0.787	647	84.22	0.7213	0.309
170	79.17	0.8543	0.786	648	84.24	0.7209	0.308
171	79.18	0.8539	0.785	649	84.26	0.7205	0.307
172	79.18	0.8535	0.784	650	84.28	0.7200	0.306
173	79.19	0.8531	0.783	651	84.29	0.7196	0.305
174	79.20	0.8527	0.782	652	84.31	0.7192	0.304
175	79.21	0.8523	0.781	653	84.33	0.7187	0.303
176	79.22	0.8519	0.780	654	84.35	0.7183	0.302
177	79.23	0.8515	0.779	655	84.37	0.7179	0.301
178	79.24	0.8511	0.778	656	84.39	0.7174	0.300
179	79.24	0.8508	0.777	657	84.41	0.7170	0.299
180	79.25	0.8504	0.776	658	84.43	0.7165	0.298
181	79.26	0.8500	0.775	659	84.45	0.7161	0.297
182	79.27	0.8496	0.774	660	84.47	0.7156	0.296
183	79.28	0.8493	0.773	661	84.49	0.7152	0.295
184	79.29	0.8489	0.772	662	84.51	0.7147	0.294
185	79.30	0.8485	0.771	663	84.53	0.7142	0.293
186	79.30	0.8481	0.770	664	84.55	0.7138	0.292
187	79.31	0.8478	0.769	665	84.57	0.7133	0.291
188	79.32	0.8474	0.768	666	84.59	0.7129	0.290
189	79.33	0.8470	0.767	667	84.62	0.7124	0.289
190	79.34	0.8467	0.766	668	84.64	0.7119	0.288
191	79.35	0.8463	0.765	669	84.66	0.7114	0.287
192	79.36	0.8459	0.764	670	84.68	0.7110	0.286
193	79.36	0.8456	0.763	671	84.70	0.7105	0.285
194	79.37	0.8452	0.762	672	84.72	0.7100	0.284

#	T [°C]	y, Ethanol	x, Ethanol	#	T [°C]	y, Ethanol	x, Ethanol
195	79.38	0.8449	0.761	673	84.74	0.7095	0.283
196	79.39	0.8445	0.760	674	84.76	0.7090	0.282
197	79.40	0.8442	0.759	675	84.79	0.7085	0.281
198	79.41	0.8438	0.758	676	84.81	0.7080	0.280
199	79.42	0.8434	0.757	677	84.83	0.7075	0.279
200	79.42	0.8431	0.756	678	84.85	0.7070	0.278
201	79.43	0.8427	0.755	679	84.87	0.7065	0.277
202	79.44	0.8424	0.754	680	84.89	0.7060	0.276
203	79.45	0.8421	0.753	681	84.92	0.7055	0.275
204	79.46	0.8417	0.752	682	84.94	0.7050	0.274
205	79.47	0.8414	0.751	683	84.96	0.7045	0.273
206	79.48	0.8410	0.750	684	84.98	0.7040	0.272
207	79.49	0.8407	0.749	685	85.01	0.7034	0.271
208	79.49	0.8403	0.748	686	85.03	0.7029	0.270
209	79.50	0.8400	0.747	687	85.05	0.7024	0.269
210	79.51	0.8397	0.746	688	85.08	0.7019	0.268
211	79.52	0.8393	0.745	689	85.10	0.7013	0.267
212	79.53	0.8390	0.744	690	85.12	0.7008	0.266
213	79.54	0.8387	0.743	691	85.14	0.7002	0.265
214	79.55	0.8383	0.742	692	85.17	0.6997	0.264
215	79.55	0.8380	0.741	693	85.19	0.6991	0.263
216	79.56	0.8377	0.740	694	85.22	0.6986	0.262
217	79.57	0.8373	0.739	695	85.24	0.6980	0.261
218	79.58	0.8370	0.738	696	85.26	0.6975	0.260
219	79.59	0.8367	0.737	697	85.29	0.6969	0.259
220	79.60	0.8364	0.736	698	85.31	0.6964	0.258
221	79.61	0.8360	0.735	699	85.34	0.6958	0.257
222	79.61	0.8357	0.734	700	85.36	0.6952	0.256
223	79.62	0.8354	0.733	701	85.38	0.6946	0.255
224	79.63	0.8351	0.732	702	85.41	0.6941	0.254
225	79.64	0.8347	0.731	703	85.43	0.6935	0.253
226	79.65	0.8344	0.730	704	85.46	0.6929	0.252
227	79.66	0.8341	0.729	705	85.48	0.6923	0.251
228	79.67	0.8338	0.728	706	85.51	0.6917	0.250
229	79.68	0.8335	0.727	707	85.53	0.6911	0.249
230	79.68	0.8332	0.726	708	85.56	0.6905	0.248
231	79.69	0.8328	0.725	709	85.58	0.6899	0.247
232	79.70	0.8325	0.724	710	85.61	0.6893	0.246
233	79.71	0.8322	0.723	711	85.64	0.6887	0.245
234	79.72	0.8319	0.722	712	85.66	0.6881	0.244
235	79.73	0.8316	0.721	713	85.69	0.6875	0.243

#	T [°C]	y, Ethanol	x, Ethanol	#	T [°C]	y, Ethanol	x, Ethanol
236	79.74	0.8313	0.720	714	85.71	0.6868	0.242
237	79.74	0.8310	0.719	715	85.74	0.6862	0.241
238	79.75	0.8307	0.718	716	85.77	0.6856	0.240
239	79.76	0.8304	0.717	717	85.79	0.6849	0.239
240	79.77	0.8301	0.716	718	85.82	0.6843	0.238
241	79.78	0.8298	0.715	719	85.85	0.6836	0.237
242	79.79	0.8295	0.714	720	85.87	0.6830	0.236
243	79.80	0.8292	0.713	721	85.90	0.6823	0.235
244	79.80	0.8289	0.712	722	85.93	0.6817	0.234
245	79.81	0.8286	0.711	723	85.96	0.6810	0.233
246	79.82	0.8283	0.710	724	85.98	0.6804	0.232
247	79.83	0.8280	0.709	725	86.01	0.6797	0.231
248	79.84	0.8277	0.708	726	86.04	0.6790	0.230
249	79.85	0.8274	0.707	727	86.07	0.6783	0.229
250	79.86	0.8271	0.706	728	86.09	0.6776	0.228
251	79.87	0.8268	0.705	729	86.12	0.6769	0.227
252	79.87	0.8265	0.704	730	86.15	0.6762	0.226
253	79.88	0.8262	0.703	731	86.18	0.6755	0.225
254	79.89	0.8259	0.702	732	86.21	0.6748	0.224
255	79.90	0.8256	0.701	733	86.24	0.6741	0.223
256	79.91	0.8254	0.700	734	86.27	0.6734	0.222
257	79.92	0.8251	0.699	735	86.29	0.6727	0.221
258	79.93	0.8248	0.698	736	86.32	0.6720	0.220
259	79.93	0.8245	0.697	737	86.35	0.6712	0.219
260	79.94	0.8242	0.696	738	86.38	0.6705	0.218
261	79.95	0.8239	0.695	739	86.41	0.6698	0.217
262	79.96	0.8236	0.694	740	86.44	0.6690	0.216
263	79.97	0.8234	0.693	741	86.47	0.6683	0.215
264	79.98	0.8231	0.692	742	86.50	0.6675	0.214
265	79.99	0.8228	0.691	743	86.53	0.6668	0.213
266	79.99	0.8225	0.690	744	86.56	0.6660	0.212
267	80.00	0.8222	0.689	745	86.59	0.6652	0.211
268	80.01	0.8220	0.688	746	86.63	0.6644	0.210
269	80.02	0.8217	0.687	747	86.66	0.6636	0.209
270	80.03	0.8214	0.686	748	86.69	0.6629	0.208
271	80.04	0.8211	0.685	749	86.72	0.6621	0.207
272	80.05	0.8209	0.684	750	86.75	0.6613	0.206
273	80.05	0.8206	0.683	751	86.78	0.6605	0.205
274	80.06	0.8203	0.682	752	86.81	0.6596	0.204
275	80.07	0.8200	0.681	753	86.85	0.6588	0.203
276	80.08	0.8198	0.680	754	86.88	0.6580	0.202

#	T [°C]	y, Ethanol	x, Ethanol	#	T [°C]	y, Ethanol	x, Ethanol
277	80.09	0.8195	0.679	755	86.91	0.6572	0.201
278	80.10	0.8192	0.678	756	86.94	0.6563	0.200
279	80.11	0.8190	0.677	757	86.98	0.6555	0.199
280	80.11	0.8187	0.676	758	87.01	0.6546	0.198
281	80.12	0.8184	0.675	759	87.04	0.6538	0.197
282	80.13	0.8182	0.674	760	87.08	0.6529	0.196
283	80.14	0.8179	0.673	761	87.11	0.6520	0.195
284	80.15	0.8176	0.672	762	87.14	0.6512	0.194
285	80.16	0.8174	0.671	763	87.18	0.6503	0.193
286	80.17	0.8171	0.670	764	87.21	0.6494	0.192
287	80.17	0.8168	0.669	765	87.24	0.6485	0.191
288	80.18	0.8166	0.668	766	87.28	0.6476	0.190
289	80.19	0.8163	0.667	767	87.31	0.6467	0.189
290	80.20	0.8161	0.666	768	87.35	0.6457	0.188
291	80.21	0.8158	0.665	769	87.38	0.6448	0.187
292	80.22	0.8155	0.664	770	87.42	0.6439	0.186
293	80.23	0.8153	0.663	771	87.45	0.6429	0.185
294	80.23	0.8150	0.662	772	87.49	0.6420	0.184
295	80.24	0.8148	0.661	773	87.52	0.6410	0.183
296	80.25	0.8145	0.660	774	87.56	0.6401	0.182
297	80.26	0.8143	0.659	775	87.60	0.6391	0.181
298	80.27	0.8140	0.658	776	87.63	0.6381	0.180
299	80.28	0.8137	0.657	777	87.67	0.6371	0.179
300	80.29	0.8135	0.656	778	87.71	0.6361	0.178
301	80.29	0.8132	0.655	779	87.74	0.6351	0.177
302	80.30	0.8130	0.654	780	87.78	0.6341	0.176
303	80.31	0.8127	0.653	781	87.82	0.6331	0.175
304	80.32	0.8125	0.652	782	87.85	0.6320	0.174
305	80.33	0.8122	0.651	783	87.89	0.6310	0.173
306	80.34	0.8120	0.650	784	87.93	0.6300	0.172
307	80.34	0.8117	0.649	785	87.97	0.6289	0.171
308	80.35	0.8115	0.648	786	88.01	0.6278	0.170
309	80.36	0.8112	0.647	787	88.05	0.6268	0.169
310	80.37	0.8110	0.646	788	88.08	0.6257	0.168
311	80.38	0.8107	0.645	789	88.12	0.6246	0.167
312	80.39	0.8105	0.644	790	88.16	0.6235	0.166
313	80.40	0.8102	0.643	791	88.20	0.6224	0.165
314	80.40	0.8100	0.642	792	88.24	0.6213	0.164
315	80.41	0.8097	0.641	793	88.28	0.6201	0.163
316	80.42	0.8095	0.640	794	88.32	0.6190	0.162
317	80.43	0.8093	0.639	795	88.36	0.6178	0.161

#	T [°C]	y, Ethanol	x, Ethanol	#	T [°C]	y, Ethanol	x, Ethanol
318	80.44	0.8090	0.638	796	88.40	0.6167	0.160
319	80.45	0.8088	0.637	797	88.44	0.6155	0.159
320	80.46	0.8085	0.636	798	88.49	0.6143	0.158
321	80.46	0.8083	0.635	799	88.53	0.6131	0.157
322	80.47	0.8080	0.634	800	88.57	0.6119	0.156
323	80.48	0.8078	0.633	801	88.61	0.6107	0.155
324	80.49	0.8076	0.632	802	88.65	0.6095	0.154
325	80.50	0.8073	0.631	803	88.69	0.6082	0.153
326	80.51	0.8071	0.630	804	88.74	0.6070	0.152
327	80.52	0.8068	0.629	805	88.78	0.6057	0.151
328	80.52	0.8066	0.628	806	88.82	0.6045	0.150
329	80.53	0.8064	0.627	807	88.87	0.6032	0.149
330	80.54	0.8061	0.626	808	88.91	0.6019	0.148
331	80.55	0.8059	0.625	809	88.95	0.6006	0.147
332	80.56	0.8056	0.624	810	89.00	0.5993	0.146
333	80.57	0.8054	0.623	811	89.04	0.5979	0.145
334	80.58	0.8052	0.622	812	89.09	0.5966	0.144
335	80.58	0.8049	0.621	813	89.13	0.5952	0.143
336	80.59	0.8047	0.620	814	89.18	0.5938	0.142
337	80.60	0.8045	0.619	815	89.22	0.5925	0.141
338	80.61	0.8042	0.618	816	89.27	0.5911	0.140
339	80.62	0.8040	0.617	817	89.31	0.5897	0.139
340	80.63	0.8038	0.616	818	89.36	0.5882	0.138
341	80.64	0.8035	0.615	819	89.41	0.5868	0.137
342	80.64	0.8033	0.614	820	89.45	0.5853	0.136
343	80.65	0.8031	0.613	821	89.50	0.5839	0.135
344	80.66	0.8028	0.612	822	89.55	0.5824	0.134
345	80.67	0.8026	0.611	823	89.60	0.5809	0.133
346	80.68	0.8024	0.610	824	89.64	0.5794	0.132
347	80.69	0.8021	0.609	825	89.69	0.5779	0.131
348	80.70	0.8019	0.608	826	89.74	0.5763	0.130
349	80.70	0.8017	0.607	827	89.79	0.5748	0.129
350	80.71	0.8014	0.606	828	89.84	0.5732	0.128
351	80.72	0.8012	0.605	829	89.89	0.5716	0.127
352	80.73	0.8010	0.604	830	89.94	0.5700	0.126
353	80.74	0.8007	0.603	831	89.99	0.5684	0.125
354	80.75	0.8005	0.602	832	90.04	0.5667	0.124
355	80.76	0.8003	0.601	833	90.09	0.5651	0.123
356	80.76	0.8001	0.600	834	90.14	0.5634	0.122
357	80.77	0.7998	0.599	835	90.19	0.5617	0.121
358	80.78	0.7996	0.598	836	90.24	0.5600	0.120

#	T [°C]	y, Ethanol	x, Ethanol	#	T [°C]	y, Ethanol	x, Ethanol
359	80.79	0.7994	0.597	837	90.30	0.5583	0.119
360	80.80	0.7991	0.596	838	90.35	0.5565	0.118
361	80.81	0.7989	0.595	839	90.40	0.5548	0.117
362	80.82	0.7987	0.594	840	90.45	0.5530	0.116
363	80.82	0.7985	0.593	841	90.51	0.5512	0.115
364	80.83	0.7982	0.592	842	90.56	0.5494	0.114
365	80.84	0.7980	0.591	843	90.61	0.5475	0.113
366	80.85	0.7978	0.590	844	90.67	0.5457	0.112
367	80.86	0.7976	0.589	845	90.72	0.5438	0.111
368	80.87	0.7973	0.588	846	90.78	0.5419	0.110
369	80.88	0.7971	0.587	847	90.83	0.5399	0.109
370	80.89	0.7969	0.586	848	90.89	0.5380	0.108
371	80.89	0.7967	0.585	849	90.95	0.5360	0.107
372	80.90	0.7964	0.584	850	91.00	0.5340	0.106
373	80.91	0.7962	0.583	851	91.06	0.5320	0.105
374	80.92	0.7960	0.582	852	91.12	0.5300	0.104
375	80.93	0.7958	0.581	853	91.17	0.5279	0.103
376	80.94	0.7955	0.580	854	91.23	0.5258	0.102
377	80.95	0.7953	0.579	855	91.29	0.5237	0.101
378	80.96	0.7951	0.578	856	91.35	0.5216	0.100
379	80.96	0.7949	0.577	857	91.41	0.5194	0.099
380	80.97	0.7946	0.576	858	91.47	0.5172	0.098
381	80.98	0.7944	0.575	859	91.53	0.5150	0.097
382	80.99	0.7942	0.574	860	91.59	0.5128	0.096
383	81.00	0.7940	0.573	861	91.65	0.5105	0.095
384	81.01	0.7938	0.572	862	91.71	0.5082	0.094
385	81.02	0.7935	0.571	863	91.77	0.5059	0.093
386	81.03	0.7933	0.570	864	91.83	0.5035	0.092
387	81.03	0.7931	0.569	865	91.89	0.5012	0.091
388	81.04	0.7929	0.568	866	91.96	0.4987	0.090
389	81.05	0.7926	0.567	867	92.02	0.4963	0.089
390	81.06	0.7924	0.566	868	92.08	0.4938	0.088
391	81.07	0.7922	0.565	869	92.15	0.4913	0.087
392	81.08	0.7920	0.564	870	92.21	0.4888	0.086
393	81.09	0.7918	0.563	871	92.28	0.4862	0.085
394	81.10	0.7915	0.562	872	92.34	0.4836	0.084
395	81.10	0.7913	0.561	873	92.41	0.4810	0.083
396	81.11	0.7911	0.560	874	92.47	0.4783	0.082
397	81.12	0.7909	0.559	875	92.54	0.4756	0.081
398	81.13	0.7907	0.558	876	92.61	0.4728	0.080
399	81.14	0.7904	0.557	877	92.67	0.4701	0.079

#	T [°C]	y, Ethanol	x, Ethanol	#	T [°C]	y, Ethanol	x, Ethanol
400	81.15	0.7902	0.556	878	92.74	0.4672	0.078
401	81.16	0.7900	0.555	879	92.81	0.4644	0.077
402	81.17	0.7898	0.554	880	92.88	0.4615	0.076
403	81.18	0.7896	0.553	881	92.95	0.4586	0.075
404	81.19	0.7893	0.552	882	93.02	0.4556	0.074
405	81.19	0.7891	0.551	883	93.09	0.4526	0.073
406	81.20	0.7889	0.550	884	93.16	0.4495	0.072
407	81.21	0.7887	0.549	885	93.23	0.4464	0.071
408	81.22	0.7884	0.548	886	93.30	0.4432	0.070
409	81.23	0.7882	0.547	887	93.38	0.4400	0.069
410	81.24	0.7880	0.546	888	93.45	0.4368	0.068
411	81.25	0.7878	0.545	889	93.52	0.4335	0.067
412	81.26	0.7876	0.544	890	93.60	0.4302	0.066
413	81.27	0.7873	0.543	891	93.67	0.4268	0.065
414	81.28	0.7871	0.542	892	93.75	0.4234	0.064
415	81.28	0.7869	0.541	893	93.82	0.4199	0.063
416	81.29	0.7867	0.540	894	93.90	0.4163	0.062
417	81.30	0.7865	0.539	895	93.97	0.4127	0.061
418	81.31	0.7862	0.538	896	94.05	0.4091	0.060
419	81.32	0.7860	0.537	897	94.13	0.4054	0.059
420	81.33	0.7858	0.536	898	94.21	0.4016	0.058
421	81.34	0.7856	0.535	899	94.29	0.3978	0.057
422	81.35	0.7854	0.534	900	94.37	0.3939	0.056
423	81.36	0.7851	0.533	901	94.45	0.3899	0.055
424	81.37	0.7849	0.532	902	94.53	0.3859	0.054
425	81.38	0.7847	0.531	903	94.61	0.3819	0.053
426	81.39	0.7845	0.530	904	94.69	0.3777	0.052
427	81.39	0.7843	0.529	905	94.77	0.3735	0.051
428	81.40	0.7840	0.528	906	94.86	0.3692	0.050
429	81.41	0.7838	0.527	907	94.94	0.3649	0.049
430	81.42	0.7836	0.526	908	95.03	0.3604	0.048
431	81.43	0.7834	0.525	909	95.11	0.3559	0.047
432	81.44	0.7831	0.524	910	95.20	0.3514	0.046
433	81.45	0.7829	0.523	911	95.28	0.3467	0.045
434	81.46	0.7827	0.522	912	95.37	0.3420	0.044
435	81.47	0.7825	0.521	913	95.46	0.3371	0.043
436	81.48	0.7823	0.520	914	95.55	0.3322	0.042
437	81.49	0.7820	0.519	915	95.64	0.3272	0.041
438	81.50	0.7818	0.518	916	95.73	0.3221	0.040
439	81.51	0.7816	0.517	917	95.82	0.3170	0.039
440	81.52	0.7814	0.516	918	95.91	0.3117	0.038

#	T [°C]	y, Ethanol	x, Ethanol	#	T [°C]	y, Ethanol	x, Ethanol
441	81.53	0.7811	0.515	919	96.00	0.3063	0.037
442	81.54	0.7809	0.514	920	96.09	0.3008	0.036
443	81.54	0.7807	0.513	921	96.19	0.2952	0.035
444	81.55	0.7805	0.512	922	96.28	0.2896	0.034
445	81.56	0.7803	0.511	923	96.38	0.2838	0.033
446	81.57	0.7800	0.510	924	96.47	0.2779	0.032
447	81.58	0.7798	0.509	925	96.57	0.2718	0.031
448	81.59	0.7796	0.508	926	96.67	0.2657	0.030
449	81.60	0.7794	0.507	927	96.76	0.2594	0.029
450	81.61	0.7791	0.506	928	96.86	0.2530	0.028
451	81.62	0.7789	0.505	929	96.96	0.2465	0.027
452	81.63	0.7787	0.504	930	97.06	0.2398	0.026
453	81.64	0.7785	0.503	931	97.17	0.2330	0.025
454	81.65	0.7782	0.502	932	97.27	0.2260	0.024
455	81.66	0.7780	0.501	933	97.37	0.2190	0.023
456	81.67	0.7778	0.500	934	97.48	0.2117	0.022
457	81.68	0.7775	0.499	935	97.58	0.2043	0.021
458	81.69	0.7773	0.498	936	97.69	0.1967	0.020
459	81.70	0.7771	0.497	937	97.79	0.1890	0.019
460	81.71	0.7769	0.496	938	97.90	0.1810	0.018
461	81.72	0.7766	0.495	939	98.01	0.1729	0.017
462	81.73	0.7764	0.494	940	98.12	0.1647	0.016
463	81.74	0.7762	0.493	941	98.23	0.1562	0.015
464	81.75	0.7760	0.492	942	98.34	0.1475	0.014
465	81.76	0.7757	0.491	943	98.46	0.1386	0.013
466	81.77	0.7755	0.490	944	98.57	0.1295	0.012
467	81.78	0.7753	0.489	945	98.68	0.1202	0.011
468	81.79	0.7750	0.488	946	98.80	0.1106	0.010
469	81.80	0.7748	0.487	947	98.92	0.1008	0.009
470	81.81	0.7746	0.486	948	99.03	0.0907	0.008
471	81.82	0.7743	0.485	949	99.15	0.0804	0.007
472	81.83	0.7741	0.484	950	99.27	0.0698	0.006
473	81.84	0.7739	0.483	951	99.39	0.0590	0.005
474	81.85	0.7737	0.482	952	99.52	0.0478	0.004
475	81.86	0.7734	0.481	953	99.64	0.0363	0.003
476	81.87	0.7732	0.480	954	99.77	0.0246	0.002
477	81.88	0.7730	0.479	955	99.89	0.0125	0.001
478	81.89	0.7727	0.478	956	100.02	0.0000	0.000

A-6: Vapor Density Data of Ethanol-Water Test System at 1.013 bar Pressure

The vapor density data of the ethanol-water mixture used to calculate the gas capacity factor, F-factor, is shown in Figure 10.4 and Table 10.3. In this work, the f-factor is calculated mostly at the eye of the rotor unless otherwise specified. To estimate the vapor density of an ethanol-water mixture, the temperature at the eye of the rotor and the vapor outlet is assumed to be equal.

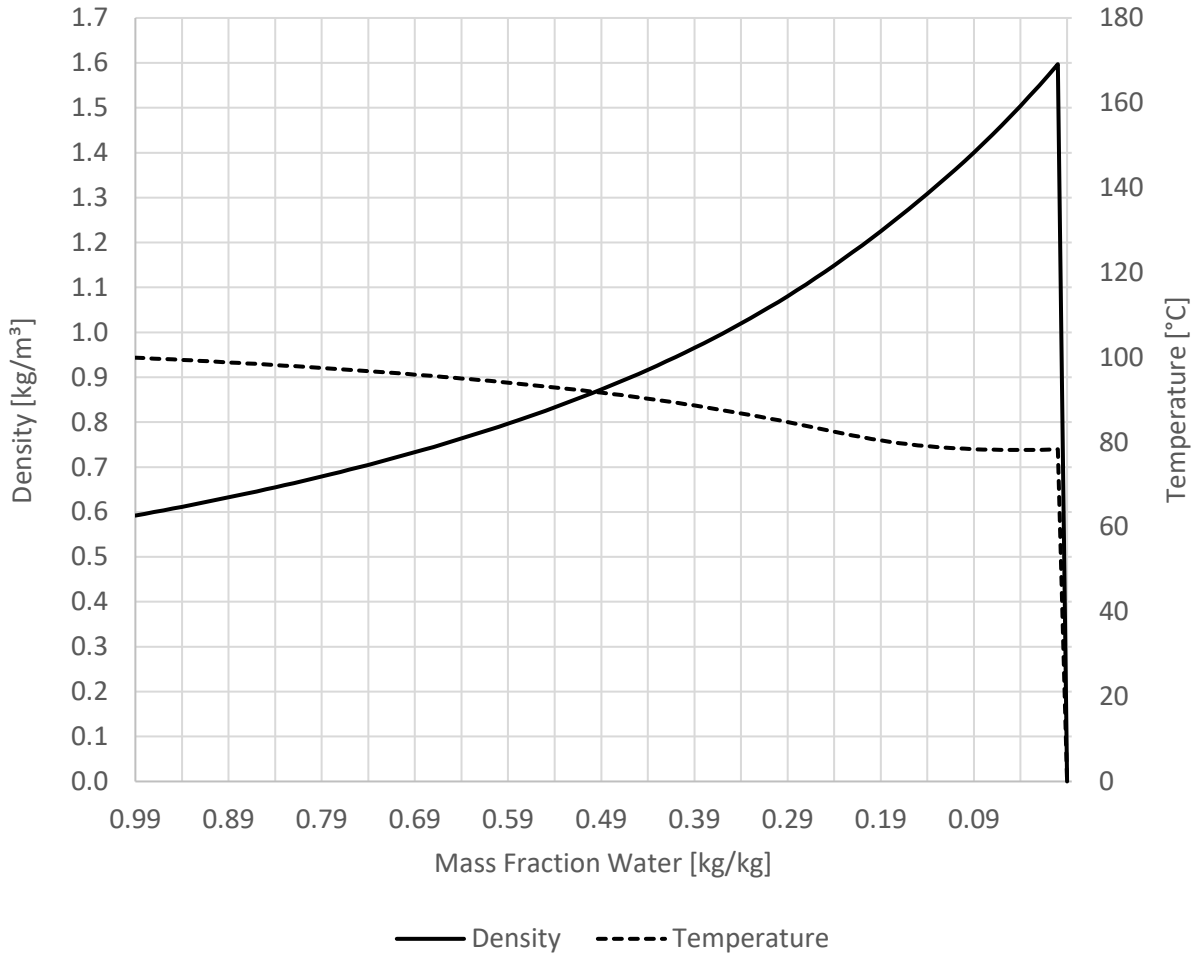

Figure 10.4: Vapor density of ethanol-water test system at 1.013 bar pressure.

Table 10.3: Vapor density data of ethanol-water test system at 1.013 bar pressure

#	y, ethanol [kg/kg]	ρ_{vap}^{mix} [kg/m³]	T [°C]	#	y, ethanol [kg/kg]	ρ_{vap}^{mix} [kg/m³]	T [°C]
1	0	0.588	100.01	39	0.38	0.776	94.64
2	0.01	0.592	99.91	40	0.39	0.783	94.44
3	0.02	0.596	99.81	41	0.4	0.790	94.23
4	0.03	0.600	99.70	42	0.41	0.797	94.03
5	0.04	0.604	99.59	43	0.42	0.804	93.81
6	0.05	0.608	99.49	44	0.43	0.811	93.59
7	0.06	0.612	99.38	45	0.44	0.818	93.37
8	0.07	0.616	99.26	46	0.45	0.825	93.14
9	0.08	0.620	99.15	47	0.46	0.833	92.91
10	0.09	0.624	99.04	48	0.47	0.841	92.67
11	0.1	0.628	98.92	49	0.48	0.848	92.42
12	0.11	0.632	98.80	50	0.49	0.856	92.17
13	0.12	0.637	98.68	51	0.5	0.864	91.92
14	0.13	0.641	98.56	52	0.51	0.873	91.65
15	0.14	0.646	98.43	53	0.52	0.881	91.38
16	0.15	0.650	98.30	54	0.53	0.890	91.11
17	0.16	0.655	98.17	55	0.54	0.899	90.83
18	0.17	0.660	98.04	56	0.55	0.907	90.53
19	0.18	0.664	97.91	57	0.56	0.917	90.24
20	0.19	0.669	97.77	58	0.57	0.926	89.93
21	0.2	0.674	97.63	59	0.58	0.935	89.62
22	0.21	0.679	97.49	60	0.59	0.945	89.30
23	0.22	0.684	97.35	61	0.6	0.955	88.97
24	0.23	0.689	97.20	62	0.61	0.965	88.63
25	0.24	0.694	97.05	63	0.62	0.976	88.28
26	0.25	0.700	96.90	64	0.63	0.986	87.92
27	0.26	0.705	96.75	65	0.64	0.997	87.56
28	0.27	0.710	96.59	66	0.65	1.008	87.18
29	0.28	0.716	96.43	67	0.66	1.020	86.79
30	0.29	0.722	96.27	68	0.67	1.031	86.40
31	0.3	0.727	96.10	69	0.68	1.043	85.99
32	0.31	0.733	95.93	70	0.69	1.055	85.57
33	0.32	0.739	95.76	71	0.7	1.068	85.15
34	0.33	0.745	95.58	72	0.71	1.081	84.71
35	0.34	0.751	95.40	73	0.72	1.094	84.27
36	0.35	0.757	95.22	74	0.73	1.107	83.82
37	0.36	0.764	95.03	75	0.74	1.121	83.37
38	0.37	0.770	94.84	76	0.75	1.135	82.91

#	y, ethanol [kg/kg]	ρ_{vap}^{mix} [kg/m^3]	T [°C]
77	0.76	1.149	82.45
78	0.77	1.164	82.00
79	0.78	1.179	81.57
80	0.79	1.194	81.15
81	0.8	1.209	80.76
82	0.81	1.225	80.40
83	0.82	1.241	80.07
84	0.83	1.258	79.77
85	0.84	1.274	79.50
86	0.85	1.291	79.26
87	0.86	1.308	79.04
88	0.87	1.326	78.85
89	0.88	1.344	78.69
90	0.89	1.363	78.55
91	0.9	1.381	78.43
92	0.91	1.401	78.34
93	0.92	1.420	78.26
94	0.93	1.440	78.21
95	0.94	1.461	78.17
96	0.95	1.482	78.15
97	0.96	1.504	78.15
98	0.97	1.526	78.16
99	0.98	1.549	78.19
100	0.99	1.573	78.24
101	1	1.597	78.30

A-7: Temperature Measurement Data of Rotor Telemetry

The raw data used to calculate the radial separation efficiency of knit mesh and empty rotor (as represented in Figure 4.8 – Figure 4.13) is shown below in Table 10.4. The experimental data given is an average of two measurements.

Table 10.4: Temperature measurements along the radius of the rotor at an F-factor of 2.1 $Pa^{0.5}$ and 1.013 bar pressure.

	Knit mesh			**Empty rotor**		
Rotational speed [1/min]	300	600	900	300	600	900
Reflux flow [kg/h]	43	43	41	39	41	39
Temperature	°C	°C	°C	°C	°C	°C
T1	78.69	78.89	78.97	79.82	79.6	79.61
T2	78.84	79.03	79.11	79.93	79.6	79.72
T3	78.75	78.96	79	79.82	80	80.06
T4	79.19	79.11	79.16	79.9	80.1	80.29
T5	78.72	78.83	79.06	80.1	79.9	80.25
T6	78.86	79.08	79.53	80.38	80.1	80.52
T7	79.05	79.22	79.36	80.54	80.3	80.61
T8	78.74	79.66	79.96	80.64	80.3	80.69
T9	79.55	79.94	80.21	81.3	80.4	81.05
T10	-	-	-	80.96	80.6	80.99
T11	-	-	-	80.89	80.6	81.17
T12	-	-	-	81.55	80.8	81.21

Regression Results

The temperature profiles are plotted from the raw temperature data in Table 10.4 after applying the assumptions in section 4.2.2. Figure 10.5, Figure 10.6, and Figure 10.7 below show the results of selected temperature profiles for knit mesh packing, empty rotor, and zickzack packing, respectively.

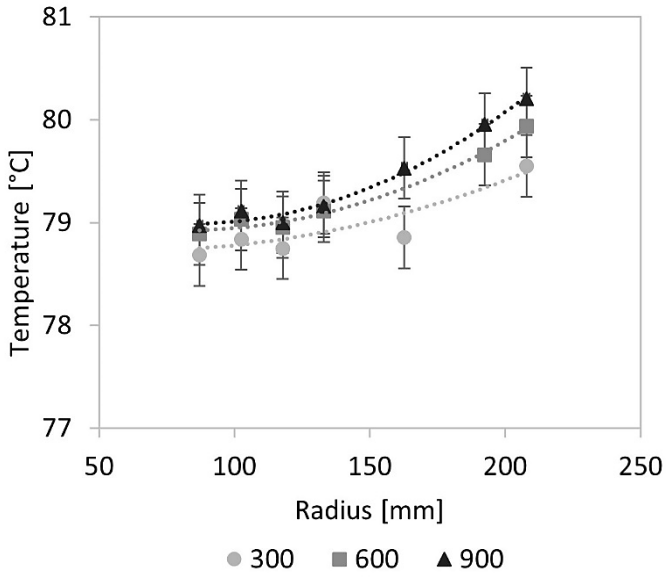

Figure 10.5: Selected temperature profile for the **knit mesh** (KM) at an F-factor 2.1 $Pa^{0.5}$. Dashed lines represent 2nd degree polynomials fitted to the data points.

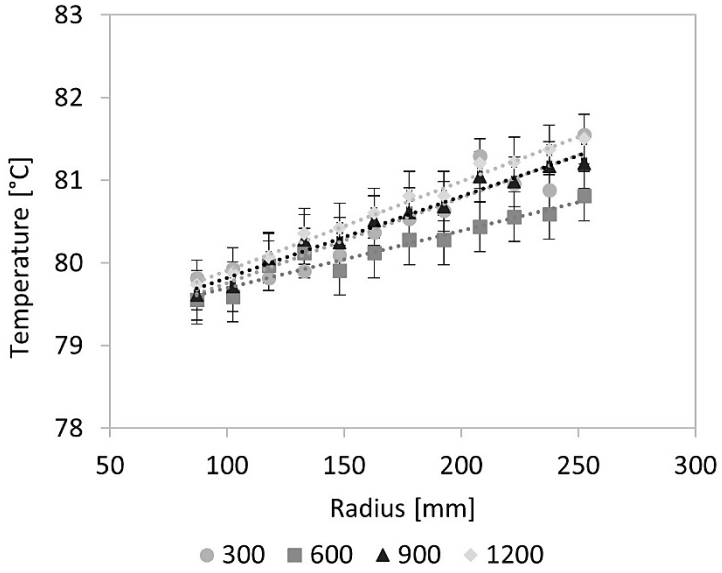

Figure 10.6: Selected temperature profile for **empty rotor** (ER) at an F-factor 2.1 $Pa^{0.5}$. Dashed lines represent a linear fit. All the measured temperature data points are considered after applying the assumptions.

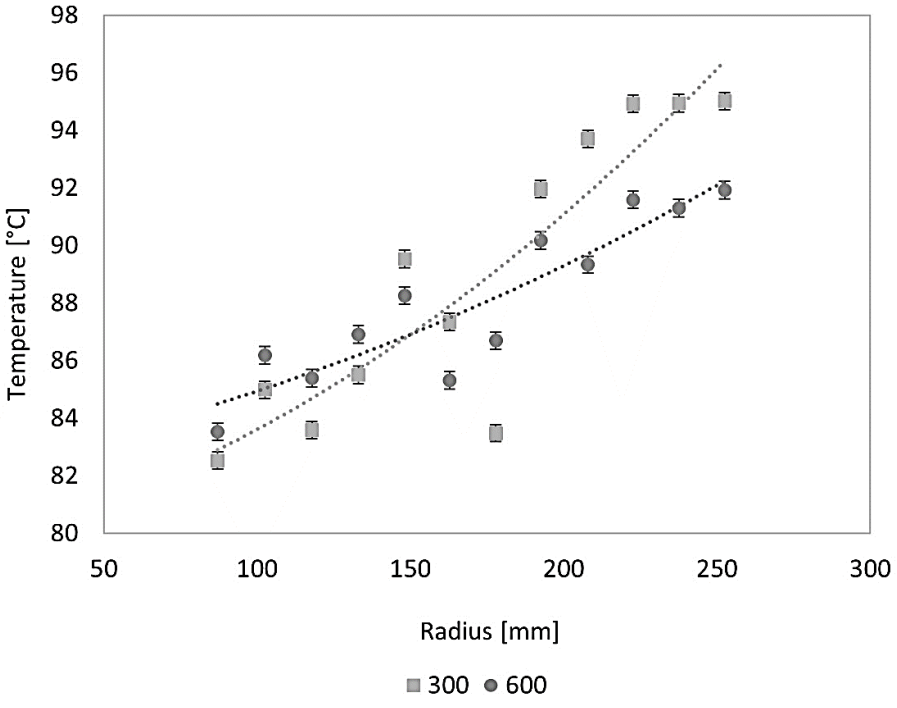

Figure 10.7: Selected temperature profile for **Zickzack** (ZZ) at an F-factor 0.3 $Pa^{0.5}$. Dashed lines represent 2nd-degree polynomials fitted to the data points. All the measured temperature data points are considered after applying the assumptions.

A-8: Vapor-liquid equilibrium data of the methanol-ethanol test system

VLE data used for calculating $K_G a$ using Mondal's model for the methanol-ethanol system were taken from Onken [88]. Where x and y are the molar fractions of methanol in the liquid and vapor, respectively. α is the relative volatility.

Table 10.5: VLE data of methanol-ethanol test system at 1.01325 bar pressure.

x	y	T (°C)	α
0	0	78.3	-
0.05	0.0795	77.4	1.641
0.1	0.1531	76.7	1.628
0.15	0.2224	75.9	1.621
0.2	0.288	75.1	1.618
0.25	0.3505	74.4	1.619
0.3	0.4104	73.6	1.624
0.35	0.4677	72.9	1.632
0.4	0.5228	72.2	1.643
0.45	0.5756	71.5	1.657
0.5	0.626	70.8	1.674
0.55	0.6741	70.1	1.692
0.6	0.7197	69.4	1.712
0.65	0.763	68.8	1.733
0.7	0.8038	68.1	1.756
0.75	0.8421	67.5	1.778
0.8	0.8781	66.9	1.801
0.85	0.9118	66.3	1.824
0.9	0.9432	65.7	1.845
0.95	0.9726	65.1	1.866
1	1	64.55	-

Chapter 11 Declaration

Parts of this thesis were developed in cooperation with ISPT (Institute for Sustainable Process Technology) within the scope of the research project ImPaCCt (Improved Process Performance by Process Intensification in Centrifugal Contactors). Selected results of this work have been previously published in journal articles (Chapter 12). Some chapters/sections include data derived from student theses (Chapter 13) supervised by the author at the Laboratory of Fluid Separation, Biochemical and Chemical Engineering Department, TU Dortmund University. Details are given below.

Chapter	Section		Scientific Work
2	2.3.1	Partly adapted from	C, G
	2.3.3	Partly adapted from	A, a
	2.3.4	Partly adapted from	E, d
3	3.1	Partly adapted from	B, C, a-f
	3.2.1, 3.2.2, 3.3.1, 3.2.3	Partly adapted from	C, f, e
	3.4	Partly adapted from	B, F, d, f
	3.5	Partly adapted from	B, b, f, d
4	4.2, 4.3.1, 4.3.2	Partly adapted from	A, C, D, E, d, e
	4.3.3, 4.3.4, 4.4	Partly adapted from	D
5	5.1	Partly adapted from	C, a-f
	5.2	Partly adapted from	C, D, e, f,
	5.3	Partly adapted from	e. f
10	A-2	Partly adapted from	e, f
	A-3	Partly adapted from	e
	A-4	Partly adapted from	B, a, c
	A-6	Partly adapted from	E
	A-7	Partly adapted from	D

Chapter 12 List of Publications

Articles	
A	**Qammar, H.;** Hecht, F.; Skiborowski, M.; Górak, A.: Experimental Investigation and Design of Rotating Packed Beds for Distillation, Chemical Engineering Transactions, 2018, 69, 655-660 https://doi.org/10.3303/CET1869110
B	**Qammar, H.;** Gładyszewski, K.; Górak, A.; Skiborowski, M.: Towards the Development of Advanced Packing Design for Distillation in Rotating Packed Beds, Chem. Ing. Tech., 2019, 91, 11, 1663 – 1673, https://doi.org/10.1002/cite.201900053
C	**Qammar, H.:** Rotating Packed Beds in Distillation: Binary Distillation, in: M. Skiborowski, A. Górak (Eds.), Process Intensification, De Gruyter, 2022, pp. 159–188. https://doi.org/10.1515/9783110724998-006
D	**Qammar, H.;** Pyka, T.; Koop, J.; Górak, A.; Schembecker, G.: Radial Temperature Profile Measurements to Understand Mass Transfer in Rotating Packed Bed Distillation, Ind. Eng. Chem. Res., 2023. https://doi.org/10.1021/acs.iecr.3c01068
E	Hampel, U.; …, Górak, A.; Skiborowski, M.; Groß, K.; **Qammar, H.:** Recent Advances in Experimental Techniques for Flow and Mass Transfer Analyses in Thermal Separation Systems, Chem. Ing. Tech. 92, 2020, 926–948. https://doi.org/10.1002/cite.202000076
F	Kruber, K.F.**; Qammar, H;** Skiborowski, M.: Optimization-Based Design of Rotating Packed Beds with Zickzack Packings, Computer Aided Chemical Engineering, 2020, 48 997–1002. https://doi.org/10.1016/B978-0-12-823377-1.50167-1
G	Neumann, K.; Gladyszewski, K.; Groß, K.; **Qammar, H.;** Wenzel, D.; Górak, A.; Skiborowski, M.: A guide on the industrial application of rotating packed beds, CHERD, 2018, 134, 443 – 462, http://doi.org/10.1016/j.cherd.2018.04.024

Oral and Poster Presentations	
1	**Qammar, H**.; Gładyszewski, K.; Górak, A.; Skiborowski, M. Towards Improved Packing Design for Rotating Packed Beds Presentation at Jahrestreffen der ProcessNet-Fachgemeinschaften "Prozess-, Apparate- und Anlagentechnik" unterstützt durch „Sustainable Production, Energy and Resources‘‘ (2019), Dortmund, Germany.
2	**Qammar, H**.; Hecht, F.; Skiborowski, M.; Górak, A. Experimental Investigation and Design of Rotating Packed Beds for Distillation Presentation at 11th International Conference on Distillation & Absorption (2018), Florence, Italy
3	**Qammar, H**.; Gladyszewski, K.; Skiborowski, M.; Górak, A. Performance Evaluation of Rotating Packed Beds for Distillation Using Improved Packing Design Presentation at ProcessNet-Jahrestagung und 33. DECHEMA-Jahrestagung der Biotechnologen (2018), Aachen, Germany
4	**Qammar, H**; Gladyszewski, K.; Li, Y.; Skiborowski, M.; Gorak, A. Detailed Analysis of an Improved Packing Design for Distillation in Rotating Packed Beds Poster at 2nd International Process Intensification Conference (2019), Leuven, Belgium
5	**Qammar, H**.; Skiborowski, M.; Górak, A. Experimental Investigation of Rotating Packed Beds for Vapour-Liquid Processes Poster at 10th World Congress of Chemical Engineering (2017), Barcelona, Spain
6	Groß, K.; Neumann, K.; **Qammar, H**.; Wenzel, D. Current Status of Rotating Packed Beds (RPBs): Applications in Chemical Industry Poster at Jahrestreffen der ProcessNet Fachgruppen Fluidverfahrenstechnik und Membrantechnik (2017), Köln, Germany

Chapter 13 List of Supervised Theses

a	Jörn Felix Hecht, Development and Experimental Investigation of Distillation in a Pilot-Scale Rotating Packed Bed, 2017	B.Sc.
b	Lisa-Marie Rombach, Investigation of the Influence of Nozzle and Packing Type on the Separation Efficiency of Rotating Packed Beds for Distillation Operation, 2017	B.Sc.
c	Nils Gerdes, Performance Evaluation of Rotating Packed Beds for Distillation Using Different Packing Types, 2018	B.Sc.
d	Yutong Li, Quantitative Characterization of Mass Transfer in the Packing and the Casing using Rotor Telemetry in RPBs, 2019	M.Sc
e	Leonie Kadau, Extending the Operating Window for Distillation in Pilot Scale Rotating Packed Bed, 2020	M.Sc.
f	Sarah Barcikowski, Characterization of Mass Transfer Distribution for Distillation in Rotating Packed Bed (RPB), 2020	B.Sc.